INTERACTION BETWEEN FERRIC HYDROXIDES AND DISSOLVED SULFIDE IN ANOXIC AQUIFERS:

Pathway and Kinetics of iron and sulfur products formation

Dissertation zur Erlangung des Grades

Doktor der Naturwissenschaften

(Dr. rer.nat)

an der Bayreuther Graduiertenschule für Mathematik und Naturwissenschaften (BayNAT)

der Universität Bayreuth

Vorgelegt von

Moli Wan

Geb. am 20.06.1982 in Guangdong, VR China

Die vorliegende Arbeit wurde in der Zeit von 02.2010 bis 07.2015 in Bayreuth am Lehrstuhl für Hydrologie unter Betreuung von Herrn Professor Dr. Stefan Peiffer angefertigt.

Vollständiger Abdruck der von der Bayreuther Graduiertenschule für Mathematik und Naturwissenschaften (BayNAT) der Universität Bayreuth genehmigten Dissertation zur Erlangung des akademischen Grades eines Doktors der Naturwissenschaften (Dr. rer. nat)

Dissertation eingereicht am: 20.03.2015

Zulassung durch das Leitungsgremium: 15.04.2015

Wissenschaftliches Kolloqium: 29.07.2015

Amtierender Direktor: Prof. Dr. Franz Xaver Schmid

Prüfungsausschuss:

Prof. Dr. Stefan Peiffer	(Erstgutachter)
Prof. Dr. Stefan Haderlein (Uni Tübingen)	(Zweitgutachter)
Prof. Dr. Gehard Gebauer	(Vorsitz)
Prof. Dr. Britta Planer-Friedrich	

Table of Contents

List of Figures IV
List of Tables VIII
Summary 1
Zusammenfassung 4
1. General introduction and summary 7
1.1 General introduction and research questions 7
1.1.1 Fe(III) reduction coupled to carbon and sulfur 7
1.1.2 Complexity of interaction between ferric (hydr)oxides and adsorbed species 11
1.1.3 Product formation during interaction between sulfide and ferric (hydr)oxides 14
1.1.4 Pyrite formation from iron monosulfide 15
1.1.5 Research questions 16
1.2 Research objectives and outline of the dissertation 18
1.3 Materials and methods 20
1.3.1 Iron phases 20
1.3.2 Experimental set-up 21
1.3.3 Optimization of wet chemical analytic methods 22
1.3.4 Solid phases analysis 24
1.4 Summary of results and discussion 25
1.4.1 Chemical speciation 25
1.4.1 Characterization of sulfur and iron products during sulfidation of ferric hydroxides 25
1.4.2 Kinetics and pathway of pyrite formation affected by the initial Fe/S ratio 27
1.4 Conclusions and perspective 28
2. Occurrence of Surface Polysulfides during the Interaction between Ferric (Hydr)Oxides and Aqueous Sulfide 34
2.1 Abstract 35
2.2 Introduction 36
2.3 Materials and methods 38
2.3.1 Ferric (hydr)oxides 38
2.3.2 Experimental set-up 38
2.3.3 Wet chemical analysis 40
2.3.4 Cryogenic XPS 41
2.4 Results and Discussion 43
2.4.1 Reaction progress as derived from wet chemical analysis 43

2.4.2 Sulfur surface-speciation as detected by Cryogenic XPS 45
2.4.3 Sulfur mass balance 50
2.5 Implication for sulfur biogeochemistry 55
2.6 Reference 59
2.7 Supporting Information 62
3. Pyrite formation and mineral transformation pathways upon sulfidation of ferric hydroxides depend on mineral type and sulfide concentration 70
3.1 Abstract 71
3.2 Introduction 73
3.3 Materials and methods 76
3.3.1 Ferric (hydr)oxides 76
3.3.2 Experimental Set-up 76
3.3.3 Sampling and analysis 78
3.4 Results 83
3.4.1 Chemical speciation 83
3.4.2 Spectroscopic and microscopic results 87
3.5 Discussion 97
3.5.1 Formation of excess Fe(II) 97
3.5.2 The role of excess Fe(II) as a driver of secondary phase formation 100
3.6 Conclusion 104
3.7 References 109
4. Fe/S ratio controls pathway and kinetics of pyrite formation during Fe(III)-S(-II) interaction 112
4.1 Abstract 113
4.2 Introduction 114
4.3 Materials and methods: 117
4.3.1 Ferric hydroxides 117
4.3.2 Experimental set-up: 117
4.4 Sampling and analysis 121
4.4.1 Wet chemical analysis 121
4.4.2 Mössbauer Spectroscopy 123
4.5 Results 123
4.5.1 Chemical speciation 124
4.5.2 Mössbauer spectroscopy 128
4.6 Discussion 133
4.6.1 Kinetics of pyrite formation 133
4.6.2 Ferrous iron species interface pyrite formation 138

4.7 Conclusion and implication 144
4.8 References 147
4.9 Supporting Information 150
5. Electromagnetic Properties of FeS Phases: Insights from Mössbauer Spectroscopy 160
5.1 Abstract 161
5.2 Introduction 162
5.3 Materials and methods 164
5.3.1 Mineral synthesis and sample preparation 164
5.3.2 Filtered FeS precipitate from Fe(II) and S(-II) solution 164
5.3.3 Freeze-dried FeS 164
5.3.4 FeS from interaction between Fe(III) and S(-II) with different Fe/S ratios 164
5.3.5 Mössbauer spectroscopy 165
5.4 Results and discussion 166
5.5 Conclusions and outlook 172
5.6 References 174
Contribution to the studies 176
Acknowledgements 178
Versicherungen und Erklärungen 179

List of Figures

Fig. 1.1 Redox-Driven Conveyor Belt mechanism to explain electron movement from the aqueous Fe2+ to bulk ferric (hydr)oxides and release to the solution. Fe2+ is adsorbed onto the surface of ferric (hydr)oxides (1) and then electron transfer occurs between adsorbed Fe2+ and Fe3+ at the surface of ferric (hydr)oxides (2). As a consequence, adsorbed Fe2+ is oxidized to Fe3+, leading to a new layer of oxide growth (3). The injected electron can move through the bulk mineral (4) and be released as Fe2+ at the other mineral facet (5). (Figure taken from Gorski and Scherer, 2011)……..……..12

Fig. 1.2. Conceptual model of interaction between aqueous Fe^{2+} and ferric (hydr)oxides. The electrons taken from oxidation of adsorbed Fe^{2+} is transferred into the conduction band (CB), from where electrons have three fates: they can 1) be localized in a trapping site; 2) be transferred to a foreign species as environmental contaminants; 3) be released into solution as mentioned in Fig. 1.1. (Figure taken from Gorski and Scherer, 2011)…….……..13

Fig. 1.3 Representive recovery ratios of FeS with and without five different ferric hydroxides: commercial goethite (comm. Gt), commercial lepidocrocite (comm. Lp), synthetic goethite (syn. Gt), synthetic lepidrocite (syn. Lp) and synthetic ferrihydrite (Fh). ……..……..23

Fig. 2. 1 Sulfur speciation during reaction between aqueous sulfide and goethite for iron excess (HR) and sulfide excess (LR) conditions. Note the different time scales between HR_Gt and LR_Gt……..……..….44

Fig. 2. 2 Concentrations of $Fe(II)_{HCl}$ of all runs. Note the two different time scales. The data with closed symbols refer to the top x axis……..….44

Fig. 2. 3 Survey XPS spectra of samples in experiments with goethite. ……...45

Fig. 2. 4 High resolution Fe 2p spectra of goethite and corresponding spectral area concentration of each species before and after reaction. Compound colours in bar chart are the same as in the spectra……..46

Fig. 2. 5 High-resolution S 2p spectra and corresponding spectral area concentration of each species in all runs. Compound colours in bar chart are the same as in the spectra. …….……..……...47

S2. 1 Sulphur speciation during reaction between aqueous sulfide and lepidocricite for iron excess (HR) and sulfide excess (LR) conditions. Note the different time scales between HR_Lp and LR_Lp…….……..……64

S2. 2 Survey XPS spectra of samples in experiments with lepidocrocite..……65

S2. 3 High resolution Fe 2p spectra of lepidocrocite and corresponding spectral area concentration of each species before and after reaction. Compound colours in bar chart are the same as in the spectra…….…….…….……...66

S2. 4 High resolution O 1s spectra of goethite and corresponding spectral area concentration of each species before and after reaction. Compound colours in bar chart are the same as in the spectra…….…….…….……...…67

S2. 5 High resolution O 1s spectra of lepidocrocite and corresponding spectral area concentration of each species before and after reaction. Compound colours in bar chart are the same as in the spectra……..…….…….…….…….68

S2. 6 High resolution S 2p spectra of LR_Lp after leaving in the analysis chamber overnight without cooling. The corresponding spectral area concentration of each species has the same color as in the spectra……..…….….69

Fig. 3.1 Time evolution of sulphur and iron species during the reaction between dissolved sulfide and ferrihydrite (A), lepidocrocite (B), and goethite (C). Note the different time scale for goethite……...…….……85

Fig. 3.2 pH progress (bottom) and H^+ consumption (top) during the reaction between ferrihydrite, lepidocrocite, and goethite with dissolved sulfide……..……..86

Fig. 3.3 Mössbauer spectra of lepidocrocite reacted with sulfide after 1 hour, 1 day, 1 week, and 2 weeks. White sextets correspond to lepidocrocite, and gray shaded to FeS_2. All spectra were collected at a temperature of 4.2 K. The scale bar represents 2% absorption for each spectrum. Solution conditions are listed in Table 3.1, and model parameters are listed in Table 3.3….....…89

Fig. 3.4 Mössbauer spectra of goethite reacted with sulfide after 1 hour, 1 day, 1 week, and 2 weeks. White sextets correspond to goethite and gray shaded doublets to FeS_2. All spectra were collected at a temperature of 4.2 K. The scale bar represents 2% absorption for each spectrum. Solution conditions are listed in Table 1, and model parameters are listed in Table 3.3……..…..90

Fig.3.5 Mössbauer spectra of ferrihydrite reacted with sulfide after 1 week and 2 weeks. White sextets are bulk models for all Fe(III) (hydr)oxides present and may represent a combination of the goethite, hematite, and magnetite observed by TEM. Gray shaded doublets reflect signals from FeS_2. All spectra were collected at a temperature of 4.2 K. The scale bar represents 2% absorption for each spectrum. Solution conditions are listed in Table 1, and model parameters are listed in Table 3.3…….....91

Fig. 3.6 High resolution TEM image (a) and electron diffraction pattern (b) of ferrihydrite after 2 hours reaction with dissolved sulfide. Dark-field STEM image (c) and EDX maps of iron [Fe Kα] (d) and sulphur [S Kα] distribution (e) show that sulphur was evenly distributed on the solid phase……..…..92

Fig. 3.7 Bright field TEM image (a) of the apparently pristine particle size and morphology of goethite after 2 hours of reaction. High resolution TEM images (b, c) reveal sulphur rich rims on goethite crystals. Lattice fringes in these rims are characteristic for mackinawite (FeS). EDX spectra (d) taken from the rims (black) and in the centre of goethite crystals (white) reveal the formation of iron sulfide with a Fe:S ratio close to 1:1 on the goethite surface …….94

Fig. 3.8 Bright field (a, c) and high resolution (b, d, e) TEM images after 2 weeks of reaction between ferrihydrite and dissolved sulfide. Pyrite crystals are characterized by quadratic outlines and occur separated from ferric oxides (a, c). The aggregates consisted of agglomerated nanocrystalline domains (b). Ferrihydrite was completely transformed into hematite (arrow in c, d, e) and magnetite (e)……95

Fig.3.9 Bright field TEM image (a) showing the distribution of goethite and pyrite after 2 weeks reaction. The pyrite crystals consisted of nanocrystalline aggregates (b). Bright field TEM images (c, d) and FFT electron diffraction pattern (inset in d) revealed that minor amounts of goethite were transformed into hematite, preferably at the top of the acicular goethite crystals……96

Fig. 3.10 Scheme for the classification of environments according to their potential for rapid pyrite formation……...105

Fig. 4.1 pH value and H^+ consumption at the first 2.5 h in the high Fe/S ratio with goethite and lepidocrocite……..……124

Fig. 4.2 Iron and sulfur speciation in the HR runs……..……..125

Fig.4.3 Iron and sulfur species in the short-term LR runs within 168 h. ……..……127

Fig. 4.4 $Fe(II)_{sol.}$ concentration in the long-term LR runs……..……128

Fig. 4.5 Representive Mössbauer spectra of HR runs. Corresponding parameters were listed in Table 4.2……..129

Fig. 4.6 Representive Mössbauer spectra of long-term LR runs (left: Lp; right: Gt) in the precence of high concentration of remaining aqueous sulfide. Corresponding parameters were listed in Table 4.2……...……130

Fig. 4.7 Mössbauer spectra of long-term LR_Lp run in the presence of low concentration of remaining aqueous sulfide. Corresponding parameters were listed in Table 4.2……131

Fig. 4.8 Pyrite concentration measured with Mössbauer spectroscopy. The diamond point at 2160 h in LR_Lp run with low initial $S(-II)_{aq}$ (L. $S(-II)_{ini}$) means that pyrite was calculated according to the wet chemical analyais.……134

Fig. 4.9 Representive plot of the concentration of MES and Fe(II) bound with pyrite at each individual time step in HR run……..……134

Fig. 4.10 Plot of logarithm of MES consumption versus time for HR runs.....135

Fig. 4.11 Measured $FeS_{2,py}$ concentration in LR_Gt and LR_Lp with high concentration of initial $S(II)_{aq}$ compared to predicted $FeS_{2,py}$ concentration forming via the polysulfide pathway (eq 3)……..…...137

Fig. 4.12 The relationship between logarithm of the mean pyrite formation rate and the molar ratio of surface sites of ferric hydroxides to sulfide...……...138

Fig. 4.13 Novel polysulfide pathway near the surface of ferric hydroxides. The iron supply for rapid pyrite formation was marked in red. The initial electron transfer (dark fat arrows) between sulfide and ferric iron generates ferrous iron and S^o/S^-. A fraction of ferrous iron was in the form of excess Fe(II) (marked in red), which can either transfer electrons into the bulk ferric hydroxides and later on reduce S^o to form polysulfide (dot line and arrow) or stayed at the surface readily bound with surface polysulfide to form pyrite. The pyrite nucleation leads to a decrease of $Fe(II)_{excess}$, which induced FeS dissolution (green thin arrows) and a second electron transfer (pinky fat arrows) between sulfide and ferric iron, resulting in excess Fe(II) (pinky fat arrows) and polysulfide (black arrows) generation. The increase of $Fe(II)_{aq}$ was originated from FeS dissolution (green arrows) or release of excess Fe(II) (red arrow).……..…….……145

SI 4.1 $Fe(II)_{py}$ and MES concentration in selected HR_Gt runs……...…….153

Figure 5.1 Mössbauer spectra collected at sample temperatures of ~5 K from (from top) wet-filtered FeS; freeze—dried FeS; FeS from interaction between Fe(III) and S(-II), Fe/S = 0.5; FeS from interaction between Fe(III) and S(-II), Fe/S = 2.8; and lepidocrocite. The black solid line marks the position of the single line subspectrum (dark grey) representing FeS and the dashed black lines mark the outer two lines of the six-line subsepctrum (grey) representing FeS. The subspectrum representing lepidocrocite is shaded in light grey……..167

List of Tables

Table 1.1. Characterization of ferric hydroxides……20

Table 2.1 Initial experimental conditions. All runs were conducted at pH 7……...39

Table 2.2 The XPS fitting parameters of Fe and S species……..49

Table 2.3 S^o obtained as MES and from XPS calculation……..…..52

Table 3.1 Initial experimental conditions for experimental runs where both TEM and Mössbauer spectroscopy was performed. All runs were conducted at pH 7……77

Table 3.2 Model Parameters used for evaluation of 4.2 K Mössbauer spectra and abundances of the minerals identified…….81-82

Table 3.3 Concentrations of products during the reaction of H_2S with the three ferric (hydr)oxides after constant values were reached. Values for ferrihydrite and lepidocrocite correspond to t = 2 h, while those for goethite to t = 8 h……...…83

Table 3.4 Interplanar spacings and corresponding lattice planes of the phases formed after 14 days of reaction of ferrihydrite with sulfide identified by electron diffraction and fast Fourier transformation of high resolution images……..……....93

Table 3.5 Relationship between fraction of excess Fe(II) after 2 h (lepidocrocite and ferrihydrite) or 8 h (goethite) reaction time and pyrite yield after 14 days……...100

Table 4.1 Initial conditions for all runs. pH was kept at 7.0±0.1……...……..120

Table 4.2 Model parameters for 4.2 K Mössbauer spectra of ^{57}Fe hydroxides……..131

Table S4.1 Area concentration of iron mineral in the Mössbauer spectra in Fig 4.5,4.6 and 4.7……..151

Table S4.2 recalculation of rate constants k_{py} from original dataset from Rickard (1975). Recalculated data are in an italic typeface…….155-156

Table S4.3 supersaturation ratio Ω_{py} with respect to pyrite in the solution (LR runs) and near the ferric hydroxides' surface……..……158

Table 5.2 Mössbauer Parameters used to fit the samples…….……..168

Summary

The interaction between ferric iron (Fe(III)) and sulfide (S(-II)) is of great importance in permanent or temporary anoxic environments. It is a major component of the biogeochemical cycling of both iron and sulfur and eventually of carbon. Electron transfer between ferric iron and sulfide leads to elemental sulfur and metastable iron sulfide minerals and finally to a thermodynamically more stable iron sulfide, which is pyrite. Pyrite formation, as a significant early diagenesis process, plays an undeniable role as a global sink for the elements Fe and S. Therefore, the interaction of ferric iron and sulfide, especially pyrite formation, has been studied for quite a long time. However, questions remain regarding the role of electron transfer between ferric iron and sulfide on the intermediates and pyrite (end product) formation. The objectives of this dissertation are therefore i) to understand the influence of chemical properties of ferric hydroxides on the kinetics of electron transfer between S(-II) and Fe(III) and eventually on the formation of different intermediated products, ii) to characterize the properties and the fates of intermediate products, iii) to study the pathway and kinetics of the end product, i.e. pyrite formation and, iv) to develop a framework of sulfide reacting with ferric iron at the surface or near-surface regime. We investigated the reactions between aqueous sulfide and ferric hydroxides at neutral pH in an anoxic glove box. The initial ratio of Fe/S was adjusted to be 'high' (HR) where excess ferric iron remained after a complete consumption of sulfide and 'low' (LR) where excess sulfide remained after a complete consumption of ferric iron. Species were examined with wet chemical analysis as well as solid phase analytic methods including Transmission Electron Microscopy (TEM), Mössbauer spectroscopy and X-ray photoelectron spectroscopy (XPS).

Results indicate complex interactions between ferric iron and sulfide. Wet chemical analysis suggests different dynamics in HR and LR experiments. In all experiments sulfide was oxidized within the first 3 h, and a pool of acid extractable ferrous iron ($Fe(II)_{HCl}$) and methanol extractable sulfur (MES) built up. In HR experiments a decrease of $Fe(II)_{HCl}$ and MES, which was accompanied by pyrite formation, occurred after 24 - 48 h. By contrast, no pyrite formation was observed up to 2160 h in the LR

experiments. A significant fraction of generated $Fe(II)_{HCl}$, could not be recovered as stoichiometric FeS (or mackinawite), which is consistent with previous studies ("excess Fe(II)") (Hellige et al., 2012; Poulton, 2003; Poulton et al., 2004). The formation of the "excess Fe(II)" seems compete with the formation of FeS/mackinawite. The excess Fe(II) concentration depends on the initial ratio of Fe/S as well as the mineralogical reactivity (represented by mineral types and surface area) of ferric iron. Higher Fe/S ratio and higher reactivity lead to higher excess Fe(II) concentration and less FeS/mackinawite concentration. Furthermore, XPS analysis confirmed that not only elemental sulfur but also polysulfides were the main oxidized sulfur products.. The polysulfides, with predominance of disulfide, accumulated mainly at the mineral surface and could be extracted by methanol with an appropriate pre-treatment with zinc acetate. Therefore, the MES pool comprised elemental sulfur, aqueous polysulfides and surface polysulfides. Rapid pyrite formation in HR experiments is closely linked to the formation of excess Fe(II). The presence of excess Fe(II) and polysulfides at the surface may lead to the potential formation of non-crystalline iron-polysulfide species and a supersaturation with respect to pyrite, thereby inducing rapid pyrite formation in the HR experiment. The rapid pyrite formation has been proposed as a 'novel' polysulfide pathway because ferrous iron and disulfide for pyrite formation originate directly from the excess Fe(II) and surface polysulfide. The rapid pyrite formation via this 'novel' polysulfide pathway is not kinetically controlled by the FeS dissolution. By contrast, pyrite in LR experiments formed via the normal polysulfide pathway that ferrous iron for pyrite formation is only from FeS dissolution. Pyrite formation in LR experiments is therefore kinetically controlled by FeS dissolution. The formation of iron polysulfide may influence the electromagnetic properties of ferrous iron in FeS/mackinawite, leading to an occurrence of magnetic ordering at 4.2 K. The magnetic ordering is represented by an asymmetric six-line in the Mössbauer spectrum (at 4.2 K). The spectrum of mixed iron sulfide phases generated during Fe(III)-S(-II) interaction is very different from that of pure FeS freshly precipitated from homogeneous solution of ferrous iron and sulfide, which showed no magnetic ordering (a single-line spectrum) at 4.2 K. The pure FeS phase is not stable and tends to transform into the mixed iron sulfide phases.

Three key findings from this thesis can be highlighted that help to understand the interaction between iron and sulfur biogeochemistry:

1) The occurrence of surface polysulfide subverts the previous consideration that polysulfide presents only in the solution and may play an overlooked role in both abiotic and biotic sulfur cycling.
2) The Fe/S ratio controlling the kinetics and pathway of pyrite can be applied as an indicator to predict rapid pyrite formation, especially in the temporary anoxic environments.
3) Complex Mössbauer spectra of iron sulfide phases reveal that the properties, especially the electromagnetic property of Fe in mackinawite, can be easily altered by impurities. Results call for the characterization of different iron sulfide minerals (especially mackinawite) with Mössbauer spectroscopy combining a strict synthesis protocol and the investigation of phase transformation among these iron sulfide minerals.

Zusammenfassung

Die Wechselwirkungen zwischen Eisen(III) und Sulfid sind in durchgehend oder vorübergehend anoxischen Umgebungen von großer Bedeutung. Sie sind eingebunden im biogeochemischen Kreislauf von Eisen, Schwefel und schließlich auch von Kohlenstoff. Die Elektronenübertragung zwischen Eisenhydroxiden und Sulfid führt zu elementarem Schwefel und metastabilen Eisensulfidmineralen und schließlich zu Pyrit, einem thermodynamisch stabileren Eisensulfid. Die Pyritbildung, die ein bedeutender frühzeitiger Diagenese-Prozess ist, spielt eine unbestreitbare Rolle als globale Senke für die Elemente Fe und S. Deshalb wurden die Wechselwirkungen zwischen Eisen(III) und Sulfid, besonders die Pyritbildung, seit sehr langer Zeit untersucht. Jedoch bleiben Fragen bezüglich der Rolle der Elektronenübertragung zwischen Eisenhydroxiden und Sulfid für die Bildung der Zwischenprodukte und von Pyrit. Die Ziele dieser Doktorarbeit sind deshalb i) den Einfluss der chemischen Eigenschaften der Eisenhydroxide auf die Kinetik der Elektronenübertragung zwischen S(-II) und Fe(III) und schließlich auf die Bildung verschiedener Zwischenprodukte zu verstehen, ii) die Eigenschaften und das Verhalten von Zwischenprodukten zu charakterisieren, iii) den Verlauf und die Kinetik der Ausbildung des Endproduktes, d.h. die Pyritbildung, zu verstehen, und iv) ein Konzept zu entwickeln, das die Elektronenübertragung zwischen Sulfid und Eisenhydroxiden an Oberflächen und in deren Nähe beschreibt.

Deshalb untersuchte diese Arbeit die Reaktionen von gelöstem Sulfid und verschiedenen Eisenhydroxiden bei neutralem pH unter anoxischen Bedingungen. Das anfängliche Verhältnis von Fe/S wurde auf „hoch“ (HR) eingestellt, wenn die Eisenhydroxidkonzentration nach vollständigem Verbrauch von Sulfid im Übermaß blieb und auf „niedrig“ (LR) im umgekehrten Fall. Spezies wurden durch nasschemische Analytik sowie Transmissionselektronenmikroskopie (TEM), Mößbauerspektroskopie und Röntgenstrahlphotoelektronenspektroskopie (XPS) charakterisiert.

Die Reaktion zwischen Eisenhydroxiden und Sulfid erwies sich als sehr kompliziert. Die nasschemische Analytik zeigte verschiedene Reaktionsmuster zwischen HR- und

LR-Experimenten. Sulfid wurde innerhalb der ersten 3 h verbraucht und $Fe(II)_{HCl}$ und MES bildeten sich. Nach 24 – 48 h trat in HR-Experimenten eine Abnahme von $Fe(II)_{HCl}$ und MES auf, die von Pyritbildung begleitet wurde. In LR-Experimenten wurde jedoch bis zu 2160 h keine Pyritbildung beobachtet. Ein Teil von $Fe(II)_{HCl}$ konnte nicht als stöchiometrisches FeS (sog. „excess Fe(II)“) wiedergefunden werden (Hellige et al., 2012; Poulton, 2003; Poulton et al., 2004). Die Bildung von „excess Fe(II)“ konkurrierte mit der von FeS/Mackinawit. Die Konzentration von „excess Fe(II)“ zeigte eine positive Korrelation zum anfänglichen Verhältnis von Fe/S und zur mineralogischen Reaktivität von Eisenhydroxiden.

Die XPS-Analyse bestätigte, dass nicht nur elementarer Schwefel, sondern auch Polysulfide die Hauptschwefelprodukte waren. Die Polysulfide, überwiegend Disulfid, die sich an der Oberfläche der Eisenhydroxide bildeten, konnten mit Zinkacetat vorbehandeltem Methanol extrahiert werden. Deshalb beinhaltete MES nicht nur elementaren Schwefel und gelöste Polysulfide, sondern auch Oberflächenpolysulfide. Die Anwesenheit von Polysulfiden und „excess Fe(II)“ an der Oberfläche könnte zur potenziellen Bildung von Eisen-Polysulfiden und einer Übersättigung von Pyrit geführt haben und dadurch die schnelle Pyritbildung in HR-Experimenten veranlasst haben. Die schnelle Pyritbildung wurde als „neuartiger“ Polysulfidpfad vorgeschlagen, weil Fe(II) und Disulfid direkt aus „excess Fe(II)“ und Oberflächenpolysulfiden entstanden. Deshalb wurde die Pyritbildung nicht kinetisch durch die Auflösung von FeS kontrolliert, das als wichtigste Quelle von Fe(II) für die Pyritbildung im normalen Polysulfidpfad betrachtet wird. Letzeres trat in den LR-Experimenten auf. Die elektromagnetischen Eigenschaften von Eisen(II) in FeS/Mackinawit könnten sich aufgrund der Assoziierung von Eisen-Polysulfiden verändert haben und darum zeigte sich ein asymmetrisches Sechs-Linien Mößbauerspektrum. Das Spektrum der gemischten Eisensulfidphasen, die sich in der Reaktion zwischen Fe(III) und S(-II) bildeten, unterschied sich von dem des FeS, das aus einer homogenen Lösung von Eisen(II) und Sulfid ausfiel.Die FeS-Phase war jedoch instabil und wandelte sich langsam in die Mischphase um.

Drei wichtige Entdeckungen dieser Arbeit sind von großer Bedeutung.

1) Das Vorkommen von Oberflächenpolysulfiden wurde bisher noch nicht berichtet und kann eine bisher übersehene Rolle sowohl im abiotischen als auch im biotischen Schwefelkreislauf spielen.
2) Das Fe/S-Verhältnis, das die Kinetik und den Verlauf der Pyritbildung kontrolliert, kann als ein Indikator angewandt werden, um eine schnelle Pyritbildung in vorübergehend anoxischen Umgebungen vorherzusagen.
3) Die Sechs-Linien-Mößbauer-Spektren von Eisensulfidphasen zeigten, dass die elektromagnetischen Eigenschaften von Eisen(II) in FeS/Mackinawit leicht durch Verunreinigungen verändert werden könnten. Deshalb ist, i) eine Mößbauer-Charakterisierung von Mackinawit, der nach einem genauen Syntheseplan hergestellt wurde, und ii) die Untersuchung der Transformation zwischen verschiedenen Eisensulfidphasen erforderlich.

1. General introduction and summary

This chapter reviews the ferric iron reduction coupled with sulfur and carbon cycling in both marine sediments and highly fluctuating environments with a focus on abiotic iron reduction by sulfide and its relation to the formation of different iron sulfide minerals.

1.1 General introduction and research questions

1.1.1 Fe(III) reduction coupled to carbon and sulfur

Origin of ferrous iron

The process of ferric iron reduction is part of the global iron cycling and of great importance in permanent or temporarily anoxic environments being involved in the biogeochemical cycling of many different elements such as carbon and sulfur (Berner, 1984; Lovley and Phillips, 1987; Raiswell and Canfield, 2012; Rickard and Luther, 2007). The reduction of ferric iron can be biotic or abiotic. Biotic iron reduction is induced by microorganisms utilizing organic carbon (Lovley, 1987; Mortimer et al., 2011; Raiswell and Canfield, 2012). Microorganisms take electrons from organic matter during anaerobic respiration and then transfer to ferric iron, sulfate and other electron acceptors (Lovley and Phillips, 1987; Raiswell and Canfield, 2012). By contrast, abiotic iron reduction occurs without carbon mineralization (Lovley, 1987; Mortimer et al., 2011). It can be induced by a mixing between oxic and anoxic water columns/sediments caused by physical forcings (wind, storm events etc.) and/or bioturbations (plant roots, microbial etc.) (Ferreira et al., 2007; Ho et al., 2004; Raiswell and Canfield, 2012; Rickard and Luther, 2007). One of the most important abiotic iron reductions is the interaction between ferric iron and sulfide (Canfield et al., 1992; Dos Santos Afonso and Stumm, 1992; Hellige et al., 2012; Peiffer et al., 1992; Poulton, 2003; Poulton et al., 2004; Price and Shieh, 1979; Pyzik and Sommer, 1981).

Ferrous iron generates as a consequence of both biotic and abiotic iron reductions (Lovley, 1987; Raiswell and Canfield, 2012; Rickard and Luther, 2007). In the presence of different sulfur species, a series of ferrous iron sulfide minerals form.

Amorphous FeS and/or mackinawite form upon precipitation of ferrous iron with sulfide, and then slowly transforms to the thermodynamically more stable iron sulfide pyrite(Berner, 1970; Canfield et al., 1992; Hellige et al., 2012; Luther, 1991; Peiffer et al., 1992; Poulton, 2003; Poulton et al., 2004; Pyzik and Sommer, 1981; Raiswell and Berner, 1985; Rickard and Luther, 1997; Schoonen and Barnes, 1991b; Schoonen, 2004; Wilkin and Barnes, 1996; Yao and Millero, 1996). Pyrite formation is an important sink for both Fe and S by removing iron and sulfate from the anoxic water and is one of the most important reactions during early diagenesis (Raiswell and Canfield, 2012).

Interlinkage of the Fe, C, and S cycle in marine sediments

Because of the significant interlinkage among these three elements, the relations between C, S and Fe have been developed as geochemical indicators to understand the evolution of ocean chemistry with the presence of limited oxygen (RAISWELL and CANFIELD, 2012 and the references therein). The indicators comprise: 1) organic carbon to pyrite sulfur ratio (C/S), 2) degree of pyritization (also pyrite-Fe/(pyrite-Fe + reactive Fe)) and 3) (pyrite-Fe + reactive Fe)/total Fe.

The C/S ratio is applied to distinguish between marine sediments with low C/S and freshwater sediments with relative high C/S (Berner and Raiswell, 1984). The C/S ratio is controlled by three factors which are closely coupled to each other (Morse and Berner, 1995). The essential factors are 1) the ratio of total organic carbon to the organic carbon which is metabolised (C_T/C_M), 2) the fraction of metabolised organic matter used by sulfate reduction (C_S/C_M) and 3) the fraction of total reduced sulfur buried as pyrite (S_p/S_T) (Morse and Berner, 1995; Raiswell and Canfield, 2012). Here, the S_p/S_T ratio is closely linked to the sedimentation rate (Raiswell and Canfield, 2012). A low sedimentation rate is accompanied by relatively high disturbances between oxic and anoxic water column/sediments. Due to the disturbances a re-oxidation of sulfide can occur and ferric iron can be brought to the reducing layer and favored over sulfate in accepting electron from organic carbon (Raiswell and Canfield, 2012). As a consequence, sulfate reduction is constrained and a low S_p/S_T high C/S are expected (Raiswell and Canfield, 2012). However, it was later recognized that the sulfate reduction rate in sediments rich in organic carbon is usually high enough to convert all iron into pyrite (Raiswell and Canfield, 2012). Therefore, reactive iron

plays even a more important role and turns out to be the major control on pyrite formation in the sediments, especially under euxinic condition (Canfield, 1989). In fact, Raiswell and coworkers (RAISWELL and CANFIELD, 2012 and the references therein) have successfully distinguished different types of depositional environments including normal marine (oxygenated overlaying water with normal ocean salinity), euxinic (anoxic, dissolved sulfide dominated, iron limited) and anoxic ferruginous (dissolved ferrous iron dominated, sulfide limited) based on the proportion of different iron species, i.e. Degree of Pyritization and (pyrite-Fe + reactive Fe)/total Fe.

By using the series of C-S-Fe geochemical indicators, the evolution of ancient ocean can be demonstrated. For insistence, ancient ocean was more anoxic ferruginous in the Archean Eon, and became more and more euxinic after great oxygenation event (great increase of oxygen in Earth's atmosphere) happening 2.3 to 2.4 billion years ago and finally predominantly euxinic in the Phanerozoic Eon (c.f. RAISWELL and CANFIELD, 2012 and the references therein).

There is a great advantage in applying the geochemical indicators to study paleo-environments. Most of the redox reactions, regarding the reduction of sulfate and ferric iron as well as the formation of iron sulfides, happen rapidly during early diagenesis (c.f. RICKARD and LUTHER, 2007) and the system approaches equilibrium on the geologic time scale (of Ma to Ga) (Raiswell and Canfield, 2012). This means consideration of thermodynamic equilibrium of iron, sulfur, carbon and other elements is required when applying C-S-Fe indicators. They are mostly applied to study marine sediments and ancient sedimental rocks (e.g. the works in (Berner, 1964a; Berner, 1970; Berner, 1984; Berner and Raiswell, 1983, 1984; Morse and Berner, 1995; Raiswell and Berner, 1985)).

Interlinkage of the Fe, C, and S cycle under dynamic conditions

When concerning highly fluctuating and dynamic aquatic environments, investigations regarding kinetics and pathways become important to understand the iron cycle and its linkages with many other species, such as oxygen, sulfur, carbon, (Ferreira et al., 2007; Ho et al., 2004; Raiswell and Canfield, 2012), nitrogen and phosphorus (Duce, 1986; Jensen et al., 1992; Raiswell and Canfield, 2012). One of the important reactions regarding iron flux is the ferric iron reduction with sulfide

(sulfidation) (Canfield et al., 1992; Dos Santos Afonso and Stumm, 1992; Peiffer et al., 1992; Pyzik and Sommer, 1981; Yao and Millero, 1996). The kinetics of sulfidation processes depend on mineral reactivities as mineral structure, crystallinity, crystal size as well as impurities (Cornell and Schwertmann, 2006; Poulton et al., 2004; Torrent et al., 1987). For example, ferrihydrite and lepidocrcite (low degree of crystallinity) are more reactive than goethite, hematite and magnetite (high degree of crystallinity) (Canfield, 1989; Canfield et al., 1992; Poulton et al., 2004; Torrent et al., 1987). Due to the wide distribution of highly reactive ferric (hydr)oxides (ferrihydrite, lepidocrocite and goethite) in the nature sediments most of the sulfidation processes are relatively fast (Canfield et al., 1992; Cornell and Schwertmann, 2006; Poulton et al., 2004; Raiswell and Canfield, 2012). Hence, they become significant in the highly fluctuating environments where cycling of species (oxidation-reduction-reoxidation) occurs rapidly as it may control electron flow by competing with other slower reactions and may potentially have an impact on biological communities (Duce, 1986).

Sulfidation of ferric iron leads to FeS and subsequent pyrite formation as mentioned above (Berner, 1970; Canfield et al., 1992; Luther, 1991; Peiffer et al., 1992; Pyzik and Sommer, 1981; Raiswell and Berner, 1985; Rickard and Luther, 1997; Schoonen and Barnes, 1991b; Schoonen, 2004; Wilkin and Barnes, 1996; Yao and Millero, 1996). The reaction formulas regarding sulfidation of ferric iron (eq 1, take FeOOH as example)

$$2FeOOH + 3HS^- \rightleftharpoons 2FeS + S^o + 3HS^- \quad (1)$$

and subsequent pyrite formation (eq 2)

$$FeS + S^o \rightleftharpoons FeS_2 \quad (2)$$

are simple, yet details with respect to kinetics and pathways for product formation are rather complex.

1.1.2 Complexity of interaction between ferric (hydr)oxides and adsorbed species

It has been long suggested that sulfidation of ferric (hydr)oxides is a ligand promoted reductive dissolution process controlled by reactive surface sites of ferric (hydr)oxides (Dos Santos Afonso and Stumm, 1992) and proceeded by the adsorption of sulfide onto ferric oxides' surface and the formation of an inner-sphere surface complex of sulfide formed with ferric iron (eq. 3a) (Dos Santos Afonso and Stumm, 1992; Peiffer et al., 1992; Pyzik and Sommer, 1981). It has been proposed that one-electron transfer between sulfide and ferric iron occurs (eq. 3b), which is followed by formation of a sulfur radical (eq.3c) and detachment of generated ferrous iron from surface (eq. 3d) (Dos Santos Afonso and Stumm, 1992).

$$> FeOH + \ HS^- \rightleftharpoons > Fe^{III}S^- + H_2O \qquad (3a)$$

$$> Fe^{III}S^- \rightleftharpoons > Fe^{II}S^{\cdot} \qquad (3b)$$

$$> Fe^{II}S^{\cdot} + H_2O \ \rightleftharpoons > Fe^{II}OH_2^+ + S^{\cdot -} \qquad (3c)$$

$$> Fe^{II}OH_2^+ \xrightarrow{H^+} new\ surface\ site + Fe^{2+} \qquad (3d)$$

The dissolution rate of Fe^{2+} is kinetically controlled by the concentration of aqueous sulfide and surface complex $>Fe^{III}S^-$, which is proportional to reactive surface sites of ferric (hydr)oxides (Dos Santos Afonso and Stumm, 1992; Peiffer et al., 1992; Poulton, 2003). When the ratio of initial ferric iron to sulfide is low, more reactive surface sites become saturated with sulfide. As a consequence, the rate of Fe^{2+} dissolution can be influenced (Poulton, 2003; Poulton et al., 2004).

Recent observations have demonstrated a strong interaction between adsorbed Fe(II) and the bulk ferric (hydr)oxide mineral. Once aqueous Fe^{2+} stays adsorbed at the ferric (hydr)oxides' surface, electrons can transfer from Fe^{2+} to ferric (hydr)oxides (electron transfer), pass through the bulk mineral (conduction) and finally release into the solution (atom exchange) (Fig. 1.1) (Gorski et al., 2012; Handler et al., 2009; Williams and Scherer, 2004). Electron transfer between Fe^{2+} and bulk mineral leads to oxide growth while atom exchange between bulk electron and surface Fe^{3+} leads to a reductive dissolution of ferric Fe^{3+} (Fig. 1.1) (Gorski et al., 2012; Handler et al., 2009; Larese-Casanova and Scherer, 2007; Rosso et al., 2009; Williams and Scherer, 2004;

Yanina and Rosso, 2008). The model has been further developed by investigating the fates of electrons injected into the ferric (hydr)oxides' bulk (Gorski and Scherer, 2011). Injected electrons go to conduction band and from there, they can 1) be temporarily or permanently immobilized in trapping sites to heal the structure defects, 2) release into solution as Fe^{2+} (reductive dissolution) and 3) be donated to other electron acceptors (Fig. 1.2) (Gorski and Scherer, 2011; Mulvaney et al., 1988). It has been documented that nitrobenzenes can be reduced by Fe(II), but only with the presence of ferric (hydr)oxides (Klausen et al., 1995; Williams and Scherer, 2004). Hence, electrons donated to the reduction of nitrobenzenes originate probably from those injected into the bulk of ferric (hydr)oxides by adsorbed Fe(II).

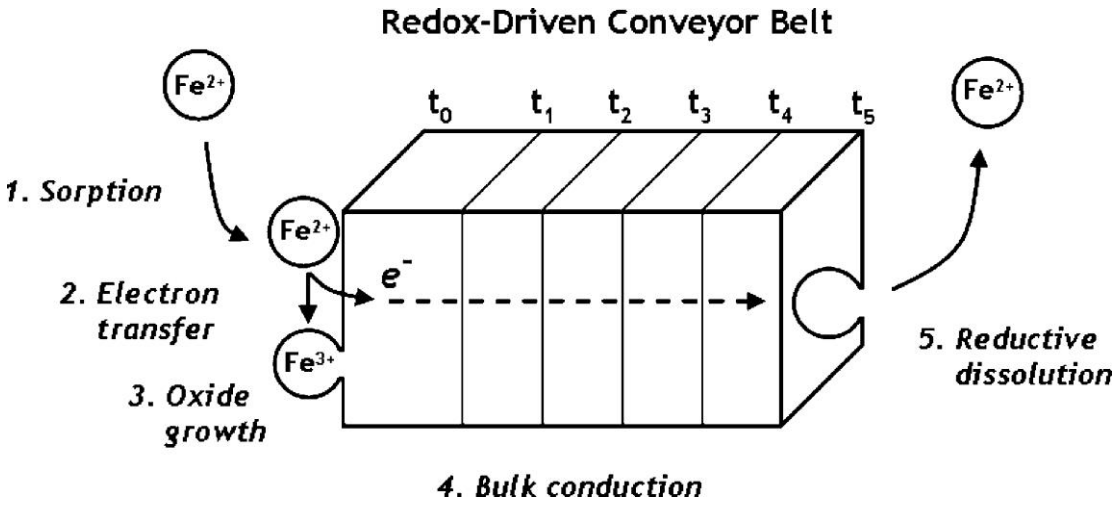

Fig. 1.1 Redox-Driven Conveyor Belt mechanism to explain electron movement from the aqueous Fe^{2+} to bulk ferric (hydr)oxides and release to the solution. Fe^{2+} is adsorbed onto the surface of ferric (hydr)oxides (1) and then electron transfer occurs between adsorbed Fe^{2+} and Fe^{3+} at the surface of ferric (hydr)oxides (2). As a consequence, adsorbed Fe^{2+} is oxidized to Fe^{3+}, leading to a new layer of oxide growth (3). The injected electron can move through the bulk mineral (4) and be released as Fe^{2+} at the other mineral facet (5). (Figure taken from Gorski and Scherer, 2011)

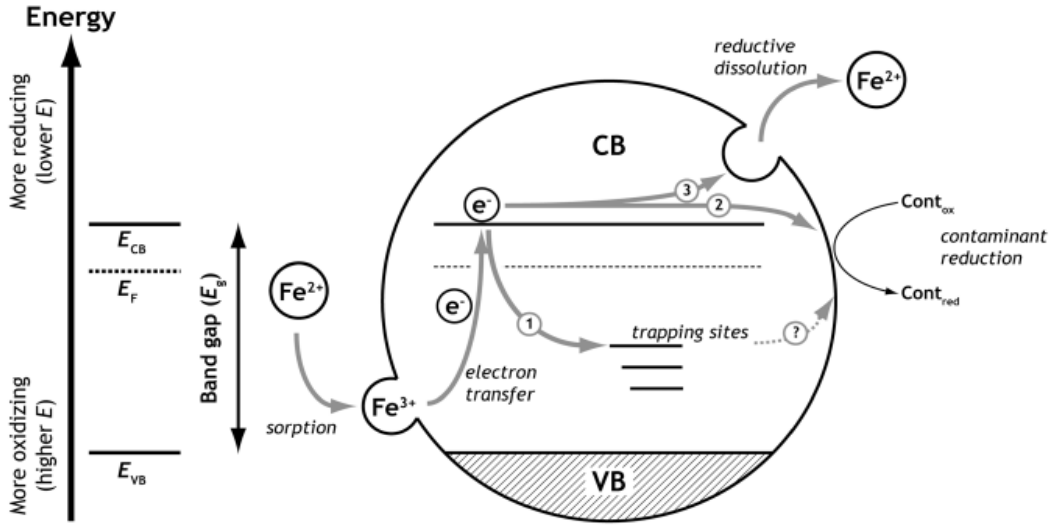

Fig. 1.2. Conceptual model of interaction between aqueous Fe^{2+} and ferric (hydr)oxides. The electrons taken from oxidation of adsorbed Fe^{2+} is transferred into the conduction band (CB), from where electrons have three fates: they can 1) be localized in a trapping site; 2) be transferred to a foreign species as environmental contaminants; 3) be released into solution as mentioned in Fig. 1.1. (Figure taken from Gorski and Scherer, 2011)

The model demonstrated in Fig. 1.2 can be generalized to the interaction between ferric (hydr)oxides and other species which are able to transfer electrons with ferric (hydr)oxides (Gorski and Scherer, 2011). Katz et al. (2010) traced a Fe(II) formation in maghemite nanoparticle after accepting electrons donated by organic molecule. Sulfide, whose interaction with ferric (hydr)oxides has been long studied, can be merged into this model as well.

The model of Dos Santos Afonso and Stumm (1992) describes the very initial electron transfer between sulfide and ferric iron and has disadvantages on explaining e.g. intermediated products formation. From the model of Gorski and Scherer (2011), electrons donated from sulfide can be injected into the bulk mineral of ferric (hydr)oxides and may have significant effects on mineral reactivity, on healing defects of crystal structure (Gorski and Scherer, 2011) and for the interest of this thesis, on the formation of secondary mineral. Combining these two models can

achieve a better explanation of the sulfidation process of ferric (hydr)oxides and subsequent pyrite formation.

1.1.3 Product formation during interaction between sulfide and ferric (hydr)oxides

Mackinawite and elemental sulfur are regarded to be dominant products during the interaction between sulfide and ferric (hydr)oxides (Peiffer et al., 1992; Poulton, 2003; Pyzik and Sommer, 1981). The very initial products during electron transfer between ferric iron and sulfide, however, are ferrous iron and sulfur radicals according to the model of Dos Santos Afonso and Stumm (1992) (eq 3c and eq 3d). Generated ferrous iron detached from the surface (eq 3d) precipitates as iron monosulfide/mackinawite in the presence of aqueous sulfide (eq.4) (Pyzik and Sommer, 1981).

$$Fe^{2+} + HS^{-} \rightleftharpoons FeS + H^{+} \qquad (4)$$

However, generated ferrous iron can be in excess to that required for the precipitation of stoichiometric FeS (Hellige et al., 2012; Poulton, 2003; Poulton et al., 2004). The concentration of the excess Fe(II) depends on the ratio between surface area of ferric (hydr)oxides and sulfide (Hellige et al., 2012). Hellige et al. (2012) proposed that the excess Fe(II) could be stored in the bulk mineral as electrons and might be involved in the secondary mineral formation of e.g. magnetite at the surface of lepidocrocite.

Not only ferrous iron species, but also the nature of oxidized sulfur products after sulfidation of ferric (hydr)oxides remain unclear. Due to the instability of sulfur radicals (eq 3c), zero-valent sulfur (S^o) is expected to form as the initial oxidized sulfur which is typically considered as elemental sulfur (Hellige et al., 2012; Poulton, 2003; Pyzik and Sommer, 1981; Yao and Millero, 1996). A rapid equilibrium between S^o and aqueous sulfide leads to the formation of polysulfide species under environmentally relevant conditions (Kamyshny et al., 2009). Trace amounts of aqueous polysulfides are detected on a basis of indirect measurement with great uncertainty (Poulton, 2003; Pyzik and Sommer, 1981). Besides elemental sulfur and polysulfides, thiosulfate is documented during the reaction between sulfide and ferrihydrite and goethite (Poulton, 2003; Pyzik and Sommer, 1981).

The generated FeS is unstable and transforms to pyrite in the presence of polysulfides and/or elemental sulfur (Berner, 1970; Canfield et al., 1992; Luther, 1991; Schoonen and Barnes, 1991b; Schoonen, 2004; Wilkin and Barnes, 1996). Numerous studies on pyrite formation concern the transformation from FeS (c.f. (Luther, 1991; Rickard, 1975; Schoonen and Barnes, 1991b). It has been found that with the presence of ferric (hydr)oxides pyrite formation can occur rapidly within days to weeks (Hellige et al., 2012; Price and Shieh, 1979).

1.1.4 Pyrite formation from iron monosulfide

The formation of crystalline pyrite is suggested to pass through all less stable phases as amorphous FeS, mackinawite and Fe_3S_4 because the energy barrier leading to less stable phases is less than that leading to pyrite formation (De Yoreo and Vekilov, 2003; Nancollas and Matthews, 1982; Schoonen and Barnes, 1991a). Pyrite is generated through reactions of metastable iron sulfide minerals (in most of the cases FeS and/or mackinawite) with different sulfur species (Benning et al., 2000; Berner, 1970; Berner, 1984; Butler and Rickard, 2000; Kraal et al., 2013; Raiswell and Berner, 1985; Rickard, 1997; Rickard and Luther, 2007; Rickard and Luther, 1997; Rickard, 1975; Schoonen and Barnes, 1991b; Schoonen, 2004; Wang and Morse, 1996; Wilkin and Barnes, 1996). Two major pathways regarding pyrite formation have been established as polysulfide pathway (eq 5) (Luther, 1991; Rickard and Luther, 2007; Rickard, 1975)

$$FeS_m + S_n^{2-} \rightarrow FeS_2 + S_{n-1}^{2-} \qquad (5)$$

and hydrogen sulfide pathway (eq 6) (Drobner et al., 1990; Rickard and Luther, 2007; Rickard and Luther, 1997).

$$FeS_m + H_2S \rightarrow FeS_2 + H_2 \qquad (6)$$

The third pathway “iron loss pathway” reported by Wilkin and Barnes (1996) can be regarded as a modified hydrogen sulfide pathway (Butler et al., 2004; Rickard and Luther, 2007).

Pyrite formation via hydrogen sulfide pathway is insignificant in environments where different sulfur species are present, although the hydrogen sulfide pathway seems to generate pyrite rapidly (Rickard, 1997). Luther (1990) argued that as H_2S is less nucleophilic compared with polysulfide species and HS^- ion, in the presence of other sulfur ions with higher nuclophilicities H_2S is not as effective in attacking Fe^{2+} and triggering pyrite formation so that the pathway becomes insignificant (Butler and Rickard, 2000). For example, pyrite formed rapidly with freeze-dried mackinawite and hydrogen sulfide gas (Butler and Rickard, 2000; Drobner et al., 1990; Rickard, 1997; Rickard and Luther, 1997), but slowly in the solution containing aqueous sulfide (Benning et al., 2000; Wilkin and Barnes, 1996). Rapid transformation of mackinawite to pyrite in the presence of hydrogen sulfide gas may be due to the higher nuclophilicities of H_2S and the absence of HS^- and S^{2-} ions. Benning et al. (2000) argued, however, that mackinawite may be at least slightly oxidized during the freeze drying process to activate the rapid pyrite formation.

1.1.5 Research questions

By exploring the processes of sulfidation of ferric (hydr)oxides and the subsequent pyrite formation, it is clear that the early studies regarding sulfidation of ferric (hydr)oxides deal mainly with the kinetics of sulfide oxidation at the oxides' surface and less with the product formation (Dos Santos Afonso and Stumm, 1992; Peiffer et al., 1992). In general, only mackinawite and elemental sulfur are regarded to be the main products (Peiffer et al., 1992; Pyzik and Sommer, 1981; Yao and Millero, 1996) and it appears the investigation of the products has been oversimplified. The model of Gorski and Scherer (2011) reveals that electron injection into the bulk of ferric (hydr)oxides is expected and may have an interesting effect on the formation of secondary minerals. Recently it has been found that not all of the Fe(II) can be recovered as stoichiometric FeS (mackinawite) and that the excess Fe(II) (to FeS) can be significant intermediates (Hellige et al., 2012; Poulton, 2003; Poulton et al., 2004). The concentration of excess Fe(II) depends on the ratio of surface area of ferric (hydr)oxides to sulfide (Hellige et al., 2012) and probably also the mineral reactivity according to the data from Poulton (2003) and Poulton et al. (2004). Furthermore,

Hellige et al. (2012) applied Transmission Electron Microscopy (TEM) and successfully traced the product formation at different time steps during the reaction between sulfide and lepidocrocite. A product rim rich in Fe and S forms at the surface of lepidocrocite after 2 h reacting with sulfide, within which mackinawite is present only as several nano-scale fingerprints among an amorphous phase (c.f. Fig. 6 in Hellige et al 2012). Magnetite forms in the boundary area between lepidocrocite and product rim (c.f. Fig. 6 in Hellige et al 2012). After 1 week, the product rim starts to dissolve and from the dissolved phase pyrite crystals form (c.f. Fig. 8 in Hellige et al 2012). They linked the rapid pyrite formation to occurrence of excess Fe(II) and proposed that excess Fe(II) could reduce S^o to form polysulfide that trigger rapid pyrite formation (Hellige et al., 2012).

Hence, it seems that product compositions are complicated during sulfidation of ferric (hydr)oxides and respond to both electron transfer between sulfide and ferric (hydr)oxides (model from Dos Santos Afonso and Stumm (1992)) and the fate of electrons which are donated by sulfide (model from Gorski and Scherer (2011)), both of which depend on the ferric (hydr)oxides' reactivity towards sulfide. Questions arise therefore regarding:

1) the dependence of electron transfer and subsequent generated electrons on characteristics of ferric (hydr)oxides;

2) the impact of electron transfer and subsequent generated electrons on the build-up of iron and sulfur products with respect to

3) the properties of intermediated products other than nano mackinawite at the surface of ferric (hydr)oxides and

4) the kinetics and pathway of pyrite formation with the presence of generated electrons during sulfidation of ferric (hydr)oxides.

1.2 Research objectives and outline of the dissertation

The overarching goal of the studies presented in this dissertation is to develop a framework of sulfide reacting with ferric iron at the surface or near-surface regime. The four studies, which are presented in the following chapters of the dissertation, apply optimized wet chemical analysis and solid phase analytical techniques to address the outlined research questions and hypotheses.

Chapter 2 (Study 1): Occurrence of surface polysulfides during the interaction between ferric (hydr)oxides and aqueous sulfide

In order to address the research questions regarding the property of sulfur products during sulfidation of ferric (hydr)oxides, experiments are applied to specify oxidized sulfur with an emphasis on identifying and locating polysulfides. Instead of indirect measurements (Poulton, 2003; Pyzik and Sommer, 1981), the highly selective method of single-phase derivatization combined with HPLC analysis is used to determine aqueous polysulfides and X-ray photoelectron spectroscopy is introduced to investigate the sulfur as well as iron species at the mineral surface. Synthetic goethite and lepidocrocite are applied to react with sulfide at neutral pH under anoxic conditions (in a glove box). Two initial molar ratios of Fe/S are selected to investigate the impact of electron transfer on iron and sulfur speciation during sulfidation of ferric (hydr)oxides.

Chapter 3 (Study 2): Pyrite formation and mineral transformation pathways upon sulfidation of ferric hydroxides depend on mineral type and sulfide concentration

The electron transfer is influenced by the characteristics of the ferric (hydr)oxides. To understand the effect of this dependence on the formation of metastable intermediates, a systematic examination is performed in Study 2, which relates the mineralogy of the ferric hydroxides to the kinetics and pathways of the formation of intermediated reaction products over time. Three types of ferric hydroxides (synthetic ferrihydrite (Fh), commercial lepidocrocite (comm. Lp) and commercial goethite (comm. Gt)), which have apparent differences regarding their mineral reactivity and reactive surface area, are chosen to react with aqueous sulfide at neutral pH under anoxic

conditions (in a glove box). An excess of ferric hydroxides to aqueous sulfide is applied in order to study the influence of mineral reactivity on the pathway of intermediates formation. This study combines wet chemical analysis, TEM and Mössbauer spectroscopy (MB) to investigate the products, in particular iron minerals at different time steps.

Chapter 4 (Study 3): Fe/S ratio controls pathway and kinetics of pyrite formation during Fe(III)-S(-II) interaction

Study 3 investigates the kinetics and pathway of pyrite formation during the anoxic reaction between ferric hydroxides and sulfide at neutral pH, and is designed to understand the influence of both ferric iron and sulfide on pyrite formation by modifying the initial ratios of Fe/S. Synthetic lepidocrocite (syn. Lp) and goethite (syn. Gt) are applied. ^{57}Fe enriched lepidocrocite and goethite are synthesized for a better tracing of iron mineral with Mössbauer spectroscopy. In combination with wet chemical analysis kinetics and pathway of pyrite formation in the experiments with different initial ratio of Fe/S are investigated.

Chapter 5 (Study 4): Electromagnetic properties of FeS phases: Insights from Mössbauer Spectroscopy

The main objective of Study 4 is to characterize the property of iron sulfide generated during sulfidation of ferric (hydr)oxides and to distinguish different types of iron sulfide with a stoichiometric form of FeS. To these ends, FeS precipitated from homogeneous solution with ferrous iron and sulfide is compared with iron sulfide intermediates generated during sulfidation of ferric hydroxides.

1.3 Materials and methods

Experimental details are presented in the individual studies. This chapter presents a summary of materials and methods of all studies, the necessary modifications of experiments and methods and the tests of those non-standard methods.

1.3.1 Iron phases

Ferric hydroxides: both commercial and synthetic ferric hydroxides are applied for different research purposes. Goethite, lepidocrocite and ferrihydrite were synthesized after standard protocols (Schwertmann and Cornell, 2008). For the purpose of Mössbauer spectroscopic measurement, the amount of ^{57}Fe was enriched to 20 wt% of total iron in the synthetic ferric hydroxides by homogenizing commercial Fe salt and corresponding ^{57}Fe salt prior to precipitation of ferric hydroxides. Commercial goethite and lepidocrocite were purchased from Lanxess (Leverkusen, Germany). The ferric hydroxides were washed to remove foreign species and freeze-dried. The characterization of the different ferric hydroxides showed almost pure phases (Table 1.1).

Table 1.1. Characterization of ferric hydroxides.

	Impurity	size (nm)	surface area (m^2 g^{-1})
comm. Gt	0	200-900	9.12
comm. Lp	5-10 wt% Gt	200-400	17.34
syn. Gt	0	600-1000	39.33
syn.Lp	0	200	70.24
Fh	0	<10	140
^{57}Fe enriched Gt	0	600-1000	39.33
^{57}Fe enriched Lp	4 wt% Gt	200	70.24

Iron sulfide: synthesis of iron sulfide was carried out in the anoxic glove box due to the sensibility of FeS to oxygen. The pre-weighted chemicals ($FeCl_2 \cdot 4H_2O$ and Na_2S, respectively) were dissolved in a 100 mL anoxic deionized water (18.2MΩ) to obtain the concentration of 2 mol L^{-1}. The Fe(II) solution was then added dropwise into the S(-II) solution. The black precipitate appeared immediately. The suspension was stirred gently with a Teflon-coated magnetic stirring bar during the whole reaction.

After all the Fe(II) solution had been added, the precipitate was left in the bottle for several hours to days. The iron sulfide mineral was filtered and immediately characterized with Mössbauer spectroscopy in order to prevent any oxidation and mineral transformation.

1.3.2 Experimental set-up

Short-term experiments with ferric hydroxides and sulfide (Study 1-4, with small modifications depending on the purposes): the experiments with a reaction time shorter than 1 week were conducted in a 4-port reactor and followed a previous study (Hellige et al., 2012). The ports allowed for pH electrode installation, acid or base charging and sample removal. The experiments were conducted by injecting the suspension with a preselected amount of ferric hydroxide into sulfide solution (c = 8 mmol L^{-1}) whose pH had been adjusted to 7. The pH was kept constant at pH = 7.0 ± 0.1 with HCl (c= 0.1 mol L^{-1}) using a pH-Stat device. The solution was gently stirred with a Teflon-coated magnetic stirring bar during the whole experiment. The initial molar ratios of Fe/S were adjusted to be 'high' with iron concentrations being in excess to sulfide (HR, Fe/S > 2.5) and 'low' with excess sulfide to Fe in ferric (hydr)oxides (LR, Fe/S <0.6). A blank experiment running for 168 h with only sulfide at pH 7 yielded a linear sulfide loss rate of 0.014 mmol L^{-1} h^{-1} (R^2 = 0.914).

Long-term experiments with ferric hydroxides and sulfide (Study 3): in order to prevent a significant loss of sulfide, long-term aging experiments (> 336 h) were performed in serum bottles sealed with thick Butyl-septa and an aluminum cap through which only trace amounts of sulfide escaped during sampling. pH was maintained neutral either by regular adjustment with HCl and/or NaOH (c = 0.1 mol L^{-1}) or by a buffer (PIPES buffer, c = 50 mmol L^{-1}). The suspensions were regularly shaken.

Synthetic iron sulfide aging experiment (Study 4): synthetic iron sulfide was washed with deionized water and freeze-dried. The dry mineral was placed in 5 mL vials and sealed with Butyl-septa and aluminum cap and stored in the dark in the glove box.

1.3.3 Optimization of wet chemical analytic methods

Iron Species Determination (Study 1-3): iron species were determined photometrically with the phenantroline method (Tamura et al., 1974). Aqueous ferrous iron ($Fe(II)_{aq}$), total iron (Fe(TOT)) and acid extractable ferrous iron ($Fe(II)_{HCl}$) were analyzed. An overestimation of $Fe(II)_{HCl}$ could occur during the extraction through reaction of the released H_2S (simply the reversed form of eq 4) with ferric iron (eq 7) in the acidic extraction solution due to the high reactivity of ferric hydroxides in all studies.

$$H_2S + 2FeOOH + 4H^+ = 2Fe^{2+} + S^o + 4H_2O \qquad (7)$$

In order to test the effect of this reaction on the yield of Fe(II), aliquots of FeS suspension were added to a suspension with predefined amounts of the respective ferric hydroxide to obtain different final concentrations FeS and 2 g L^{-1} of ferric hydroxide, aliquots of which (mixture of FeS and ferric hydroxide) were taken to extract Fe(II) with 0.5 N HCl. Ferrihydrite was tested with four FeS concentrations (2, 4, 7 and 13.5 mmol L^{-1}) due to its higher reactivity. Goethite and lepidocrocite were tested with two FeS concentrations (8 and 13.5 mmol L^{-1}). Samples were taken at different time steps, filtered (0.45 µm, Nylon) and analyzed using the phenanthroline method (Tamura et al., 1974). The stock solution of FeS (c=0.2 mmol L^{-1}) was prepared by precipitation from Na_2S (c = 0.4 mol L-1) and $FeCl_2 .4H_2O$ (c = 0.4 mol L^{-1}) in a glove box. Aqueous sulfide and $Fe(II)_{aq}$ in the stock solution were 68 µmol L^{-1} and 16 µmol L^{-1} respectively.

Recovery rates of $Fe(II)_{HCl}$ with the presence of different ferric hydroxides seemed to be related to mineral reactivities. The synthesized lepidocrocite which has a larger surface area of 70.24 m^2 g^{-1} led to a significant overestimation of 120 % FeS concentration already after 15 min than the commercial one, which recovered 101% of FeS (Fig. 1.3). 97% and 95% of FeS were recovered in the presence of synthesized and commercial goethite, respectively. In the case of ferrihydrite, between 196 % and 232 % for the four FeS concentrations (2, 4, 7 and 13.5 mmol L^{-1}) were detected after 1 h. Therefore, measured $Fe(II)_{HCl}$ concentrations were overestimated by about a factor of 1.2 and 2 when FeS was extracted simultaneously in the presence of synthesized lepidocrocite and ferrihydrite, respectively. Therefore, an overestimation

with respect to $Fe(II)_{HCl}$ occurred in the case of synthesized lepidocrocite and ferrihydrite. Yet in the experiments with goethite and commercial lepidocrocite the variation of Fe(II) was within the rage of uncertainty. To correct $Fe(II)_{HCl}$ we stopped the acid extraction after 1 h in Study 2 and applied the factor of 2, 1 and 1 for ferrihydrite, commercial lepidocrocite and goethite, respectively. In Study 1 & 3 we extracted $Fe(II)_{HCl}$ for 15 min and applied the factor of 1 and 1.2 for goethite and synthesized lepidocrocite.

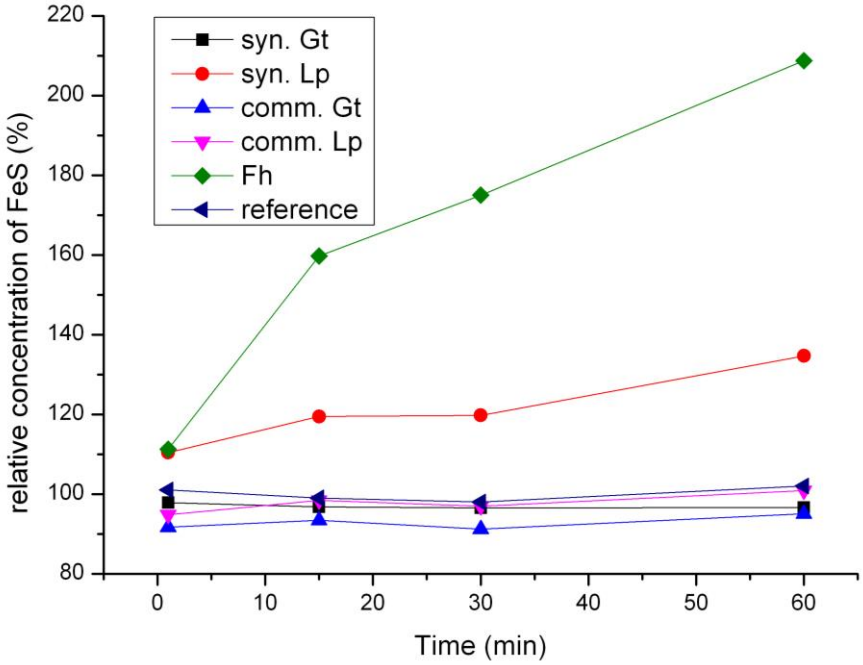

Fig. 1.3 Representive recovery ratios of FeS with and without five different ferric hydroxides: commercial goethite (comm. Gt), commercial lepidocrocite (comm. Lp), synthetic goethite (syn. Gt), synthetic lepidrocite (syn. Lp) and synthetic ferrihydrite (Fh).

Sulfur species determination (Study 1-3): aqueous sulfide ($S(-II)_{aq}$) was determined photometrically with the methylene blue method (Fonselius et al., 1999). Methanol extractable sulfur (MES) was extracted after pre-treatment of the suspension with zinc acetate (ZnAc) to precipitate free sulfide, following a procedure modified after Kamyshny et al. (2009). The extracts were analyzed for zero-valent sulfur using HPLC after filtration. Aqueous polysulfide species were transformed into more stable organic polysulfanes with triflate (trifluoromethanesulfonate) reagent prior to the measurement (Kamyshny et al., 2006). The obtained organic polysulfanes were

determined with HPLC. The total amount of aqueous polysulfides (S_n^{2-}(aq)) was calculated as the sum of the individual polysulfide fractions (S_2^{2-} (aq) to S_8^{2-} (aq)).

SO_4^{2-} was determined turbidimetrically based on $BaSO_4$ precipitation as described by Tabatabai (1974). $S_2O_3^{2-}$ was determined by ion-pair chromatography following the methods described by Steudel et al. (1987). Both of them were not detected.

1.3.4 Solid phases analysis

Samples for solid phase analysis were collected and prepared with great care either under oxygen-free gas flow or in the glove box in order to avoid possible air oxidation. After preparation they were either analyzed immediately or stored in sealed vials until analysis. The exposure time to oxygen during the migration of solid phases into the anoxic or vacuum chamber of the instrument was strictly controlled and remained under 1-2 min. Depending on the research purposes, the solid phases were analyzed with Cryogenic X-ray Photoelectron Spectroscopy (XPS) in Study 1, Transmission Electron Microscopy (TEM) in Study 2 and Mössbauer Spectroscopy (MB) in Study 2 to Study 4.

1.4 Summary of results and discussion

1.4.1 Chemical speciation

Detailed investigation of chemical speciation presented in Study 1-3 indicates the reaction processes are rather complicated already within the first several hours. The interaction between sulfide and ferric hydroxides yielded $Fe(II)_{HCl}$ and MES as the main products after minutes to hours. The formation kinetics of $Fe(II)_{HCl}$ and MES depend on the mineralogical reactivity as well as reactive surface area. Minerals with higher reactivity and/or higher surface area react faster with sulfide and consequently, faster formation of $Fe(II)_{HCl}$ and MES occurs. It appears that kinetics depend first on the crystallinity and then the surface area, with a reactivity sequence of Comm. Gt < Syn. Gt < Comm. Lp < Syn.Lp < Syn. Fh. A black precipitate appeared immediately after sulfide reacting with ferric hydroxides, revealing the metastable iron sulfide mineral, namely amorphous FeS as well as mackinawite formation according to the previous study (Hellige et al., 2012). In the LR experiments with initial ratio of Fe/S < 0.6 where $S(II)_{aq}$ is in excess to ferric hydroxides, ferric hydroxides were completely consumed and the generated $Fe(II)_{HCl}$ was completely precipitated with aqueous sulfide to form FeS. By contrast, in the HR experiments with initial ratio of Fe/S > 2.5, a significant fraction of $Fe(II)_{HCl}$ could not be recovered as stoichiometric FeS, but stayed associated at the surface of ferric hydroxides after 3 h when $S(II)_{aq}$ remained < 300 μmol L^{-1}. The observation of excess Fe(II) formation is consistent with the previous studies (Hellige et al., 2012; Poulton, 2003; Poulton et al., 2004). The concentration of excess Fe(II) is positively correlated with the initial ratio of Fe/S (Hellige et al., 2012) as well as the mineralogical reactivity of ferric hydroxides with an increasing sequence of Gt < Lp < Fh.

1.4.1 Characterization of sulfur and iron products during sulfidation of ferric hydroxides

With respect to oxidized sulfur products, XPS analysis shows that polysulfide species are one of the major intermediates, most of which are associated at the surface. The polysulfide species and elemental sulfur can be extracted by methanol with

appropriate pre-treatment with ZnAc. The reason for the pre-treatment is that ZnAc precipitates S(-II) which is in the form of $S(-II)_{aq}$ and/or S(-II) bound with polysulfides to form ZnS so that 1) oxidation of S(-II) to S^o during extraction can be minimized and 2) polysulfides can be determined by breaking S^{II}-S^o bond to form S^o atoms which can be extracted by methanol. Results indicate that the MES pool does not only comprise elemental sulfur and aqueous polysulfides as suggested by Kamyshny et al (2006), but also most of the polysulfides associated at the surface. Disulfide as the predominant polysulfide species makes up 20-34 % of generated S^o and can be potentially bound with Fe(II) to trigger pyrite formation. Due to the association of surface polysulfide and ferrous iron, a mixture phase with FeS/mackinawite and non- crystalline iron-polysulfides species is expected to form after the first several hours during Fe(III)-S(-II) interaction, which may affect the properties of ferrous iron. Results of oxidized sulfur products as polysulfides and elemental sulfur are presented in Study 1.

Mössbauer spectra of all experiments show asymmetric six-lines, which is probably due to the mixed phases of ferrous iron during the sulfidation of ferric hydroxides. No pure mackinawite can be expected according to the TEM observation (Hellige et al., 2012) and the occurrence of surface polysulfides which increase the possibility of non- crystalline iron-polysulfide species. By contrast, the Mössbauer spectrum collected from freshly precipitated FeS shows a single line. However, results show that the freshly precipitated FeS is rather unstable. After 1 month dry aging, an asymmetric six-line additional to the single-line shows up in the Mössbauer spectrum, indicating a slow transformation from freshly precipitated FeS to the FeS phase in which mackinawite mixes with the non-crystalline iron-polysulfide species. Neither of two iron sulfide minerals can be clearly identified as mackinawite because of the lack of a characteristic Mössbauer spectrum of a standard material (c.f.the studies in (Bertaut et al., 1965; Morice et al., 1969; Mullet et al., 2002; Vaughan and Ridout, 1971)). Results regarding the properties of the iron phases are discussed in Study 4.

1.4.2 Kinetics and pathway of pyrite formation affected by the initial Fe/S ratio

Study 2 and Study 3 suggest that the initial ratio of Fe/S has a strong influence on the pathway of pyrite and the formation of secondary iron oxides. In the HR experiments pyrite occurred rapidly on a time scale of days. By contrast, pyrite did not form up to months in the LR experiments. A significant mineral transformation occurred in the HR experiments with Fh in that the original Fh was completely replaced with thermodynamically more stable ferric (hydr)oxides such as hematite or magnetite. It is proposed that the formation of pyrite and secondary iron mineral is controlled by the initial ratio of Fe/S between the competing formation of excess Fe(II) and FeS/mackinawite in the early stage of the reaction and that the formation of excess Fe(II) is a prerequisite for rapid formation of pyrite as well as other secondary iron oxides. The competition between excess Fe(II) and FeS_s formation is controlled by two factors: 1) the initial molar ratio between reactive surface area to sulfide, and 2) the capability of the iron hydroxide to conduct electrons from surface bound Fe(II) to bulk Fe(III) and to accommodate structural Fe(II), which depend on the mineralogical reactivity. Alternatively, the occurrence of surface polysulfide and excess Fe(II) would lead to a possible formation of non-crystal iron-polysulfide and eventual pyrite formation within days due to the extreme supersaturation ratio near the surface of ferric hydroxides. The rapid pyrite formation is proposed to be via the 'novel' polysulfide pathway because it takes advantage of the presence of excess Fe(II) and allows pyrite to precipitate independently from FeS/mackinawite dissolution. The decrease of the Fe/S ratio favours FeS precipitation instead of the formation of excess Fe(II), and constrains pyrite formation via 'novel' polysulfide pathway. Ferrous iron precipitates completely as FeS in LR runs. As a consequence, ferrous iron for pyrite formation is originated from solubility product of FeS. Pyrite formation is therefore kinetically controlled by the FeS dissolution and follows the normal polysulfide pathway as suggested by many previous studies (Luther, 1991; Rickard, 1975; Schoonen and Barnes, 1991b).

1.4 Conclusions and perspective

By combining wet chemical analytical methods with microscropic and spectroscopic methods this dissertation is able to demonstrate the whole reaction process between ferric hydroxides and aqueous sulfide at neutral pH under anoxic conditions. The different mineral types of ferric hydroxides as well as the initial ratio of Fe/S in all of the experiments are crucial to understand the kinetics and pathways of the formation of secondary iron oxide minerals as well as pyrite. Three key findings from this thesis can be highlighted that provide substantial novelty to the understanding of the interaction between the Fe and S cycle:

1) The identification of polysulfide species located at the mineral surface in Study 1 subverts the previous consideration that polysulfide was present only in the solution (Giggenbach, 1972; Kamyshny et al., 2006; Lichtschlag et al., 2013; Luther, 1991; Rickard and Luther, 2007). Due to their high reactivity polysulfides are regarded to be involved in both abiotic and biotic reactions as electron acceptors as well as to induce sedimental pyrite formation. Yet only aqueous polysulfides were measured or taken into account (Giggenbach, 1972; Kamyshny et al., 2006; Lichtschlag et al., 2013; Luther, 1991; Rickard and Luther, 2007). The finding of Study 1 therefore calls for revisiting the overlooked role of surface polysulfide species in sulfur cycling.
2) Rapid pyrite formation in the HR runs reveals that electrons donated by sulfide to ferric iron can be temporally stored in the bulk mineral of ferric hydroxides as excess Fe(II), which can later trigger pyrite formation. Results indicate that the Fe/S ratios can be potentially used as a geochemical indicator for rapid pyrite formation via ‘novel’ polysulfide pathway in highly fluctuating, dynamic and temporary anoxic environments.
3) The Mössbauer spectroscopy of metastable iron sulfide minerals showed a pattern of an asymmetric six-line which is in conflict with many previous studies (c.f. (Bertaut et al., 1965; Morice et al., 1969; Mullet et al., 2002; Vaughan and Ridout, 1971)). Study 4 did not produce a standard Mössbauer spectrum of pure mackinawite. The finding of excess Fe(II) as well as surface polysulfide, however, suggests that the presence of these two species may influence the properties, especially the electromagnetic property of Fe in mackinawite. The finding of

Study 4 therefore calls for an investigation of phase transformation among different iron sulfide minerals which are stoichiometric FeS.

1.5 References

Benning, L. G., Wilkin, R. T., and Barnes, H., 2000. Reaction pathways in the Fe–S system below 100 C. *Chemical Geology* **167**, 25-51.

Berner, R. A., 1964. An idealized model of dissolved sulfate distribution in recent sediments. *Geochimica et Cosmochimica Acta* **28**, 1497-1503.

Berner, R. A., 1970. Sedimentary pyrite formation. *American Journal of Science* **268**, 1-23.

Berner, R. A., 1984. Sedimentary pyrite formation: an update. *Geochimica et Cosmochimica Acta* **48**, 605-615.

Berner, R. A. and Raiswell, R., 1983. Burial of organic carbon and pyrite sulfur in sediments over Phanerozoic time: a new theory. *Geochimica et Cosmochimica Acta* **47**, 855-862.

Berner, R. A. and Raiswell, R., 1984. C/S method for distinguishing freshwater from marine sedimentary rocks. *Geology* **12**, 365-368.

Bertaut, E., Burlet, P., and Chappert, J., 1965. Sur l'absence d'ordre magnetique dans la forme quadratique de FeS. *Solid State Communications* **3**, 335-338.

Butler, I. B., Böttcher, M. E., Rickard, D., and Oldroyd, A., 2004. Sulfur isotope partitioning during experimental formation of pyrite via the polysulfide and hydrogen sulfide pathways: implications for the interpretation of sedimentary and hydrothermal pyrite isotope records. *Earth and Planetary Science Letters* **228**, 495-509.

Butler, I. B. and Rickard, D., 2000. Framboidal pyrite formation via the oxidation of iron (II) monosulfide by hydrogen sulphide. *Geochimica et Cosmochimica Acta* **64**, 2665-2672.

Canfield, D. E., 1989. Reactive iron in marine sediments. *Geochimica et Cosmochimica Acta* **53**, 619-632.

Canfield, D. E., Raiswell, R., and Bottrell, S. H., 1992. The reactivity of sedimentary iron minerals toward sulfide. *American Journal of Science* **292**, 659-683.

Cornell, R. M. and Schwertmann, U., 2006. *The iron oxides: structure, properties, reactions, occurrences and uses*. John Wiley & Sons.

De Yoreo, J. J. and Vekilov, P. G., 2003. Principles of crystal nucleation and growth. *Reviews in mineralogy and geochemistry* **54**, 57-93.

Dos Santos Afonso, M. and Stumm, W., 1992. Reductive dissolution of iron(III) (hydr)oxides by hydrogen sulfide. *Langmuir* **8**, 1671-1675.

Drobner, E., Huber, H., Wächtershäuser, G., Rose, D., and Stetter, K. O., 1990. Pyrite formation linked with hydrogen evolution under anaerobic conditions. *Nature* **346**, 742-744.

Duce, R. A., 1986. The impact of atmospheric nitrogen, phosphorus, and iron species on marine biological productivity, *The role of air-sea exchange in geochemical cycling*. Springer.

Ferreira, T., Otero, X., Vidal-Torrado, P., and Macías, F., 2007. Effects of bioturbation by root and crab activity on iron and sulfur biogeochemistry in mangrove substrate. *Geoderma* **142**, 36-46.

Fonselius, S., Dyrssen, D., and Yhlen, B., 1999. *Determination of hydrogen sulphide*.

Giggenbach, W., 1972. Optical spectra and equilibrium distribution of polysulfide ions in aqueous solution at 20. deg. *Inorganic Chemistry* **11**, 1201-1207.

Gorski, C. and Scherer, M., 2011. Fe2+ sorption at the Fe oxide-water interface: A revised conceptual framework. *Aquatic Redox Chemistry* **1071**, 477-517.

Gorski, C. A., Handler, R. M., Beard, B. L., Pasakarnis, T., Johnson, C. M., and Scherer, M. M., 2012. Fe atom exchange between aqueous Fe2+ and magnetite. *Environmental Science & Technology* **46**, 12399-12407.

Handler, R. M., Beard, B. L., Johnson, C. M., and Scherer, M. M., 2009. Atom exchange between aqueous Fe (II) and goethite: An Fe isotope tracer study. *Environmental Science & Technology* **43**, 1102-1107.

Hellige, K., Pollok, K., Larese-Casanova, P., Behrends, T., and Peiffer, S., 2012. Pathways of ferrous iron mineral formation upon sulfidation of lepidocrocite surfaces. *Geochimica et Cosmochimica Acta* **81**, 69-81.

Ho, T.-Y., Taylor, G. T., Astor, Y., Varela, R., Müller-Karger, F., and Scranton, M. I., 2004. Vertical and temporal variability of redox zonation in the water column of the Cariaco Basin: implications for organic carbon oxidation pathways. *Marine Chemistry* **86**, 89-104.

Jensen, H. S., Kristensen, P., Jeppesen, E., and Skytthe, A., 1992. Iron: phosphorus ratio in surface sediment as an indicator of phosphate release from aerobic sediments in shallow lakes. *Hydrobiologia* **235**, 731-743.

Kamyshny, A., Borkenstein, C. G., and Ferdelman, T. G., 2009. Protocol for Quantitative Detection of Elemental Sulfur and Polysulfide Zero-Valent Sulfur Distribution in Natural Aquatic Samples. *Geostandards and Geoanalytical Research* **33**, 415-435.

Kamyshny, A., Ekeltchik, I., Gun, J., and Lev, O., 2006. Method for the determination of inorganic polysulfide distribution in aquatic systems. *Analytical Chemistry* **78**, 2631-2639.

Katz, J. E., Gilbert, B., Zhang, X., Attenkofer, K., Falcone, R. W., and Waychunas, G. A., 2010. Observation of transient iron (II) formation in dye-sensitized iron oxide nanoparticles by time-resolved X-ray spectroscopy. *The Journal of Physical Chemistry Letters* **1**, 1372-1376.

Klausen, J., Troeber, S. P., Haderlein, S. B., and Schwarzenbach, R. P., 1995. Reduction of substituted nitrobenzenes by Fe (II) in aqueous mineral suspensions. *Environmental Science & Technology* **29**, 2396-2404.

Kraal, P., Burton, E. D., and Bush, R. T., 2013. Iron monosulfide accumulation and pyrite formation in eutrophic estuarine sediments. *Geochimica et Cosmochimica Acta* **122**, 75-88.

Larese-Casanova, P. and Scherer, M. M., 2007. Fe (II) sorption on hematite: New insights based on spectroscopic measurements. *Environmental Science & Technology* **41**, 471-477.

Lichtschlag, A., Kamyshny Jr, A., Ferdelman, T. G., and deBeer, D., 2013. Intermediate sulfur oxidation state compounds in the euxinic surface sediments of the Dvurechenskii mud volcano (Black Sea). *Geochimica et Cosmochimica Acta* **105**, 130-145.

Lovley, D. R., 1987. Organic matter mineralization with the reduction of ferric iron: a review. *Geomicrobiology Journal* **5**, 375-399.

Lovley, D. R. and Phillips, E. J., 1987. Competitive mechanisms for inhibition of sulfate reduction and methane production in the zone of ferric iron reduction in sediments. *Applied and Environmental Microbiology* **53**, 2636-2641.

Luther, G. W., 1990. The frontier-molecular-orbital theory approach in geochemical processes. In *Aquatic Chemical Kinetics*; Stumm, W., Ed.; Wiley: New York. 173-198.

Luther, G. W., 1991. pyrite synthesis via polysulfide compounds. *Geochimica et Cosmochimica Acta*, 2839-2849.

Morice, J., Rees, L., and Rickard, D., 1969. Mössbauer studies of iron sulphides. *Journal of Inorganic and Nuclear Chemistry* **31**, 3797-3802.

Morse, J. W. and Berner, R. A., 1995. What determines sedimentary C/S ratios? *Geochimica et Cosmochimica Acta* **59**, 1073-1077.

Mortimer, R. J., Galsworthy, A. M., Bottrell, S. H., Wilmot, L. E., and Newton, R. J., 2011. Experimental evidence for rapid biotic and abiotic reduction of Fe (III) at low temperatures in salt marsh sediments: a possible mechanism for formation of modern sedimentary siderite concretions. *Sedimentology* **58**, 1514-1529.

Mullet, M., Boursiquot, S., Abdelmoula, M., Génin, J.-M., and Ehrhardt, J.-J., 2002. Surface chemistry and structural properties of mackinawite prepared by reaction of sulfide ions with metallic iron. *Geochimica et Cosmochimica Acta* **66**, 829-836.

Mulvaney, P., Cooper, R., Grieser, F., and Meisel, D., 1988. Charge trapping in the reductive dissolution of colloidal suspensions of iron (III) oxides. *Langmuir* **4**, 1206-1211.

Nancollas, G. H. and Matthews, J. L., 1982. *Biological mineralization and demineralization*. Springer.

Peiffer, S., Dos Santos Afonso, M., Wehrli, B., and Gaechter, R., 1992. Kinetics and mechanism of the reaction of hydrogen sulfide with lepidocrocite. *Environmental Science & Technology* **26**, 2408-2413.

Poulton, S. W., 2003. Sulfide oxidation and iron dissolution kinetics during the reaction of dissolved sulfide with ferrihydrite. *Chemical Geology* **202**, 79-94.

Poulton, S. W., Krom, M. D., and Raiswell, R., 2004. A revised scheme for the reactivity of iron (oxyhydr)oxide minerals towards dissolved sulfide. *Geochimica et Cosmochimica Acta* **68**, 3703-3715.

Price, F. T. and Shieh, Y., 1979. Fractionation of sulfur isotopes during laboratory synthesis of pyrite at low temperatures. *Chemical Geology* **27**, 245-253.

Pyzik, A. J. and Sommer, S. E., 1981. Sedimentary iron monosulfides: Kinetics and mechanism of formation. *Geochimica et Cosmochimica Acta* **45**, 687-698.

Raiswell, R. and Berner, R. A., 1985. Pyrite formation in euxinic and semi-euxinic sediments. *American Journal of Science* **285**, 710-724.

Raiswell, R. and Canfield, D. E., 2012. The iron biogeochemical cycle past and present. *Geochemical Perspectives* **1**, 1-2.

Rickard, D., 1997. Kinetics of pyrite formation by the H2S oxidation of iron(II) monosulfide in aqueous solutions between 25-125 °C: the rate equation. *Geochimica et Cosmochimica*, 115-134.

Rickard, D. and Luther, G. W., 1997. Kinetics of pyrite formation by the H2S oxidation of iron (II) monosulfide in aqueous solutions between 25 and 125 °C: The mechanism. *Geochimica et Cosmochimica Acta* **61**, 135-147.

Rickard, D. and Luther, G. W., 2007. Chemistry of iron sulfides. *Chemical Reviews* **107**, 514-562.

Rickard, D. T., 1975. Kinetics and mechanism of pyrite formation at low temperatures. *American Journal of Science* **275**, 636-652.

Rosso, K. M., Yanina, S. V., Gorski, C. A., Larese-Casanova, P., and Scherer, M. M., 2009. Connecting observations of hematite (α-Fe2O3) growth catalyzed by Fe (II). *Environmental Science & Technology* **44**, 61-67.

Schoonen, M. and Barnes, H., 1991a. Reactions forming pyrite and marcasite from solution: I. Nucleation of FeS_2 below 100 °C. *Geochimica et Cosmochimica Acta* **55**, 1495-1504.

Schoonen, M. and Barnes, H., 1991b. Reactions forming pyrite and marcasite from solution: II. Via FeS precursors below 100 C. *Geochimica et Cosmochimica Acta* **55**, 1505-1514.

Schoonen, M. A., 2004. Mechanisms of sedimentary pyrite formation. *SPECIAL PAPERS-GEOLOGICAL SOCIETY OF AMERICA*, 117-134.

Schwertmann, U. and Cornell, R. M., 2008. *Iron oxides in the laboratory*. Wiley-Vch.

Steudel, R., Holdt, G., Göbel, T., and Hazeu, W., 1987. Chromatographic Separation of Higher Polythionates SnO 62-(n= 3… 22) and Their Detection in Cultures of Thiobacillus ferroxidans; Molecular Composition of Bacterial Sulfur Secretions. *Angewandte Chemie International Edition in English* **26**, 151-153.

Tabatabai, M., 1974. A rapid method for determination of sulfate in water samples. *Environmental Letters* **7**, 237-243.

Tamura, H., Goto, K., Yotsuyanagi, T., and Nagayama, M., 1974. Spectrophotometric determination of iron (II) with 1, 10-phenanthroline in the presence of large amounts of iron (III). *Talanta* **21**, 314-318.

Torrent, J., Schwertmann, U., and Barron, V., 1987. The reductive dissolution of synthetic goethite and hematite in dithionite. *Clay Minerals* **22**, 329-337.

Vaughan, D. and Ridout, M., 1971. Mössbauer studies of some sulphide minerals. *Journal of Inorganic and Nuclear Chemistry* **33**, 741-746.

Wang, Q. and Morse, J. W., 1996. Pyrite formation under conditions approximating those in anoxic sediments I. Pathway and morphology. *Marine Chemistry* **52**, 99-121.

Wilkin, R. and Barnes, H., 1996. Pyrite formation by reactions of iron monosulfides with dissolved inorganic and organic sulfur species. *Geochimica et Cosmochimica Acta* **60**, 4167-4179.

Williams, A. G. and Scherer, M. M., 2004. Spectroscopic evidence for Fe (II)-Fe (III) electron transfer at the iron oxide-water interface. *Environmental Science & Technology* **38**, 4782-4790.

Yanina, S. V. and Rosso, K. M., 2008. Linked reactivity at mineral-water interfaces through bulk crystal conduction. *Science* **320**, 218-222.

Yao, W. and Millero, F. J., 1996. Oxidation of hydrogen sulfide by hydrous Fe(III) oxides in seawater. *Marine Chemistry* **52**, 1-16.

2. Occurrence of Surface Polysulfides during the Interaction between Ferric (Hydr)Oxides and Aqueous Sulfide

Moli Wan[1*], Andrey Shchukarev[2], Regina Lohmayer[3], Britta Planer-Friedrich[3], Stefan Peiffer[1]

[1] BayCEER, Department of Hydrology, University of Bayreuth, D-95440, Bayreuth, Germany

[2] Environmental and Biogeochemistry, Department of Chemistry, Umeå Iniversity, SE-901 87 Umeå, Sweden

[3] Environmental Geochemistry, University of Bayreuth, D-95440 Bayreuth, Germany

[*] Corresponding author. Phone ++49-921-553500, Fax ++49-921-552366, moli.wan@uni-bayreuth.de

Published in *Environmental science & technology*, 2014, *48* (9) , pp 5076–5084

DOI: 10.1021/es405612f

2.1 Abstract

Polysulfides are often referred to as key reactants in the sulfur cycle, especially during the interaction of ferric (hydr)oxides and sulfide, forming ferrous-sulfide minerals. Despite their potential relevance, the extent of polysulfide formation and its relevance for product formation pathways remains enigmatic. We applied cryogenic X-ray Photoelectron Spectroscopy and wet chemical analysis to study sulfur oxidation products during the reaction of goethite and lepidocrocite with aqueous sulfide at different initial Fe/S molar ratios under anoxic conditions at neutral pH. The higher reactivity of lepidocrocite leads to faster and higher electron turnover compared to goethite. We were able to demonstrate for the first time the occurrence of surface-associated polysulfides being the main oxidation products in the presence of both minerals, with a predominance of disulfide (S_2^{2-}(surf)), and elemental sulfur. Concentrations of aqueous polysulfide species were negligible (< 1%). With prior sulfide fixation by zinc acetate, the surface-associated polysulfides could be precipitated as zero-valent sulfur (S^o), which was extracted by methanol thereafter. Of the generated S^o, 20-34 % were associated with S_2^{2-}(surf). Varying the Fe/S ratio revealed that surface polysulfide formation only becomes dominant when the remaining aqueous sulfide concentration is low (<0.03 mmol L^{-1}). We hypothesize these novel surface sulfur species, particularly surface disulfide, to act as pyrite precursors. We further propose that these species play an overlooked role in the sulfur cycle.

Key words: Polysulfides, disulfide, surface-associated, XPS, sulfur extraction, iron-sulfur interaction, ferric (hydr)oxides

2.2 Introduction

The interaction between ferric (hydr)oxides and sulfide has been widely studied (Dos Santos Afonso and Stumm, 1992; Hellige et al., 2012; Peiffer et al., 1992; Poulton, 2003) due to its fundamental relevance for the cycling of sulfur in many anaerobic environments such as marine or lake sediments and aquifers and due to its potential link with sedimentary pyrite formation (Berner, 1970; Morse, 1999; Raiswell and Berner, 1985; Schoonen and Barnes, 1991b; Wang and Morse, 1996). It is generally observed that aside to an iron sulfide phase, also elemental sulfur forms during this reaction (Hellige et al., 2012; Poulton, 2003; Pyzik and Sommer, 1981; Yao and Millero, 1996). It has been suggested that the oxidation of HS^- by ferric iron occurs via a single electron step to generate sulfur radicals $S^{\cdot-}$ (Dos Santos Afonso and Stumm, 1992; Steudel, 1996). This reaction allows for the generation of polysulfides and subsequently of elemental sulfur (Steudel, 1996). Alternatively, it has been proposed that two electrons are transferred simultaneously and S(-II) is directly oxidized to S(0) (Luther, 2010), which then rapidly equilibrates with aqueous sulfide to form polysulfides under environmentally relevant conditions (Kamyshny et al., 2009). In either case, polysulfides are regarded as essential intermediates.

Some evidence exists for the occurrence of aqueous polysulfides at low concentration levels during reaction of dissolved sulfide with ferric (hydr)oxides (Poulton, 2003; Pyzik and Sommer, 1981). Unfortunately, these measurements are based on indirect methods, such as converting polysulfide species into thiosulfate and its subsequent determination (Poulton, 2003) or optical spectroscopy combined with thermodynamic calculations (Pyzik and Sommer, 1981). Recently developed selective and specific analytical tools (e. g. the single-phase derivatization technique (Kamyshny et al., 2006)) have not been applied, yet, to study these interactions.

Hellige et al. (2012) investigated the sulfidation of lepidocrocite under conditions where aqueous sulfide was completely consumed within a short time (15 min). They found a large deficit in the sulfur mass balance, which they attributed to unknown solid phase-bound sulfur species. High resolution transmission electron microscope (HRTEM) images revealed that a large fraction of surface-associated sulfur had formed in these experiments which they could not further identify. They also observed rapid pyrite formation (after several days), a process that is regarded to

require polysulfides as precursor substances (Rickard and Luther, 2007).Surface-associated polysulfides have been observed at the surface of iron sulfide minerals after surface sulfide oxidation using surface-sensitive techniques such as X-ray photoelectron spectroscopy (XPS) (Eggleston et al., 1996; Mullet et al., 2002; Nesbitt and Muir, 1994; Thomas et al., 1998). Comparable studies about their occurrence during oxidation of dissolved sulfides at ferric mineral surfaces have not been performed yet, although strong indications for the formation of surface associated sulfur exist. The extent of polysulfide formation and its relevance for product formation pathways during the reaction remains enigmatic.

This study therefore aims at resolving the fate of sulfur during the reaction between ferric (hydr)oxides and dissolved sulfide. To these ends we applied wet chemical methods in combination with XPS to determine sulfur oxidation products both in solution and at the surface of ferric (hydr)oxides. Since XPS analyzes the surface under vacuum and elemental sulfur is volatile under ultra vacuum, we performed the whole analytical procedure at cryogenic temperature (− 155 °C).

2.3 Materials and methods

All solutions were prepared in a glove box system (Inert Lab 4GB Glovebox Systems, Innovative Technology, USA) with a O_2 level in a range of 0-1 ppm. The working gas in the glove box is N_2 (99.99 %). The deionized water was purged with N_2 (99.99 %) for at least 1 h to remove O_2 before the transfer into the glove box. All reagents were of analytical grade.

2.3.1 Ferric (hydr)oxides

Synthetic ferric oxides were prepared after Schwertmann and Cornell(2008). To synthesize goethite, 100 mL $Fe(NO_3)_3$ (c = 1 mol L^{-1}) and 180 mL KOH (c = 5 mol L^{-1}) were mixed rapidly in a 2 L polyethylene flask. Red-brown ferrihydrite precipitated immediately. The suspension was then diluted to 2 L with deionized water and kept at 70 ^{o}C for 60 h. To synthesize lepidocrocite, a $FeCl_2$ (c = 0.06 mol L^{-1}) solution was oxidized by air which was pumped through the solution at a controlled flow rate of 100 mL min^{-1}.The pH was maintained at 6.8 by addition of NaOH (c = 0.5 mol L^{-1}) with a pH-stat device (Titrino, Metrohm). The oxidation was carried out at room temperature with sufficient stirring for 3 h. The synthetic goethite and lepidocrocite were washed with deionized water and freeze-dried.

The mineral characterization with Mößbauer spectroscopy demonstrated that no other Fe containing phases was present in goethite and around 4% goethite in lepidocrocite. Multi-point BET (Brunauer, Emmett and Teller) gas adsorption with N_2 (Gemini 2375 analyzer) gave a surface area of 39.33 m^2 g^{-1} and 70.24 m^2 g^{-1} for goethite and lepidocrocite, respectively.

2.3.2 Experimental set-up

The experimental set-up was similar to that used in a previous study(Hellige et al., 2012). In a closed vessel, 450 mL aqueous sulfide solution (approx. 8 mmol L^{-1} Na_2S solution, concentration $(S(-II)_{ini})$ determined prior to each experiment) was adjusted to pH 7.0 in the glove box by addition of HCl (c = 1 mol L^{-1}), to which 50 mL of a suspension containing a preselected amount of synthetic ferric (hydr)oxides (goethite or lepidocrocite) was added. The pH was kept constant at pH = 7.00 $\pm$ 0.05 with HCl

(c= 0.1 mol L^{-1}) using the pH-Stat device (Titrino, Metrohm). The solution was gently stirred with a teflon-coated magnetic stirring bar during the whole experiment. Initial

Table 2.1 Initial experimental conditions. All runs were conducted at pH 7.

Mineral	Initial Fe content	c(Fe)	c(Fe)/ c(S)	SS(Fe)/c(S) [a]
	g L^{-1}	mmol L^{-1}		
Goethite	3.6	40.4	5.05 (HR)	0.11
(Gt)	0.28	3.0	0.37 (LR)	0.01
Lepidocrocite	2	22.5	2.8 (HR)	0.10
(Lp)	0.38	3.9	0.5 (LR)	0.02

[a] concentration of surface sites (SS) was calculated based on a value of $6.3x10^{-6}$ mol/m^2 for both ferric (hydr)oxides (Peiffer and Gade, 2007b).

molar ratios of Fe/S were adjusted to be 'high' with iron concentrations being in excess to sulfide (HR runs, cf. Table 2.1) and 'low' with excess aqueous sulfide (LR runs). The runs with high Fe/S ratio are comparable to previous experiments that were performed under comparable conditions with regard to pH, anoxic atmosphere and mineral application(Hellige et al., 2012). The same concentration of surface area was used for the two minerals in HR runs. Blank experiments with pure sulfide solution were performed in order to quantify sulfide loss in the low Fe/S ratio runs due to degassing. The 168 h-experiments yielded a linear sulfide loss with time at a rate of 0.014 mmol L^{-1} h^{-1} (R^2 = 0.914).

Aqueous samples were removed regularly for wet chemical analysis. Samples for XPS analysis were taken after 3 h in HR runs and after 168 h in LR runs by removing 40 mL of the suspension from the reactor, centrifuging, decanting, then resuspending in deionized water and centrifuging again. The concentration of the residual Fe and S species was calculated as the difference between the species concentration in the suspension before centrifugation and in the supernatant after centrifugation.

All steps were done in the glove box except centrifugation. The black precipitates in HR runs were dried overnight under anoxic conditions in the glove box. LR samples

contained volatile sulfide which might damage the purification system of the glove box. Samples from LR runs were therefore freeze-dried. After drying, all samples were stored under a N_2 atmosphere in sealed crimp vials.

2.3.3 Wet chemical analysis

Aqueous sulfide was determined after filtration (0.2 µm, Nylon) by methylene blue method (Fonselius et al., 2007). However, not only hydrogen sulfide and sulfide ions, but also sulfide associated with aqueous polysulfide(Mylon and Benoit, 2001) can be determined in this way. We therefore refer to this fraction as methylene-blue-detectable sulfur (MBS). Sulfate was determined after filtration (0.2 µm, Nylon) following the turbidimetric method based on $BaSO_4$ precipitation described by Tabatabai (1974). Thiosulfate was determined immediately after filtration (0.2 µm, Nylon) by ion-pair chromatography following the method described by Steudel et al. (1987).

Aqueous polysulfides (S_n^{2-}(aq) were determined following the method developed by Kamyshny et al.(2006). Due to their instability towards oxygen and pH-changes, inorganic polysulfides were derivatized with methyl trifluoromethanesulfonate (methyl triflate) to form dimethylpolysulfanes. To this end, 200 µL of the filtered samples and 8 µL triflate (c = 8.7 mol L^{-1}) were added simultaneously into 1200 µL methanol previously buffered with 100 µL phosphate buffer (c = 50 mmol L^{-1}) at pH 7 and shaken intensively for 10 s. Dimethylpolysulfanes were determined by HPLC (Merck Hitachi, L-2130 pump, L-2200 autosampler, L-2420 UV-VIS detector) after separation on a C18 column (Waters-Spherisorb, ODS2, 5 µm, 250 x 4.6 mm) and gradient elution according to Rizkov et al.(2004). The detection was performed at a wavelength of 230 nm. The total polysulfide concentration was calculated as the sum of individual polysulfide fractions.

Methanol-extractable sulfur (MES) was extracted after pretreatment of 500 µL of unfiltered sample with 250 µL of ZnAc (c = 0.1 mol L^{-1}) to precipitate free sulfide following a procedure modified after Kamyshny et al. (2009). After 10 min, 6 mL methanol were injected into the suspension. The sample was shaken for 3 h and then filtered (0.2 µm, Nylon). The prior sulfide fixation allows ZnAc to react with S^{2-} as well as S_n^{2-} ($n \geq 2$) to precipitate ZnS and (n-1) S^o atoms, which are extracted later with methanol. MES therefore comprises of elemental sulfur and aqueous polysulfide-

bound sulfur (S_n^{2-}-S° with $n \geq 2$), as pointed out by Kamyshny et al. (2009). Since samples for MES determination were unfiltered, MES includes also sulfur associated at the mineral surface. The samples were determined by HPLC (Perkin Elmer 2000 pump and autosampler, Fa. linear-UV-VIS detector and software peaksample 409) after separation on a C18 column (Nucleosil 100-5 PAH) and isocratic elution by pure methanol with a flow rate of 0.4 mL min^{-1}. The detection was performed at a wavelength of 265 nm.

Acid-extractable Fe(II) ($Fe(II)_{HCl}$) was determined after extraction of both the precipitate and the suspension with HCl (c = 0.5 mol L^{-1}) and filtration using the phenanthroline method(1974).

Samples for HPLC measurements were stored in the freezer at around -18°C and analyzed within one week. Photometric measurements were performed within 1-2 h after sampling.

2.3.4 Cryogenic XPS

Sample loading for XPS measurements was performed in an argon atmosphere to protect the samples due to their oxygen sensitivity. Vials were opened under argon flow, samples were placed on the molybdenum holder, gently pressed to create a flat surface and immediately placed on the claw of the transfer rod that was pre-cooled at − 170 ℃. The sample was frozen in the spectrometer air-lock under dry N_2 (g) for 45 s prior to a vacuum activation of 10^{-7} Torr. The frozen sample was then transferred to the pre-cooled manipulator in the analysis chamber. During the whole analysis, the pressure and the sample temperature were maintained at 10^{-9} Torr and − 155 ℃, respectively. All XPS spectra were collected with Kratos Axis Ultra DLD electron spectrometer using monochromatized Al Kα (1486.6 eV) radiation. Survey spectra were collected from 1000 to 0 eV at pass energy of 160 eV. High resolution spectra for Fe 2p, S 2p, O 1s, C 1s, Cl 2p and Na 1s were collected at pass energy of 20 eV with a scan step of 0.1 eV. In order to verify the occurrence of elemental sulfur, selected samples were measured once under liquid N_2 temperature, and then left in the analysis chamber at the same position under vacuum overnight without cooling and measured again the next day at room temperature. Processing of the spectra was accomplished by Kratos software. High-resolution XPS spectra were fitted using linear combinations of 70:30 Gauss–Lorentz functions on Shirley background-

subtracted spectra. O 1s peak at 529.8 eV corresponding to the Fe-O bond of goethite/lepidocrocite was used as the internal standard for binding energy (BE) scale calibration. In the absence of the Fe-O bond, peak positions were referred to the aliphatic C 1s component, set at 285.0 eV.

2.4 Results and Discussion

2.4.1 Reaction progress as derived from wet chemical analysis

Ferric (hydr)oxides reacted in a different way with aqueous sulfide in runs with excess iron over sulfide (HR) compared to those with excess sulfide over iron (LR) runs. In the HR runs, the concentration of MBS decreased along with the increase of MES. Only trace amount of MBS (< 0.03 mmol L^{-1}, detection limit of MBS was 0.0009 mmol L^{-1}) could be determined after 1.5 h in the HR_Gt run (Fig. 2.1) and after 10 min in the HR_Lp run (S2.1). After 3 h, a significant fraction of the initially added S was recovered as MES (31.3% in HR_Gt run and 25.6% in HR_Lp run). Within this time, more $Fe(II)_{HCl}$ had formed in the presence of lepidocrocite (7.0 mmol L^{-1}) than in the presence of goethite (5.5 mmol L^{-1}) (Fig. 2.2). $S_n^{2-}(aq)$ was detected in the first 15 min of the HR_Gt run, the concentration of which made up 5 % of the initially added S (in a replicate run only 2 %). No $S_n^{2-}(aq)$ could be detected in HR runs after 3 h.

In LR runs the concentration of MBS decreased after 3 h to 29.2% of the initially added S in the LR_Gt run and to 6.5% in the LR_Lp run, respectively, along with which the ferric (hydr)oxides was almost complete consumed. MES increased to 16.7% and 19.3% of the initially added S, respectively. $S_n^{2-}(aq)$ remained at a low concentration, with around 2.2 % of the initially added S after 3 h and a decrease to 0.9 % after 168 h. Thiosulfate and sulfate were undetectable in all runs (data not shown, detection limits were 6 µmol L^{-1} and 28 µmol L^{-1} for thiosulfate and sulfate, respectively).

Most of the MBS as well as 18.5 % of the generated MES and 20.4 % of the generated $Fe(II)_{HCl}$ were removed with the supernatant after centrifugation. Hence, around 80 % of the MES and $Fe(II)_{HCl}$ remained in the residual solid phase.

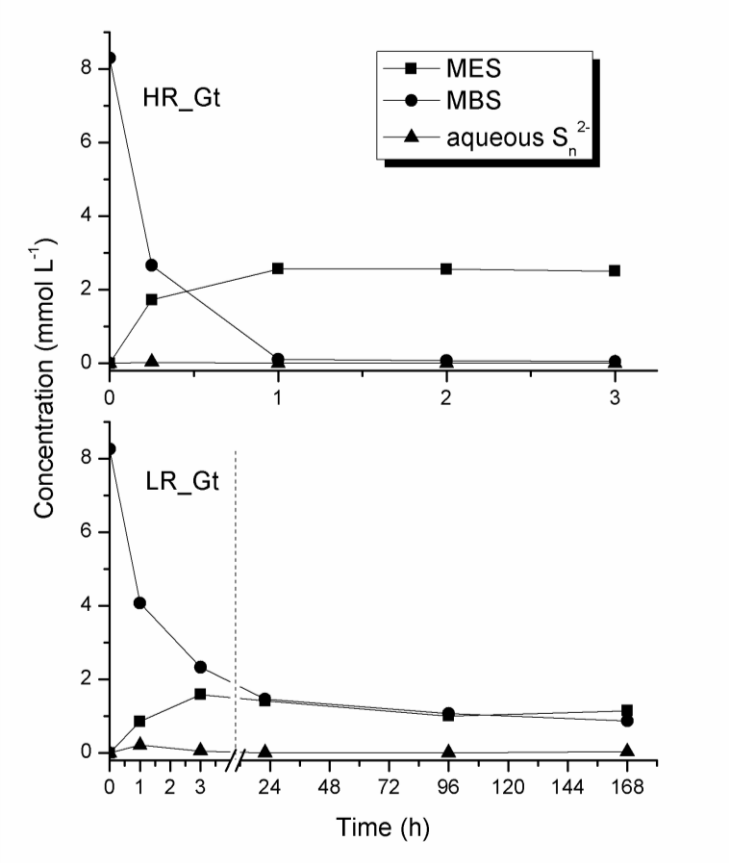

Fig. 2. 6 Sulfur speciation during reaction between aqueous sulfide and goethite for iron excess (HR) and sulfide excess (LR) conditions. Note the different time scales between HR_Gt and LR_Gt.

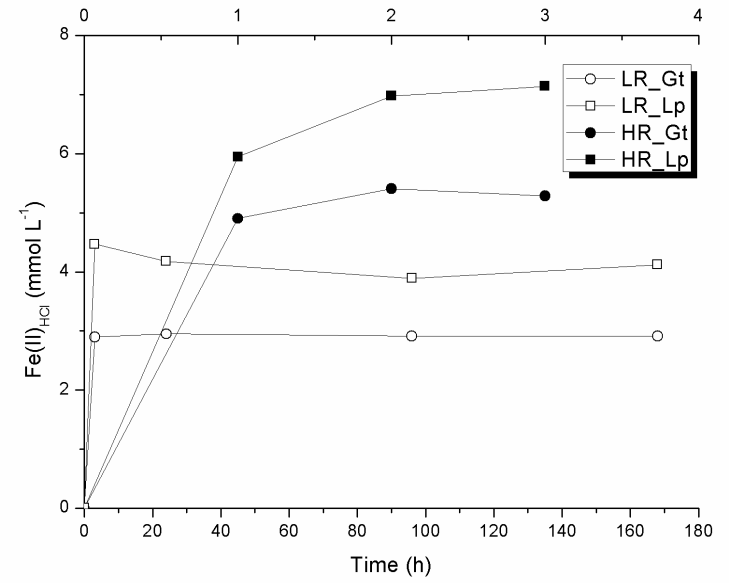

Fig. 2. 7 Concentrations of $Fe(II)_{HCl}$ of all runs. Note the two different time scales. The data with closed symbols refer to the top x axis.

2.4.2 Sulfur surface-speciation as detected by Cryogenic XPS

The survey spectra clearly demonstrate the occurrence of sulfur at the ferric (hydr)oxides´ surface after reaction with sulfide (Fig. 2.3 for goethite, S2.2 for lepidocrocite). Spectra also revealed impurities of remaining Na and Cl and contamination with organic carbon from sampling handling mainly in the LR runs.

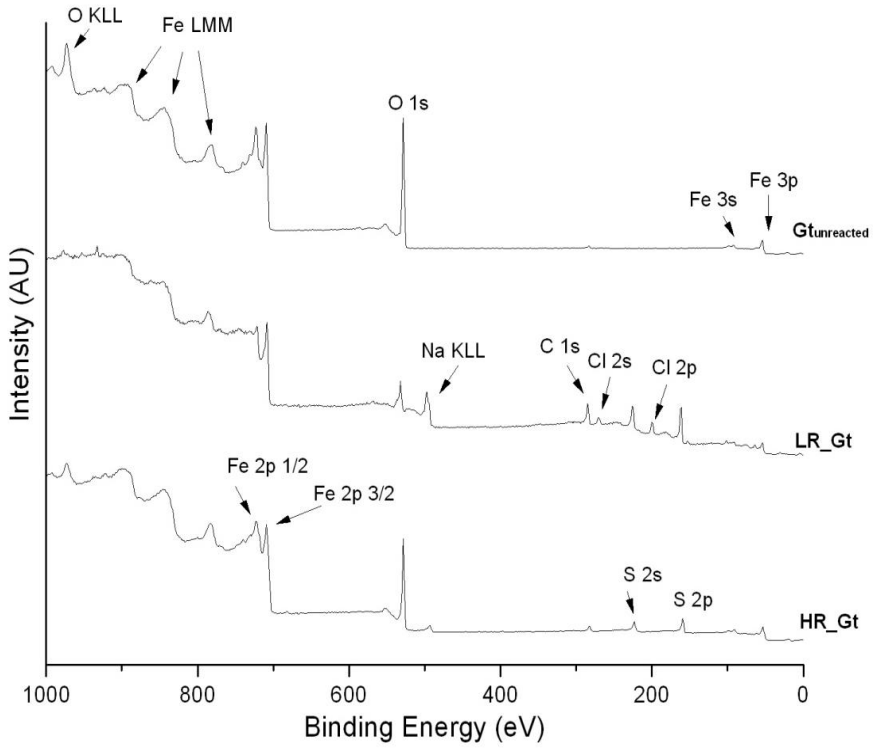

Fig. 2. 8 Survey XPS spectra of samples in experiments with goethite.

The high resolution of Fe 2p spectra were fitted following the principle of minimal number of components. The binding energies of Fe(III) $2p_{3/2}$ of goethite and lepidocrocite are located at 711.5 eV and 711.2 eV, respectively, and Fe(III) $2p_{1/2}$, both at 724.3 eV. After having reacted with sulfide, a new iron signal with a Fe $2p_{3/2}$ binding energy of 707.6 ± 0.2 eV appeared which we interpret as a sulfide-bound ferrous iron species (Fe(II)-S)(Karthe et al., 1993; Mullet et al., 2002; Nesbitt and Muir, 1994). Because of a negligible concentration of the Fe-OH and the Fe-O group in the O 1s spectra (S2.4), the Fe 2p spectra of LR runs can be assumed to reflect only Fe(II) species. The concentration of Fe(II) in the LR run was therefore 100 % (Fig. 2.4, S2.3). The Fe(II) concentration in the spectrum of HR run was calculated to be 16.7 % (Fig. 2.4) and 8.7 % (S2.3) in the HR_Gt and HR_Lp run, respectively.

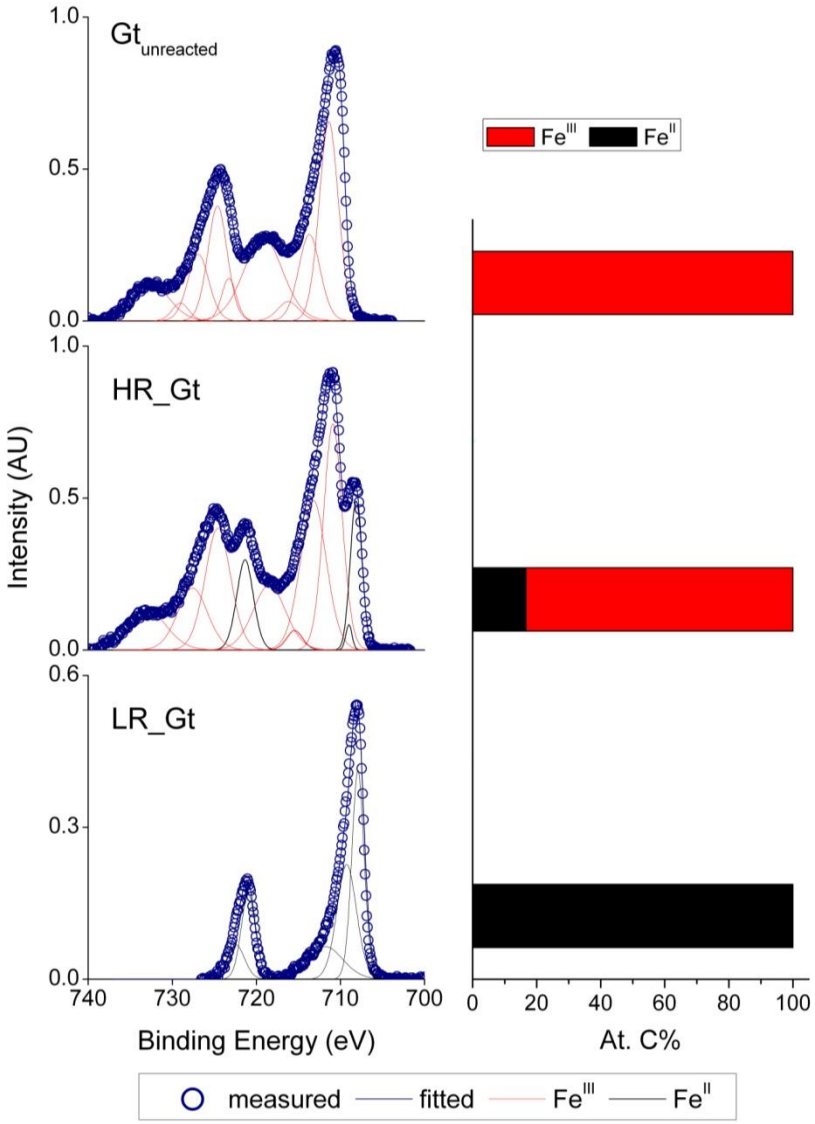

Fig. 2. 9 High resolution Fe 2p spectra of goethite and corresponding spectral area concentration of each species before and after reaction. Compound colours in bar chart are the same as in the spectra.

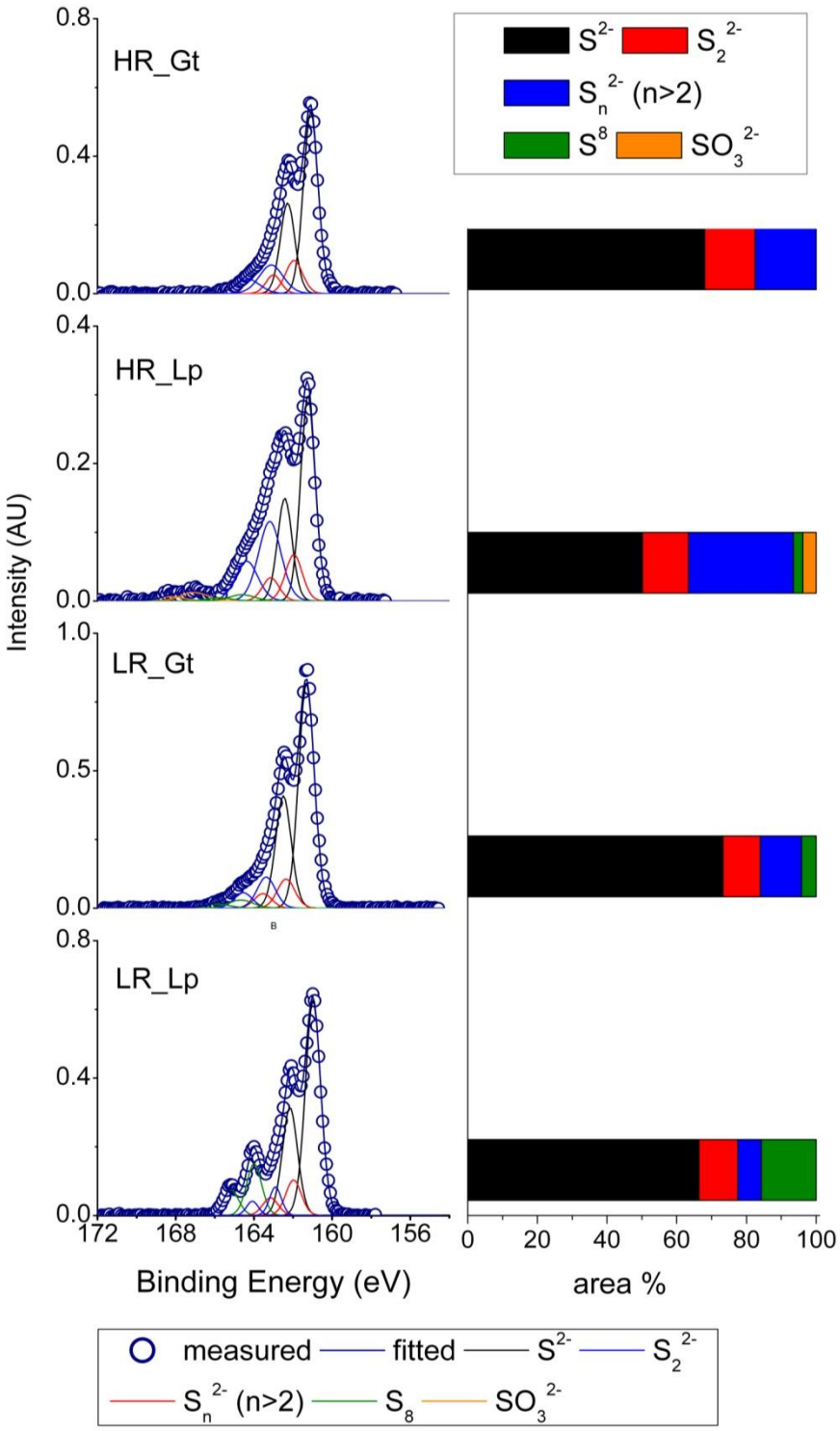

Fig. 2. 10 High-resolution S 2p spectra and corresponding spectral area concentration of each species in all runs. Compound colours in bar chart are the same as in the spectra.

S 2p spectra obtained after the reaction and the species concentrations are shown in Fig. 2.5, the corresponding fitting parameters of which were listed in Table 2.2. Each species in the S 2p spectrum was fitted with a doublet due to spin-orbit splitting of S $2p_{1/2}$ and S $2p_{3/2}$. It is reasonable to assume that a fraction of the initial sulfide was bound to Fe(II) generated from Fe(III) reduction. Hence, a species with a S $2p_{3/2}$ binding energy characteristic for the Fe(II)-S bond (S^{2-}(surf), 161.2 ± 0.3 eV)(Mullet et al., 2002; Nesbitt and Muir, 1994; Nesbitt et al., 2000) is regarded to be present in all runs, contributing to 68.1 %, 50.2 %,73.3 % and 66.4 % of the S 2p spectral area in the HR_Gt, HR_Lp, LR_Gt and LR_Lp run, respectively (Table 2.2, Fig. 2.5). Proper fitting of the spectra could, however, not be achieved by considering sulfide only. A reasonable fitting of the spectrum of the HR_Gt run was obtained with two additional species, which contributed to 14.4 % and 17.5 % of the spectral area. S $2p_{3/2}$ binding energies were 162.1 ± 0.2 eV and 163.2 ± 0.3 eV, which can be attributed to disulfide (S_2^{2-}(surf)) and polysulfide (S_n^{2-}(surf), with n>2), respectively (cf. Table 2.2 and references therein). Other three spectra were possible to fit only considering additional species besides the three species discussed above. The HR_Lp spectrum required two species with a S $2p_{3/2}$ binding energy of 164.5 eV (2.7 %) corresponding to elemental sulfur (S_8(surf)) and 167.5 eV (3.8 %) corresponding to sulphite(Baltrusaitis et al., 2007) (SO_3^{2-}(surf), Table 2.2 and Fig. 2.5). The LR_Gt and LR_Lp spectra also required consideration of the S_8 species with a binding energy of 164.4 ± 0.5 eV (4.2 % and 15.7 %, respectively) (Table 2.2). The fraction of S_8(surf) was higher in the LR_Lp run compared with the LR_Gt run after 168 h. No S_8(surf) was observed in the HR_Gt run.

There are several indications that the higher reactivity of lepidocrocite has induced a higher electron turnover in the HR_Lp run compared to the HR_Gt run(Poulton et al., 2004). The fraction of S_2^{2-}(surf) and S_n^{2-}(surf) (n>2) was higher in the HR_Lp run as well as the yield of $Fe(II)_{HCl}$. Additionally, products detected by XPS had a higher oxidation state (S_8(surf) and SO_3^{2-}(surf)) in the presence of lepidocrocite. However, formation of SO_3^{2-}(surf) from oxidation of reduced sulfur species during sample handling cannot be excluded. SO_3^{2-}(surf) was detected only in the HR_Lp run and has not been observed in previous studies on Fe(III)-S(-II) interaction. We did not analyse for dissolved SO_3^{2-} as an independent verification and sulfate and thiosulfate could

Table 2.2 The XPS fitting parameters of Fe and S species

	$Gt_{unreacted}$		$Lp_{unreacted}$		HR_Gt		HR_Lp		LR_Gt		LR_Lp		Ref. data[a]
	BE[b] (eV)	FWHM[c]	BE (eV)	FWHM	BE (eV)	FWHM	BE (eV)	FWHM	BE (eV)	FWHM	BE (eV)	FWHM	BE(eV)
S 2p $_{3/2}$													
S^{2-}	n.d.[d]	n.d.	n.d.	n.d.	161.1	0.85	161.2	0.85	161.3	0.9	161	0.9	161.2(Nesbitt et al., 2000) 161.3(Mullet et al., 2002; Nesbitt and Muir, 1994)
S_2^{2-}	n.d.	n.d.	n.d.	n.d.	162	1	161.9	1	162.3	1.05	162	0.9	162.1(Nesbitt and Muir, 1994) 162.6(Karthe et al., 1993)
S_n^{2-}	n.d.	n.d.	n.d.	n.d.	163.1	1.4	163.1	1.35	163.4	1.1	162.9	0.7	163.3 (Nesbitt and Muir, 1994) 163.2(Mullet et al., 2002) 163.4(Thomas et al., 1998)
S^8	n.d.	n.d.	n.d.	n.d.	n.d.	n.d.	164.5	1.5	164.7	1.45	164	0.9	165.3(Mullet et al., 2002) 164(Thomas et al., 1998)
SO_3^{2-}	n.d.	n.d.	n.d.	n.d.	n.d.	n.d.	167.5	1.55	n.d.	n.d.	n.d.	n.d.	166.5(Baltrusaitis et al., 2007)
Fe 2p $_{3/2}$													
Fe(II)-S	n.d.	n.d.	n.d.	n.d.	707.6	1.55	707.7	1.65	707.8	1.7	707.4	1.85	707.8(Nesbitt and Muir, 1994) 707.2(Mullet et al., 2002) 707.4(Karthe et al., 1993)
Fe(III)-O	711.5	2.6	711.2	2.3	711.4	2.55	711	2.9	n.d.	n.d.	n.d.	n.d.	711.5(Thomas et al., 1998)

[a]- all reference data were recalibrated with the internal standard of Fe-O bond at binding energy of 529.8eV.

[b]- binding energy [c]- full width at half maximum [d]- not detected

not be detected in any sample from this study, which excludes SO_3^{2-}(surf) formation from disproportionation of thiosulfate(Moses et al., 1984).

2.4.3 Sulfur mass balance

In contrast to the bulk concentration values obtained from wet chemistry data, XPS quantifies the mass percentage of surface-bound species. Hence, the question arises whether these surface species need to be considered in the overall mass balance of the reaction between aqueous sulfide and ferric (hydr)oxides and whether they affect its stoichiometry. To these ends we will in a first step test whether the mass balance for sulfur detected by wet chemistry methods is complete. In a second approach we will analyze to what extent the quantitative measurements made by XPS can be related to the bulk measurements.

Characteristic products of the reaction between aqueous sulfide and ferric (hydr)oxides are regarded to consist of elemental sulfur and FeS (amorphous FeS or mackinawite)(Hellige et al., 2012; Yao and Millero, 1996). Elemental sulfur is typically determined using the MES technique which indeed makes up a large fraction of total sulfur recovered from the experiments. Methanol extraction, however, also allows for the determination of surface-associated zero-valent sulfur(Kamyshny et al., 2009), a fraction which seems to be relevant according to the XPS results. Hence, application of the bulk techniques MBS and MES considers the concentration of the species aqueous sulfide, S(-II) associated with aqueous polysulfides (S_n^{2-} (aq)), and the concentration of total zero-valent sulfur, including S^o in the form of colloidal elemental sulfur in the suspension (S_8 (coll)) and the sulfur associated at the surface (S_8(surf), S ° bound to S_n^{2-}(aq) and S ° bound to surface associated polysulfides (S_2^{2-} (surf) and S_n^{2-}(surf).

A critical fraction in the sulfur mass balance is sulfur associated with Fe(II). This fraction can comprise crystalline pyrite, mackinawite (FeS) but also species of weak crystallinity with variable stoichiometries. Using HRTEM, Hellige et al. identified nano-mackinawite with a large amount of an amorphous phase rich in both iron and sulfur within the first 3 days of experiments comparable to the HR_LP experiment (cf. Fig. 8a in Hellige et al.[3]). Pyrite crystals were observed only after 1 week. Given that experimental conditions in this study were similar to the previous study we conclude

that pyrite did not form in the HR runs. Moreover, the absence of crystalline (i. e. not HCl extractable) pyrite in our experiments at the given reaction time scale of 3 h in the HR runs and 168 h in the LR runs can be also inferred from our wet chemical analysis of $Fe(II)_{HCl}$ and MES. Both analytical fractions remained relatively constant after their built-up (e.g. Fig. 2.2 for $Fe(II)_{HCl}$). We therefore exclude the formation of pyrite in both HR and LR runs.

The sulfide sulfur associated with Fe(II) is typically determined as acid volatile sulfide (AVS) but it apparently consists also of S(-II) bound in the polysulfide sulfur species e.g. non-crystalline surface disulfide (S_2^{2-}(surf)). The S^o atom in such species may be analyzed with the MES technique. AVS was not analyzed in this study due to the large uncertainties inherent to this methodology(Rickard and Morse, 2005). A good proxy for Fe(II)-S associations, however, would be the amount of HCl-extractable Fe(II), provided a 1:1 stoichiometry exists. Magnetite, which would be extractable with HCl and which had been observed in a previous study with lepidocrocite as an intermediate was estimated to make up < 7% of the generated $Fe(II)_{HCl}$ in our experiments (cf. SI) and seems therefore negligible. We therefore calculated the recovery of sulfur by wet chemical analysis using the concentrations measured with the bulk techniques MES, MBS and $Fe(II)_{HCl}$ (eq. 1). In LR runs the degassing rate was considered.

$$S_{recovery} = \frac{c(MES) + c(MBS) + c(Fe(II)_{HCl})}{c(S(-II)_{ini})} \qquad (1)$$

S recovery was found to be 100.8 %, 103.9 %, 95.7 % and 97.0 % for HR_Gt, HR_Lp, LR_Gt and LR_Lp, respectively. Given the errors inherent to this mass balance approach (we estimated a total error of ± 10 % based on propagation of errors of the individual methods), recovery seems to be complete.

XPS is a surface-sensitive technique which is able to detect surface coverage up to a thickness of 10 nm(Vickerman and Gilmore, 2009). A previous HRTEM study demonstrated that during the time the experiments where performed, sulfur was clearly associated with the surface of the ferric minerals(Hellige et al., 2012). We therefore assume that all solid phase-bound S quantified by wet chemical analysis is detectable by XPS and used the area percentage of the S 2p spectra to quantify surface sulfur speciation and to compare these data with the bulk concentration.

Table 2.3 S^o obtained as MES and from XPS calculation

	%	HR_Gt	HR_Lp	LR_Gt	LR_Lp
Wet chemical analysis	MES	30.5	25.6	16.7	19.3
XPS	S^o_{xps}	21.2	33.4	19.1	26.8
	S_8	0	2.7	4.2	15.7
	S^o associated with S_2^{2-}	7.2	6.6	5.4	5.6
	S^o bound to S_n^{2-} (n=5)	14.0	24.1	9.5	5.5

The amount of S° detected as polysulfide sulfur by XPS analysis was estimated using equation (2). The chain length of surface-associated polysulfides (S_n^{2-}(surf) with n = 3-8) other than disulfide cannot be identified by XPS. We assumed an average chain length of such polysulfides to be 5, in order to simplify the calculation. The total amount of S^o bound as polysulfides was 21.2%, 30.7 %, 14.8 % and 11.0 % in the HR_Gt (3 h), HR_Lp (3 h), LR_Gt (168 h) and LR_Lp run (168 h), respectively (Table 2.3).

$$c(S^o_{polysulfide}) = \frac{1}{2}c(S_2^{2-}(surf)) + \frac{4}{5}c(S_5^{2-}(surf)) \qquad (2)$$

Thus, the total amount of S° detected by XPS (S^o_{xps}), which is the sum of S_8 and polysulfide-bound S°, was 21.2 %, 33.4%, 19.1 % and 26.8 %, respectively (Table 2.3). These values can be compared to the MES fractions of the total initial sulfur determined at the time when also the XPS samples were taken, which were 30.5%, 25.6 %, 16.7 % and 19.3 %, respectively (Table 2.3). The match between the amount of S° derived from XPS measurements and the amount obtained from HPLC measurements is not perfect, but the values are at least in the same order of magnitude.

This analysis clearly indicates that surface polysulfides plus S_8 are a significant fraction of the MES pool. MES is commonly regarded to consist of S_8 sulfur (colloidal and solid phase), aqueous polysulfides (Kamyshny et al., 2009) and surface-associated S°. The absence of aqueous polysulfide in HR runs and the low concentration in LR runs (0.9 % of the initially added S) imply that MES in our experiments comprised mainly S_8 and surface-associated S°. S_8 concentrations

detected by XPS were rather low while concentrations of surface-associated polysulfides were high. We therefore conclude that the S °extracted by methanol with ZnAc pretreatment (MES) comprised the surface polysulfide species.

This conclusion raises the question about the nature of such surface associations. XPS indicates a large quantity of S to be S^{2-}(surf) which is either adsorbed to the mineral surface or bound to the generated Fe(II) (e. g. as FeS). Potentially, Fe(II) could be also associated with the surface polysulfides, e. g. as an amorphous Fe(II)-polysulfide phase. This assumption does not conflict with the 1:1 stoichiometry for Fe(II)-S associations inherent to the calculation of the S recovery in equation (1). If sulfur associated with Fe(II) contains methanol-extractable S °and solid phase-bound sulfide, as would be the case with Fe(II)-polysulfide associations, the S mass balance would still remain complete. In the presence of an amorphous phase of the stoichiometry FeS_n, our wet chemical analysis would extract such species as $Fe(II)_{HCl}$ and (n-1) S^o atoms as MES and the S recovery of FeS_n would be the sum of $Fe(II)_{HCl}$ and MES.

Unfortunately, a direct proof for the occurrence of Fe(II)-polysulfide associations was not possible with the analytical methods used in this study. We therefore tested the possibility for their occurrence based on a mass balance approach. To this end we compared the fraction $f_{Fe(II),HCl}$ of $Fe(II)_{HCl}$ formed per mol of initial S(-II)

$$f_{Fe(II),HCl} = Fe(II)_{HCl}/S(-II)_{ini} \qquad (3)$$

with the fraction $f_{S^{2-},XPS}$ of the spectral area of surface S^{2-} determined with XPS in the HR runs. Inherent to this approach is the assumption that precipitated FeS can be extracted with HCl as $Fe(II)_{HCl}$ and detected with XPS as S^{2-}(surf) (LR runs contain excess initial aqueous sulfide so that these experiments cannot be used for this comparison). Hence, in the absence of any Fe(II)-polysulfide associations the two fractions $f_{Fe(II),HCl}$ and $f_{S^{2-},XPS}$ would match each other. This was indeed the case in the HR_Gt run ($f_{Fe(II),HCl}$ = 66.8 % and $f_{S^{2-},XPS}$ = 68.1 %).

However, in the HR_Lp run a distinctly higher $Fe(II)_{HCl}$ fraction was observed ($f_{Fe(II),HCl}$ = 78.7 %, $f_{S^{2-},XPS}$ = 50.2 %) indicating that sufficient Fe(II) was available to bind surface S_2^{2-}(surf) and S_n^{2-}(surf) (n>2) species besides S^{2-}(surf) and that the occurrence of Fe(II)-polysulfide associations seems possible in this experiment.

This finding has implications for the initial reaction stoichiometry of the interaction between ferric (hydr)oxides and dissolved sulfide, in which a significant fraction of surface-bound polysulfides associated with Fe(II) should be considered additionally to S_8 and FeS. A generalized stoichiometry matching the recovery can thus be formulated (eq 4):

$$3x\ H_2S + 2x\ FeOOH \rightarrow (2x-1)\ FeS + Fe^{2+}_{surf.} + S_{y+1}{}^{2-}_{surf.} + (x-y)/8\ S_8 + 4x\ H_2O \quad (4)$$

where $S_{y+1}{}^{2-}_{surf.}$ denotes surface polysulfide and $Fe^{2+}_{surf.}$ surface-bound Fe(II). The coefficient x reflects the number of generated S° atoms and y ($0 \leq y \leq x$) is the number of S° atoms associated with surface polysulfides. Note that under conditions where y = 0, we obtain the idealized stoichiometry:

$$3\ H2S + 2\ FeOOH \rightarrow 2\ FeS + 1/8\ S_8$$

2.5 Implication for sulfur biogeochemistry

Polysulfides are regarded to be the key reactants for pyrite formation (Rickard and Luther, 2007; Schoonen and Barnes, 1991b). Pyrite occurrence has been demonstrated in solutions either rich in aqueous polysulfides (Luther, 1991; Schoonen and Barnes, 1991b; Wang and Morse, 1996) or rich in aqueous S(-II) and S_8 (Benning et al., 2000; Wang and Morse, 1996), in which aqueous polysulfides can rapidly form (Kamyshny et al., 2009). Hellige et al. (Hellige et al., 2012) have postulated the contribution of surface bound polysulfides to pyrite formation based on HRTEM measurements and on theoretical considerations. They demonstrated that pyrite formation occurred as precipitation of new a phase after 1 week following the reaction between aqueous sulfide and lepidocrocite and disaggregation of iron sulfur associations under experimental conditions comparable to this study. However, they could not further resolve the nature of these species.

Our study supports this hypothesis showing that a large fraction of S can be recovered as polysulfides at the surface of the iron minerals at a low residual concentration of aqueous sulfide (< 0.03 mmol L^{-1}, LR runs) or after aqueous sulfide has been consumed (HR runs). This finding conflicts with previous studies in which polysulfides are generally assumed to be present in the aqueous phase only or, at least, the existence of polysulfides at the solid phase was not taken into consideration (Giggenbach, 1972; Kamyshny et al., 2006; Lichtschlag et al., 2013; Luther, 1991; Rickard and Luther, 2007). Solid-phase sulfur forming during the initial interaction between dissolved sulfide and ferric (hydr)oxides is commonly regarded to consist of elemental sulfur, S^{2-} bound as FeS and S_2^{2-} bound to crystalline pyrite (Hellige et al., 2012; Yao and Millero, 1996).

Of particular relevance for pyrite formation may be the discovery of surface-associated disulfide. The cause for their formation can be related to the reaction between aqueous sulfide and the ferric (hydr)oxide´s mineral surface. Electron transfer between sulfide and ferric iron is regarded to be preceded by an adsorption step of sulfide onto the ferric (hydr)oxides´surface (Dos Santos Afonso and Stumm, 1992).

$$HS^- + >Fe^{III}OH \;<=>\; >Fe^{III}HS + OH^- \qquad (5)$$

It has been postulated that the one-electron transfer between surface-associated sulfide and ferric iron (eq. 6) generates sulfide radicals $HS^{\cdot}$.

$$>Fe^{III}HS \rightarrow >Fe^{II}HS^{\bullet} \qquad (6)$$

This species may spontaneously react with an additional $HS^{\bullet}$ radical to form a surface disulfide (Steudel, 1996) (eq. 7),

$$>Fe^{II}HS^{\bullet} + HS^{\bullet} \rightarrow >Fe^{II}S_2 + 2\ H^{+} \qquad (7)$$

which may tend to further react to form polysulfides with longer chain (S_n^{2-}, n>2) and to elemental sulfur depending on pH (Steudel, 1996).

Surface disulfide species can be regarded to be the precursor required for pyrite formation, which will trigger pyrite formation in the presence of abundant surface-associated Fe(II) either through direct combination with Fe^{2+} (eq. 8) or through reaction with FeS (eq. 9).

$$Fe^{2+} + {S_2}^{2-}{}_{surface} \rightarrow FeS_{2,\ precursor} \xrightarrow{aging} FeS_{2,\ pyrite} \qquad (8)$$

$$FeS + {S_2}^{2-}{}_{surface} \rightarrow FeS_{2,\ precursor} + S^{2-} \xrightarrow{aging} FeS_{2,\ pyrite} + S^{2-} \qquad (9)$$

Note that the $FeS_{2,\ precursor}$ is a non-crystalline form. Reaction (8) leads to FeS dissolution and subsequent reprecipitation as pyrite. HRTEM images discussed in the study of Hellige et al. support this model(Hellige et al., 2012). They observed after 2h a sulfur-rich rim coating the crystals of lepidocrocite containing domains of nano mackinawite. The coating disintegrated after 72 h of reaction and precipitated as an amorphous phase rich in Fe and S marking the onset of the formation of pyrite. The S^{2-} released from reaction (8) may be reabsorbed at the surface and react with remaining ferric (hydr)oxides.

Moreover, surface associated polysulfides may play an overlooked role in the sulfur cycle. Polysulfides are generally regarded to exert a high reactivity and to be involved in both abiotic and biotic reactions. For instance, polysulfide species were detected as intermediates during microbial sulfur disproportionation and might even be disproportionated themselves (Poser et al., 2013). They can serve as electron

acceptors for specific bacteria such as *Deltaproteobacteria* from soda lakes(Sorokin et al., 2008). Polysulfide pathway is regarded to be the important pathway of biotic oxidation of metal sulfides such as arsenopyrite (Rohwerder et al., 2003). The chemical bonds between metal and sulfur is broken by proton attach and the sulfur is then liberated as hydrogen sulfide, which could be oxidized in a one-electron step to form polysulfide species (Rohwerder et al., 2003; Steudel, 1996). However, only aqueous polysulfide species have been determined to date(Giggenbach, 1972; Kamyshny et al., 2006; Lichtschlag et al., 2013; Luther, 1991; Rickard and Luther, 2007).This study clearly demonstrates that a large amount (> 50 % of generated S^o) and previously unknown fraction of the oxidized sulfur is stabilized as polysulfides at the mineral surface. The question arises to what extent the occurrence these species may help to decipher unexplained observations such as the cryptic sulfur cycle driven by iron in the methane zone of a marine sediment (Holmkvist et al., 2011). Our findings therefore call for a revisiting of the role of polysulfide species in abiotic and biotic sulfur cycling.

Supporting Information Available

The supporting information contains the reaction pattern, the Fe 2p spectra and the calculation process of minor iron mineral in the runs with lepidocrocite as well as the O 1s spectra after reacted with sulfide in all of the runs. The S 2p spectrum without cooling showed significant elemental sulfur decrease. This information is available free of charge via the Internet at http://pubs.acs.org.

Acknowledgements

This study was financially supported by the German Research Foundation (DFG) for the research group “etrap” (electron transfer processes in anoxic aquifers) (FOR 580, PE 438/11-3 und PLA 302/7-1) and by the European Science Foundation (ESF) for the research networking programme “FIMIN” (The Functionality of Iron Minerals in Environmental Processes). We thank Professor Per Persson for granting access to the XPS analysis, and Dr. Thilo Behrends for his valuable comments and discussions. Finally, we thank the editor and the anonymous reviewers for their constructive comments.

2.6 Reference

Baltrusaitis, J., Cwiertny, D. M., and Grassian, V. H., 2007. Adsorption of sulfur dioxide on hematite and goethite particle surfaces. *Physical Chemistry Chemical Physics* **9**, 5542-5554.

Benning, L. G., Wilkin, R. T., and Barnes, H., 2000. Reaction pathways in the Fe–S system below 100 C. *Chemical Geology* **167**, 25-51.

Berner, R. A., 1970. Sedimentary pyrite formation. *American Journal of Science* **268**, 1-23.

Dos Santos Afonso, M. and Stumm, W., 1992. Reductive dissolution of iron(III) (hydr)oxides by hydrogen sulfide. *Langmuir* **8**, 1671-1675.

Eggleston, C. M., Ehrhardt, J. J., and Stumm, W., 1996. Surface structural controls on pyrite oxidation kinetics: An XPS-UPS, STM, and modeling study. *American Mineralogist* **81**, 1036-1056.

Fonselius, S., Dyrssen, D., and Yhlen, B., 2007. Determination of hydrogen sulphide. *Methods of Seawater Analysis, Third Edition*, 91-100.

Giggenbach, W., 1972. Optical spectra and equilibrium distribution of polysulfide ions in aqueous solution at 20. deg. *Inorganic Chemistry* **11**, 1201-1207.

Hellige, K., Pollok, K., Larese-Casanova, P., Behrends, T., and Peiffer, S., 2012. Pathways of ferrous iron mineral formation upon sulfidation of lepidocrocite surfaces. *Geochimica et Cosmochimica Acta* **81**, 69-81.

Holmkvist, L., Ferdelman, T. G., and Jørgensen, B. B., 2011. A cryptic sulfur cycle driven by iron in the methane zone of marine sediment (Aarhus Bay, Denmark). *Geochimica et Cosmochimica Acta* **75**, 3581-3599.

Kamyshny, A., Borkenstein, C. G., and Ferdelman, T. G., 2009. Protocol for Quantitative Detection of Elemental Sulfur and Polysulfide Zero-Valent Sulfur Distribution in Natural Aquatic Samples. *Geostandards and Geoanalytical Research* **33**, 415-435.

Kamyshny, A., Ekeltchik, I., Gun, J., and Lev, O., 2006. Method for the determination of inorganic polysulfide distribution in aquatic systems. *Analytical Chemistry* **78**, 2631-2639.

Karthe, S., Szargan, R., and Suoninen, E., 1993. Oxidation of pyrite surfaces: A photoelectron spectroscopic study. *Applied Surface Science* **72**, 157-170.

Lichtschlag, A., Kamyshny Jr, A., Ferdelman, T. G., and deBeer, D., 2013. Intermediate sulfur oxidation state compounds in the euxinic surface sediments of the Dvurechenskii mud volcano (Black Sea). *Geochimica et Cosmochimica Acta* **105**, 130-145.

Luther, G. W., 1991. pyrite synthesis via polysulfide compounds. *Geochimica et Cosmochimica Acta*, 2839-2849.

Luther, G. W., 2010. The role of one-and two-electron transfer reactions in forming thermodynamically unstable intermediates as barriers in multi-electron redox reactions. *Aquatic Geochemistry* **16**, 395-420.

Morse, J. W., 1999. Sulfides in sandy sediments: new insights on the reactions responsible for sedimentary pyrite formation. *Aquatic Geochemistry* **5**, 75-85.

Moses, C. O., Nordstrom, D. K., and Mills, A. L., 1984. Sampling and analysing mixtures of sulphate, sulphite, thiosulphate and polythionate. *Talanta* **31**, 331-339.

Mullet, M., Boursiquot, S., Abdelmoula, M., Génin, J.-M., and Ehrhardt, J.-J., 2002. Surface chemistry and structural properties of mackinawite prepared by

reaction of sulfide ions with metallic iron. *Geochimica et Cosmochimica Acta* **66**, 829-836.

Mylon, S. E. and Benoit, G., 2001. Subnanomolar Detection of Acid-Labile Sulfides by the Classical Methylene Blue Method Coupled to HPLC. *Environmental Science & Technology* **35**, 4544-4548.

Nesbitt, H. and Muir, I., 1994. X-ray photoelectron spectroscopic study of a pristine pyrite surface reacted with water vapour and air. *Geochimica et Cosmochimica Acta* **58**, 4667-4679.

Nesbitt, H., Scaini, M., Höchst, H., Bancroft, G., Schaufuss, A., and Szargan, R., 2000. Synchrotron XPS evidence for Fe2+-S and Fe3+-S surface species on pyrite fracture-surfaces, and their 3D electronic states. *American Mineralogist* **85**, 850-857.

Peiffer, S., Dos Santos Afonso, M., Wehrli, B., and Gaechter, R., 1992. Kinetics and mechanism of the reaction of hydrogen sulfide with lepidocrocite. *Environmental Science & Technology* **26**, 2408-2413.

Peiffer, S. and Gade, W., 2007. Reactivity of ferric oxides toward H2S at low pH. *Environmental Science & Technology* **41**, 3159-3164.

Poser, A., Lohmayer, R., Vogt, C., Knoeller, K., Planer-Friedrich, B., Sorokin, D., Richnow, H.-H., and Finster, K., 2013. Disproportionation of elemental sulfur by haloalkaliphilic bacteria from soda lakes. *Extremophiles* **17**, 1003-1012.

Poulton, S. W., 2003. Sulfide oxidation and iron dissolution kinetics during the reaction of dissolved sulfide with ferrihydrite. *Chemical Geology* **202**, 79-94.

Poulton, S. W., Krom, M. D., and Raiswell, R., 2004. A revised scheme for the reactivity of iron (oxyhydr)oxide minerals towards dissolved sulfide. *Geochimica et Cosmochimica Acta* **68**, 3703-3715.

Pyzik, A. J. and Sommer, S. E., 1981. Sedimentary iron monosulfides: Kinetics and mechanism of formation. *Geochimica et Cosmochimica Acta* **45**, 687-698.

Raiswell, R. and Berner, R. A., 1985. Pyrite formation in euxinic and semi-euxinic sediments. *American Journal of Science* **285**, 710-724.

Rickard, D. and Luther, G. W., 2007. Chemistry of iron sulfides. *Chemical Reviews* **107**, 514-562.

Rickard, D. and Morse, J. W., 2005. Acid volatile sulfide (AVS). *Marine Chemistry* **97**, 141-197.

Rizkov, D., Lev, O., Gun, J., Anisimov, B., and Kuselman, I., 2004. Development of in-house reference materials for determination of inorganic polysulfides in water. *Accreditation and Quality Assurance* **9**, 399-403.

Rohwerder, T., Gehrke, T., Kinzler, K., and Sand, W., 2003. Bioleaching review part A. *Applied microbiology and biotechnology* **63**, 239-248.

Schoonen, M. and Barnes, H., 1991. Reactions forming pyrite and marcasite from solution: II. Via FeS precursors below 100 C. *Geochimica et Cosmochimica Acta* **55**, 1505-1514.

Schwertmann, U. and Cornell, R. M., 2008. *Iron oxides in the laboratory*. Wiley-Vch.

Sorokin, D. Y., Tourova, T. P., Mußmann, M., and Muyzer, G., 2008. Dethiobacter alkaliphilus gen. nov. sp. nov., and Desulfurivibrio alkaliphilus gen. nov. sp. nov.: two novel representatives of reductive sulfur cycle from soda lakes. *Extremophiles* **12**, 431-439.

Steudel, R., 1996. Mechanism for the Formation of Elemental Sulfur from Aqueous Sulfide in Chemical and Microbiological Desulfurization Processes. *Industrial & Engineering Chemistry Research* **35**, 1417-1423.

Steudel, R., Holdt, G., Göbel, T., and Hazeu, W., 1987. Chromatographic Separation of Higher Polythionates SnO 62-(n= 3… 22) and Their Detection in Cultures of Thiobacillus ferroxidans; Molecular Composition of Bacterial Sulfur Secretions. *Angewandte Chemie International Edition in English* **26**, 151-153.

Tabatabai, M., 1974. A rapid method for determination of sulfate in water samples. *Environmental Letters* **7**, 237-243.

Tamura, H., Goto, K., Yotsuyanagi, T., and Nagayama, M., 1974. Spectrophotometric determination of iron (II) with 1, 10-phenanthroline in the presence of large amounts of iron (III). *Talanta* **21**, 314-318.

Thomas, J. E., Jones, C. F., Skinner, W. M., and Smart, R. S. C., 1998. The role of surface sulfur species in the inhibition of pyrrhotite dissolution in acid conditions. *Geochimica et Cosmochimica Acta* **62**, 1555-1565.

Vickerman, J. C. and Gilmore, I. S., 2009. *Surface analysis: the principal techniques*. Wiley Online Library.

Wang, Q. and Morse, J. W., 1996. Pyrite formation under conditions approximating those in anoxic sediments I. Pathway and morphology. *Marine Chemistry* **52**, 99-121.

Yao, W. and Millero, F. J., 1996. Oxidation of hydrogen sulfide by hydrous Fe(III) oxides in seawater. *Marine Chemistry* **52**, 1-16.

2.7 Supporting Information

Occurrence of Surface Polysulfides during the Interaction between Ferric (Hydr)Oxides and Aqueous Sulfide

Moli Wan[1], Andrey Shchukarev[2], Regina Lohmayer[3], Britta Planer-Friedrich[3], Stefan Peiffer[1]

[1] Department of Hydrology, University of Bayreuth, D-95440, Bayreuth, Germany

[2] Biogeochemistry, Department of Chemistry, Umeå Iniversity, SE-901 87 Umeå, Sweden

[3] Environmental Geochemistry, University of Bayreuth, D-95440 Bayreuth, Germany

8 pages and 6 figures are presented in this supporting information.

Sulphur mass balance

Magnetite was regarded to be an intermediate of minor relevance in the previous paper (Hellige et al., 2012). The concentration of magnetite was not given but it may be attributed to the fraction of $Fe(II)_{excess}$ which was calculated as:

$$Fe(II)_{excess} = Fe(II)_{HCl} - FeS = Fe(II)_{HCl} - (S(-II)_{ini} - S^{o}) \quad (1)$$

Although their S^{o} is extracted without ZnAc pretreatment, we can in a first approximation apply this equation for our experiments

$$Fe(II)_{excess} = Fe(II)_{HCl} - FeS = Fe(II)_{HCl} - (S(-II)_{ini} - MES) \quad (2)$$

The calculation shows that $Fe(II)_{excess}$ would be a minor fraction in the HR_Lp run (7%) and absent in the other three runs (negative values in HR_Gt (-2%), LR_Gt (-33%) and LR_Lp (-3%) runs, respectively). Hence magnetite should be a minor component in our experiments.

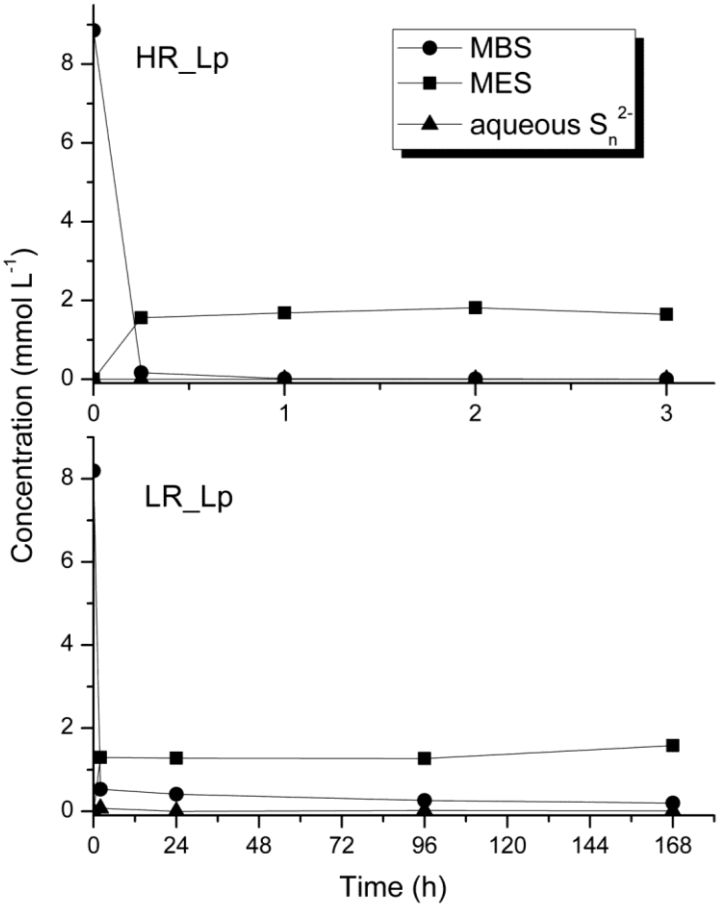

S2. 7 Sulphur speciation during reaction between aqueous sulfide and lepidocricite for iron excess (HR) and sulfide excess (LR) conditions. Note the different time scales between HR_Lp and LR_Lp.

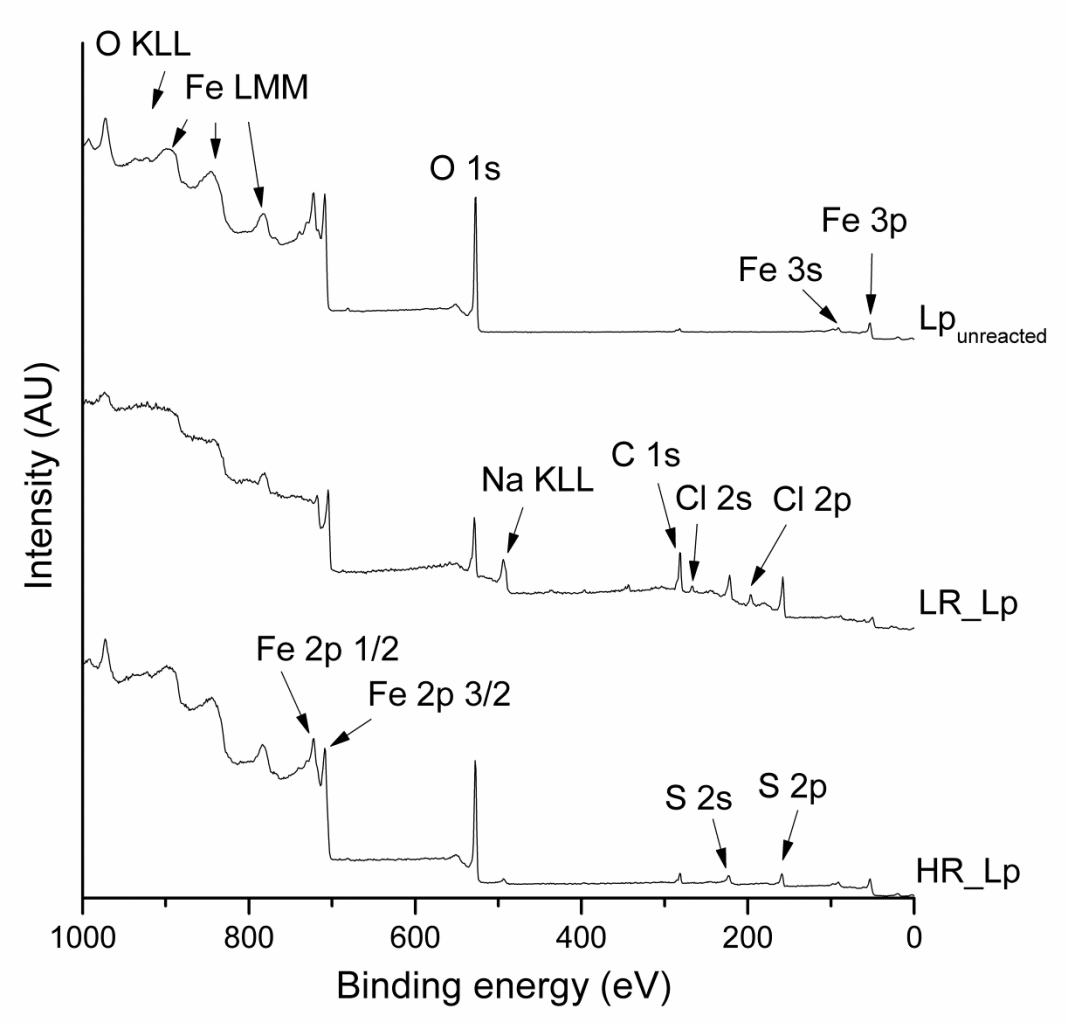

S2. 8 Survey XPS spectra of samples in experiments with lepidocrocite.

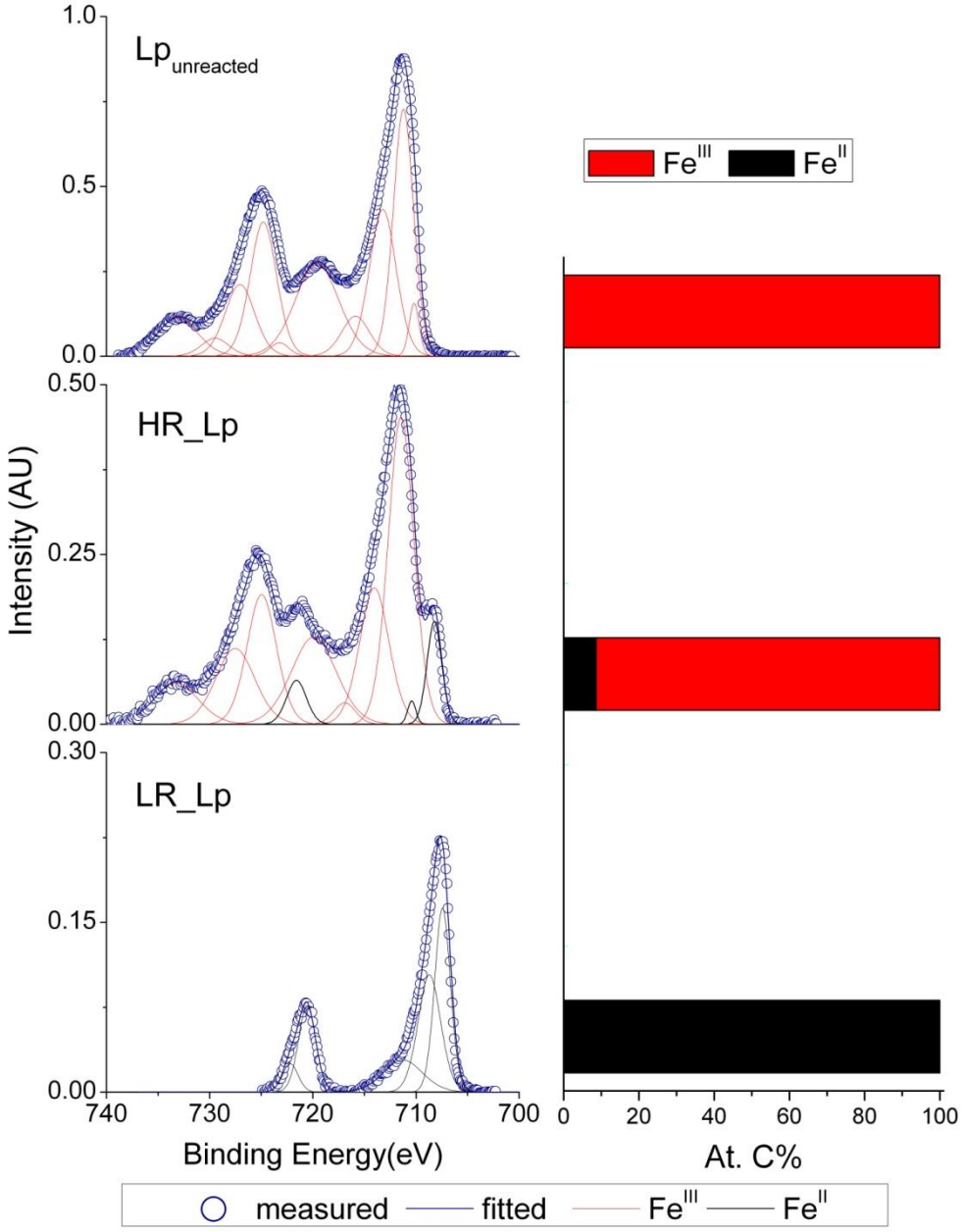

S2. 9 High resolution Fe 2p spectra of lepidocrocite and corresponding spectral area concentration of each species before and after reaction. Compound colours in bar chart are the same as in the spectra.

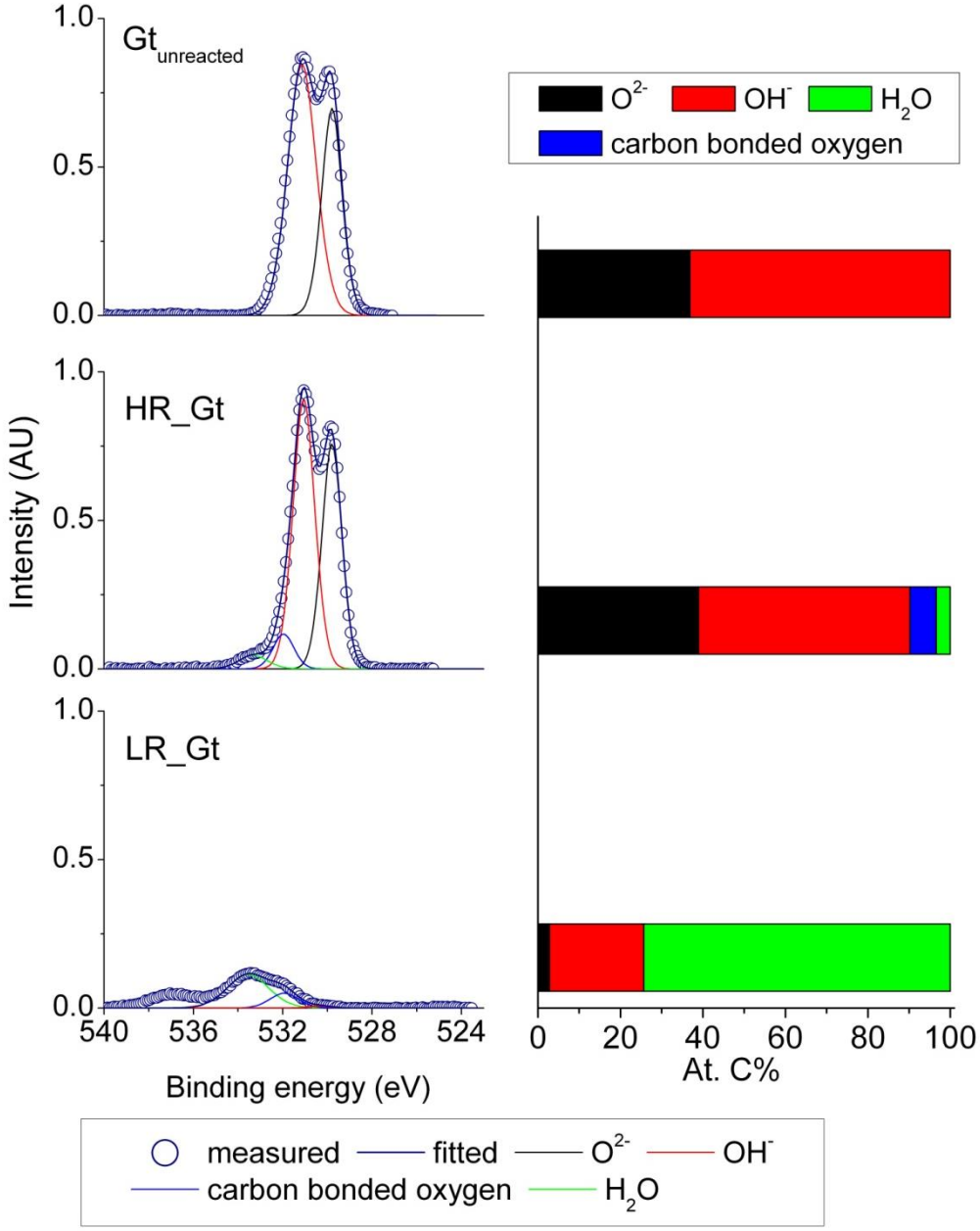

S2. 10 High resolution O 1s spectra of goethite and corresponding spectral area concentration of each species before and after reaction. Compound colours in bar chart are the same as in the spectra.

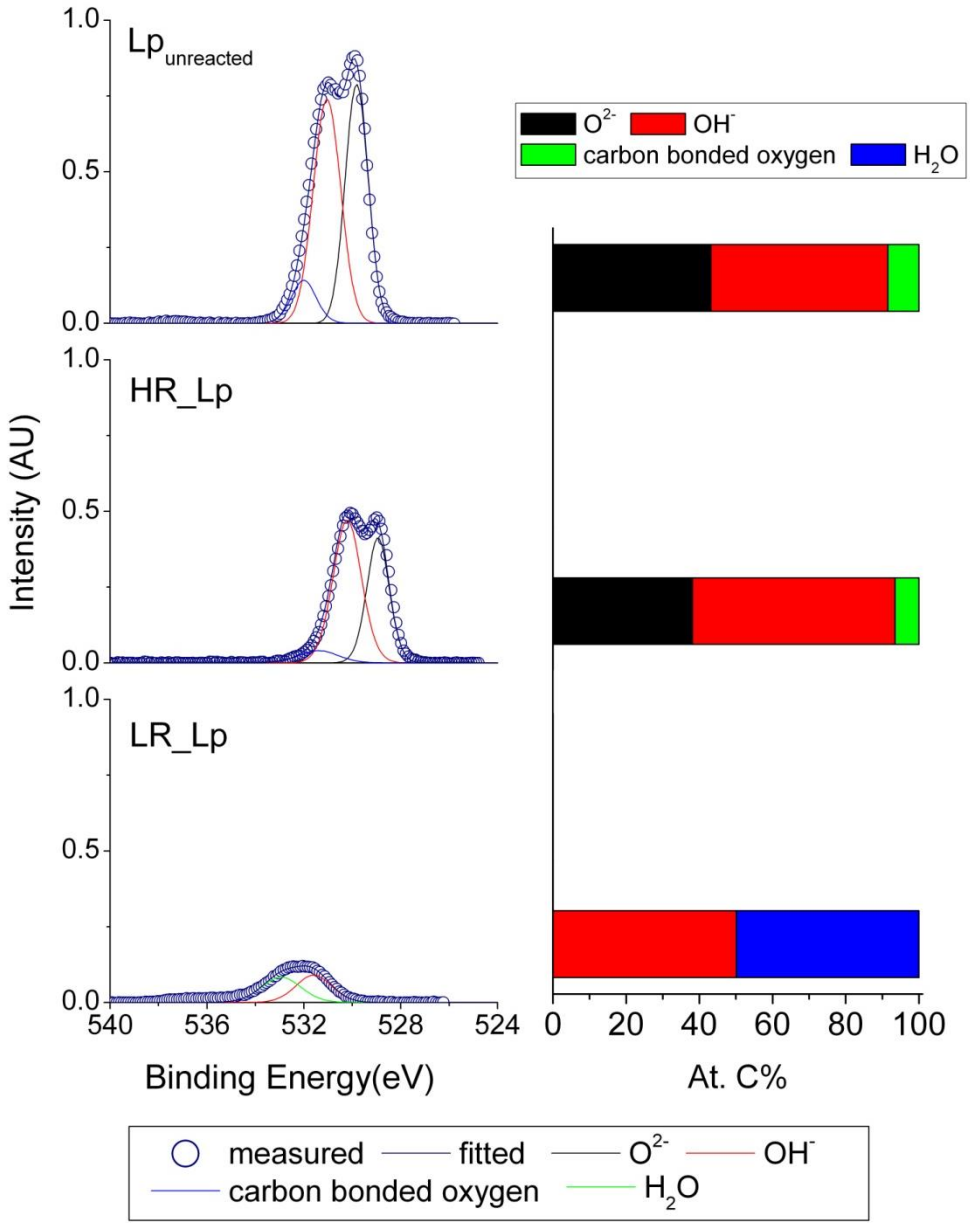

S2. 11 High resolution O 1s spectra of lepidocrocite and corresponding spectral area concentration of each species before and after reaction. Compound colours in bar chart are the same as in the spectra.

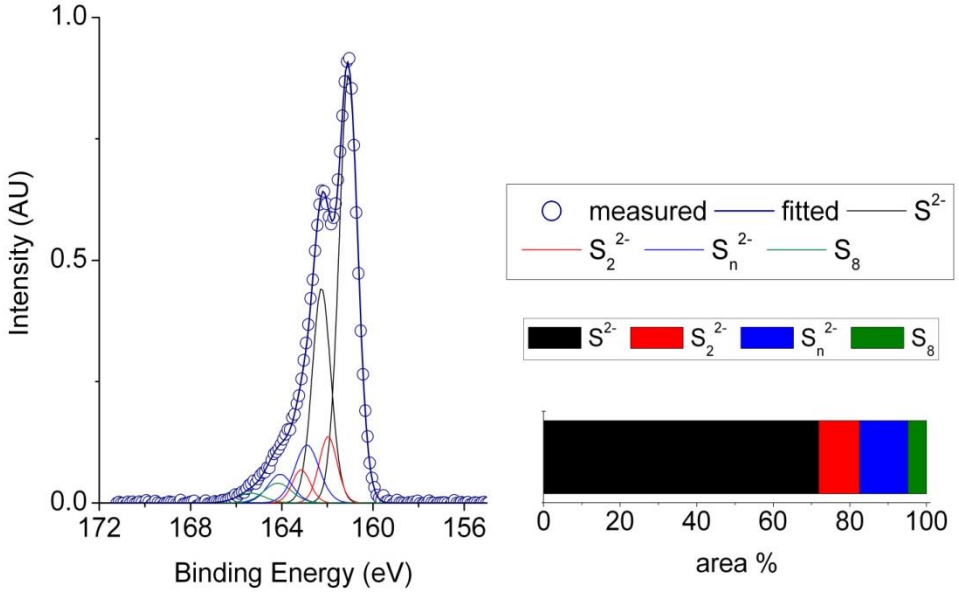

S2. 12 High resolution S 2p spectra of LR_Lp after leaving in the analysis chamber overnight without cooling. The corresponding spectral area concentration of each species has the same color as in the spectra.

References

Hellige, K., Pollok, K., Larese-Casanova, P., Behrends, T., and Peiffer, S., 2012. Pathways of ferrous iron mineral formation upon sulfidation of lepidocrocite surfaces. *Geochim. Cosmochim. Acta* **81**, 69-81.

3. Pyrite formation and mineral transformation pathways upon sulfidation of ferric hydroxides depend on mineral type and sulfide concentration

Stefan Peiffer[1]*, Thilo Behrends[2], Katrin Hellige[1], Philip Larese-Casanova[3], Moli Wan[1], and Kilian Pollok[4,5],

[1] Department of Hydrology, Universität Bayreuth, Universitätsstraße 30, D-95445 Bayreuth, Germany

[2] Department of Earth Sciences, Geochemistry, Utrecht University, P.O. Box 80021, 3508 TA Utrecht, The Netherlands

[3] Department of Civil and Environmental Engineering, Northeastern University, 469 Snell Engineering, 360 Huntington Ave, Boston, MA 02115, USA

[4] Bayerisches Geoinstitut, Universität Bayreuth, Universitätsstraße 30, D-95445 Bayreuth, Germany

[5] Institute of Geosciences, Mineralogy, Friedrich-Schiller-Universität Jena, Carl-Zeiss-Promenade 10, D-07745 Jena, Germany

* Corresponding author. Phone ++49-921-552251, Fax ++49-921-552366, s.peiffer@uni-bayreuth.de

Published in *Chemical Geology*, 2015(400): pp44-55.

DOI: 10.1016/j.chemgeo.2015.01.023

3.1 Abstract

The reaction of ferric (hydr)oxides with dissolved sulfide does not lead to the instantaneous production of thermodynamically stable products but can induce a variety of mineral transformations including the formation of metastable intermediates. The importance of the various transformation pathways depends, among other factors, on the characteristics of the ferric (hydr)oxides but a mechanistic model which relates the mineralogy of the ferric (hydr)oxides to the type of reaction products and their evolution over time is still missing. Here, we investigate the kinetics of the reaction between dissolved sulfide (6.7–7.5 mmol L^{-1} with ferrihydrite (Fh, 12 mmol L^{-1}), lepidocrocite (Lp, 26.6 mmol L^{-1}), and goethite (Gt, 22 mmol L^{-1}) in batch experiments at pH 7 and room temperature. The time evolution of solution and solid phase composition was monitored over 2 weeks while TEM, and Mössbauer spectroscopy were used to characterize the transformations of the solid phases.

Dissolved sulfide was consumed within 2 (Fh, Lp) to 8 hours (Gt) with methanol extractable sulphur and HCl extractable Fe(II) ($Fe(II)_{HCl}$) being the main products after this time. The mass balances of Fe and S indicated that a large fraction of the $Fe(II)_{HCl}$ in the reactions with Fh (46 % of $Fe(II)_{HCl}$) and Lp (36 % of $Fe(II)_{HCl}$) was solid-phase bound but not associated with sulphur. This excess Fe(II) exceeded the adsorption capacity of the solids and remained associated with the oxides. Over the time scale of days, the concentrations of MES and $Fe(II)_{HCl}$ decreased and this process was accompanied by the formation of secondary iron oxides and pyrite in all experiments. The pyrite yield after two weeks showed the same trend as the amounts of intermediately produced excess Fe(II): Fh (84 % of initial S(-II)) > Lp (50%) > Gt (13%). Besides the formation of pyrite, Fh transformed completely into thermodynamically more stable iron oxides such as hematite or magnetite. In contrast, formation of other iron oxides was only minor when Lp or Gt reacted with sulfide.

We propose that the extent of pyrite and secondary iron mineral precipitation is controlled by the ratio between the competing formation of excess Fe(II) and FeS_s in the early stage of the reaction. Formation of excess Fe(II) is a prerequisite for rapid pyrite formation and induces secondary formation of iron oxides. The competition between excess Fe(II) and FeS_s formation, in turn, is ruled by two factors: 1) the ratio between added sulfide and available surface area, and 2) the capability of the

iron(hydr)oxide to conduct electrons from surface bound Fe(II) to bulk Fe(III) and to accommodate structural Fe(II). This capability is largest for Fh and explains the most pronounced excess Fe(II) production and, by this, the greatest pyrite yield in experiments with Fh. During the reaction with Gt, in contrast, formation of FeS_s outcompetes the accumulation of excess Fe(II) and consequently the precipitation of pyrite is only minor.

This conceptual model constrains conditions at which relatively fast pyrite formation within the time scale of days or weeks might be relevant in natural environments. Suitable conditions are expected in environments with low sulfide levels in which formation of reactive iron (hydr)oxides is stimulated by redox oscillations (e. g. wetlands, riparian soils, tidal flats).

Keywords: ferric hydroxides, dissolved sulfide, ferrous iron, ferrihydrite, lepidocrocite, goethite, pyrite formation, electron transfer, bulk mineral electrons

3.2 Introduction

Reduction of ferric (hydr)oxides is a prominent pathway contributing to electron fluxes in subsurface environments (Raiswell and Canfield, 2012) and is directly connected to the bioavailability and mobility of nutrients (Einsele, 1936) and contaminants (Haderlein and Pecher, 1998). Reductive dissolution occurs either enzymatically (e. g. (Thamdrup, 2000)) or chemically (Cornell and Schwertmann, 2006) with dissolved sulfide being a powerful and ubiquitous reductant in anoxic environments (e. g. (Canfield et al., 1992)). Ferric (hydr)oxides display a wide spectrum of reactivity (Postma, 1993) as being controlled by surface area (Roden, 2003) but also by thermodynamic properties such as E_h (Fischer, 1987) or solubility product (Bonneville et al., 2009). Interaction with sulfide is regarded to be a surface controlled process (Dos Santos Afonso and Stumm, 1992). Under acidic conditions Fe(II) becomes completely dissolved (Peiffer and Gade, 2007b) whereas solid FeS is a common initial product at circumneutral pH (Pyzik and Sommer, 1981; Rickard, 1974).

It has been early recognized that sulfidation of ferric (hydr)oxides also triggers the formation of pyrite (Rickard, 1975). The accepted model for pyrite formation is the reaction between an aqueous FeS species and dissolved polysulfides, which requires solid FeS as a precursor species (cf. review in (Rickard, 2012) and references therein), irrespective of the origin of the reactants. In a recent study, it was demonstrated that sulfidation of lepidocrocite at millimolar S(-II) concentration and at pH 7 is a highly dynamic process (Hellige et al., 2012). High resolution transmission electron microscopy (HRTEM) revealed that lepidocrocite crystals were covered with FeS after 2 h when dissolved S(-II) was completely consumed. FeS started to disappear after 72 h along with the formation of amorphous Fe and S phases. Nanopyrite particles formed after only one week. Cryogenic x-ray photoelectron spectroscopy measurements demonstrate that a substantial fraction (> 50 %) of the S species consisted of surface-bound polysulfides (Wan et al., 2014) with only small amounts (< 1 %) of the initial sulfide being recovered as aqueous polysulfides.

Poulton et al. (2004) investigated the reaction of various ferric (hydr)oxides with dissolved sulfide at pH 7.5 and observed the accumulation of acid extractable Fe(II) which is neither Fe(II) extractable as acid volatile sulphur (AVS) nor is it

exchangeable with other cations. They considered this fraction to be associated with the surface, but the amount of Fe(II) in this pool exceeded the number of sites at the oxides surface by a factor of 10. The nature of this Fe(II) containing phase remained completely unknown. Similarly, a significant fraction of solid-phase Fe(II) in excess to surface Fe(II) associated with sulfur species was observed during sulfidation of lepidocrocite (Hellige et al., 2012). The excess Fe(II) was interpreted as uptake of electrons into the bulk mineral (Gorski and Scherer, 2011). The amount of produced pyrite was higher in experiments in which high concentrations of excess Fe(II) were intermediately formed. It was therefore proposed that the pool of excess Fe(II) triggered the sequence of mineral transformations and promoted the formation of pyrite.

The relative importance of excess Fe(II) formation during the reaction may also depend on the type of ferric iron (hydr)oxide. Poulton et al (2004) observed a range in reactivity towards sulfide covering two orders of magnitude when normalized to surface area. According to our proposed model, channeling of electrons into the bulk structure can therefore be expected to be less significant at low reactivity, i. e. higher crystallinity.

We therefore hypothesize that the extent of excess Fe(II) production and hence the extent of pyrite formation upon sulfidation is different for various ferric (hydr)oxides and depends on their electron transfer properties, but also on their ability to accommodate Fe(II) within the structure. Adsorption of Mössbauer-insensitive ^{56}Fe(II) to various ferric (hydr)oxides revealed dramatic variations in magnetic response of ferrihydrite (Williams and Scherer, 2004), hematite (Larese-Casanova and Scherer, 2007), magnetite (Gorski and Scherer, 2009) and goethite (Gorski and Scherer, 2011) that is being attributed to a varying degree of electron delocalization in the bulk minerals (Gorski and Scherer, 2011). As a consequence, type and concentrations of secondary Fe minerals such as pyrite forming upon the reaction with S(-II) are expected to differ between different ferric iron (hydr)oxides in relation to the relative production of excess Fe(II).

Here, we compare the reductive dissolution of lepidocrocite with those of ferrihydrite and goethite, representing a less stable and a more stable iron oxide phase,

respectively. We conducted batch experiments with the same set-up and analytical methods as described in Hellige et al. (2012) with a focus on the reactivity of these hydr(oxides) in sulfide-rich systems at pH 7 in regard to the reaction rates, intermediate phases, and final products.

3.3 Materials and methods

3.3.1 Ferric (hydr)oxides

Synthetic 6-line ferrihydrite was prepared after Schwertmann and Cornell (2008). Under rapid stirring, 20 g of $Fe(NO_3)_3 \cdot 9\ H_2O$ was added to 2 L 75 °C hot distilled water. After 12 minutes of stirring, the solution was cooled and dialysed for three days. The final product was freeze dried.

Synthetic lepidocrocite and goethite were purchased from Lanxess (Leverkusen, Germany). The trade names are Bayferrox 920 Z for goethite and Bayferrox 943 for lepidocrocite. To remove sulfate from the iron oxides surface (which commercial ferric (hydr)oxides typically contain), 1 mol L^{-1} of each hydroxide was suspended in 0.01 mol L^{-1} $NaNO_3$ and the pH was adjusted to 10 with NaOH. After 4 days of shaking the suspension was washed and freeze-dried.

The ferric (hydr)oxides were characterized using X-ray diffractometry (XRD), scanning electron microscopy (SEM), and transmission electron microscopy (TEM). Lepidocrocite contained 5-10 wt. % goethite and had a particle size of 0.2- 0.4 µm as determined by SEM. Goethite had a particle size of 0.2-0.9 µm. Ferrihydrite particles were < 10 nm as revealed by TEM (cf. Fig. 3.6). Surface area was measured by multi-point BET-N_2 (Brunauer, Emmett and Teller) method (Gemini 2375 Surface Area Analyzer). Surface areas were determined to be 140 $m^2\ g^{-1}$ for ferrihydrite, 17.34 $m^2\ g^{-1}$ for lepidocrocite and 9.12 $m^2\ g^{-1}$ for goethite.

3.3.2 Experimental Set-up

Kinetic batch experiments were conducted in an anoxic glove box at pH 7 at a constant ionic strength of I = 0.1 mol L^{-1} NaCl and at room temperature. In this publication data are presented from those three experiments only where we have a complete data set in regard to wet chemical analysis, TEM and Mössbauer spectroscopy. Additional results from lepidocrocite experiments have been published in Hellige et al (2012). Ferric (hydr)oxide concentrations in these three experiments ranged between 12 and 26.6 mmol L^{-1} and the initial dissolved sulfide concentration between 6.7 and 7.5 mmol L^{-1} (cf. Table 1). Initial sulfide concentrations were in large excess relative to initial surface site concentrations of the three mineral phases (Table 3.1). All reactions were conducted in a 500-mL glass vessel with ports for

sampling, addition of reactants and for a pH electrode. The solution was stirred with a Teflon-coated stirring bar at constant rate. With an automatic pH-stat device the pH value was kept constant by adding HCl (0.5 mol L^{-1}) in the glove box. The reaction suspension was prepared by mixing 50 mL of 0.1 mol L^{-1} NaCl solution containing approx. 1 g ferric (hydr)oxide with 450 ml of 0.1 mol L^{-1} NaCl to which appropriate amounts of NaHS (as a 1:1. mixture between $Na_2S \cdot 9 H_2O$ (0.5 mol L^{-1}) and HCl (0.5 mol L^{-1})) were added. In order to convert the mass of the ferric (hydr)oxides into molar concentrations, the molar mass of ferrihydrite was determined to be 92.3 g/mol after dissolution in 6 N HCl and determination of Fe. Molar masses of 89 g/mol were used for lepidocrocite and goethite. The sulfide concentration was determined before each run.

Table 3.3 Initial experimental conditions for experimental runs where both TEM and Mössbauer spectroscopy was performed. All runs were conducted at pH 7.

Mineral	c(Fe(TOT))[a]	SA Fe(TOT)[b]	SS Fe(TOT)[c]	$c(S(-II)_{ini})$[d]	S(-II):SS ratio
	mmol L^{-1}	m^2 L^{-1}	mmol L^{-1}	mmol L^{-1}	[-]
Ferrihydrite	12	155	0.98	7.5	7.7
Lepidocrocite	26.6	41.1	0.26	7.2	27.8
Goethite	22	17.9	0.11	6.7	57.6

[a] concentration of initial ferric hydroxides

[b] surface area of initial ferric hydroxides

[c] concentration of surface sites was calculated based on a value of $6.3 \cdot 10^{-6}$ mol m^{-2} for all minerals (Peiffer and Gade, 2007a)

[d] concentration of initial added sulfide

During the reaction reaction, aliquots were taken to monitor the time evolution of dissolved Fe(II) and S(-II), Fe(II) extractable with 0.5 N HCl, methanol extractable sulphur, and total iron. Furthermore, solids were retrieved after 1-2 hours, 24 hours, 1 week and 2 weeks and analyzed by Mössbauer spectroscopy and TEM. All solutions were prepared with distilled water and purged with N_2 prior to use to remove dissolved oxygen from solutions. All reagents were of analytical grade.

3.3.3 Sampling and analysis

Iron species. Dissolved Fe(II) ($Fe(II)_{diss}$) was determined after filtration (0.45 µm) using the phenanthroline method (Tamura et al., 1974). Total extractable iron was determined in the suspension prior to the addition of sulfide after dissolution in 6 N HCl and heating at 60 ℃ for 3 days. HCl extractable Fe(II) ($Fe(II)_{HCl}$), which comprises both dissolved and solid phase-bound Fe(II), was extracted with 0.5 N HCl for 1 hour and briefly (2-3 minutes) purged with N_2 , filtered and the Fe(II) was determined in the filtrate as described above. The occurrence of FeS_s and $FeS_{n,s}$ in the samples may lead to an overestimation of HCl extractable Fe(II) through reaction of the liberated H_2S with ferric iron in the acidic extraction solution . In order to test the effect of this reaction on the yield of Fe(II), we have added aliquots of a FeS suspension to a suspension of a predefined amount of the respective ferric hydroxide to obtain a final concentration of 2, 4, 8 and 13.5 mmol L^{-1} FeS and 2g L^{-1} of ferric hydroxide and extracted Fe(II) with 0.5 N HCl at different time steps. FeS was prepared by precipitation from Na_2S (c = 0.4 mol L^{-1}) and $FeCl_2 .4H_2O$ (c = 0.4 mol L^{-1}) in a glove box to obtain a stock solution of 0.2 mmol L^{-1} FeS. Dissolved sulfide and Fe(II)aq in the stock solution were 68 µmol L^{-1} and 16 µmol L^{-1} respectively. Recovery rates after 1 hour ranged between 196 % and 232 % for the four FeS concentrations in case of ferrihydrite. In case of lepidocrocite and goethite, only 13.5 mmol L^{-1} FeS were tested to yield a recovery of 101 % and 95 %, respectively. Hence, measured $Fe(II)_{HCl}$ concentrations were overestimated by about a factor of two when FeS and ferrihydrite were simultaneously extracted. Therefore, in experiments with ferrihydrite a correction factor of two was applied for calculating the amount of excess Fe(II) (Eq. 1). In the experiments with goethite and lepidocrocite, the increase of $Fe(II)_{HCl}$ due to the reduction of Fe(III) during HCl extraction seemed to be within the range of uncertainty.

Sulphur species. Dissolved sulfide ($S(-II)_{diss}$) was determined photometrically by the methylene blue method (Fonselius et al., 1999) after filtration. Methanol extractable sulphur (MES) was measured by high performance liquid chromatography (HPLC, Beckman) combined with UV detection (Detector 168, Beckman) after extraction of 300 µL of unfiltered sample suspended in 1200 µL methanol (modified after (Ferdelman et al., 1991)). Wan et al (2014) demonstrated that MES comprises not only elemental S_8 sulphur but also zero-valent sulphur from polysulfides associated

with the ferric (hydr)oxides surface, probably as Fe(II)-polysulfide associations. After 1 h equilibration time, the suspension was filtered (0.2 µm) and the filtrate was stored at -20 °C until analysis. The precision of this method was estimated from measurements of MES after 10 minutes of reaction of dissolved sulfide with lepidocrocite. The data were taken from five independent experiments documented in Hellige (2011). Since initial concentrations of both dissolved sulfide and lepidocrocite where different in each experiment, it was not possible to calculate the mean value and the standard deviation of the MES measurement. Hence, the relative error was calculated from the amount of MES recovered per mol lepidocrocite and was 13 %.

Mössbauer spectroscopy. 30 mL of the suspension was centrifuged outside the glove box using closed centrifuge tubes. After centrifugation, the supernatant was decanted inside the glove box and the solid phase was dried under a nitrogen stream for 1 minute. After drying, the solid phase was put on a membrane filter (13 mm diameter and 0.45 µm) and was sealed between two layers of Kapton tape (polyimide tape with very low oxygen permeability). The samples were placed in a sealed crimp vial and stored at 4 °C until measurement. Mössbauer spectra were collected with a WissEl Mössbauer gamma-ray spectrometer and a Janis closed-cycle helium gas cryostat at 4.2 K. A Co-57 gamma-ray source was used with a constant acceleration drive system operated in transmission mode. Spectra were calibrated against a spectrum of alpha-Fe(0) foil at room temperature. Data acquisition times were usually about 12-20 hours per spectrum. Spectral fitting was performed using Recoil® software (University of Ottawa, Canada) and Voigt-based spectral lines. Model parameters from the various specimen are listed in Table 3.2. The concentrations of iron mineral phases were calculated by multiplying total Fe concentration by their fitted spectral area, which represents the percentage of the individual mineral phases. The detection limit of Mössbauer spectroscopy is ~ 2% of total Fe.

Transmission electron microscopy. Aliquots of the reacting suspension (after 2 h and 2 weeks) were analyzed by a Philips CM 20-FEG TEM (Bayerisches Geoinstitut, University of Bayreuth), operating at 200 kV. In order to minimize oxidation in air during sample preparation the aliquots collected from the experimental suspension were stored in gas-tight vials until TEM analysis. Immediately before transfer of the sample into the TEM, a drop of the suspension was then taken with a syringe and put

onto a Lacey carbon-coated copper grid. The grid was immediately transferred to the TEM holder and inserted into the high vacuum of the TEM. The short exposure of the sample to air was limited to 1-2 minutes at maximum with this procedure. The chemical composition and the distribution of elements were determined by energy dispersive X-ray (EDX) spectroscopy (Thermo Noran Ge detector).

Table 3.2 Model Parameters used for evaluation of 4.2 K Mössbauer spectra and abundances of the minerals identified.

			Fe(III) sextet						FeS_2		
Sample Time	I[a] mms^{-1}	χ^{2} [b]	<CS>[c] $mm\ s^{-1}$	<QS>[d] $mm\ s^{-1}$	<H>[e] T	# of comp. [f]	Hp [g] T	Abundance	<CS> $mm\ s^{-1}$	<QS> $mm\ s^{-1}$	Abundance
Ferrihydrite			Fe(III) sextet								
1 hr	—	—	—	—	—	—	—	—	—	—	—
1 d	—	—	—	—	—	—	—	—	—	—	—
1 wk	0.11	4.0	0.49	-0.11	49.1	2	50.1	70.7	0.41	0.62	29.3
2 wk	0.11	2.0	0.48	-0.10	48.8	2	49.9	73.6	0.40	0.64	26.4
Lepidocrocite			Lepidocrocite sextet								
1 hr	0.11	1.4	0.50	0.04	44.8	2	45.4	100	—	—	—
1 d	0.11	2.0	0.50	0.04	43.7	3	45.5	100	—	—	—
1 wk	0.11	1.3	0.50	0.04	43.9	3	45.5	98.2	0.42	0.60	1.8
2 wk	0.11	2.0	0.50	0.03	44.4	2	45.4	93.4	0.40	0.65	6.6
Goethite			Goethite sextet								
1 hr	0.11	1.6	0.49	-0.23	50.6	1	50.6	100	—	—	—
1 d	0.11	2.9	0.49	-0.23	50.6	1	50.6	100	—	—	—
1 wk	0.11	2.3	0.49	-0.23	50.6	1	50.6	91.6	0.40	0.64	8.4
2 wk	0.11	1.5	0.49	-0.23	50.6	1	50.6	98.0	0.40	0.64	2.0

Mineral Standards								
Ferrihydrite, 4.2 K		0.48	-0.02	47.4	2	49.9		
Goethite, 4.2 K		0.48	-0.25	50.6	1	50.6		
Pyrite, 77K							0.36	0.64
Pyrite, 4.2 K							0.43	0.66
Marcasite, 80 K							0.37	0.50
Magnetite, 4.2 K	^{IV}Fe(III)	0.37	-0.02	50.1				
	^{VI}Fe(III) 1^{h}	0.49	0.00	52.2				
	^{VI}Fe(III) 2^{h}	0.83	-0.27	49.8				
	^{VI}Fe(II) 1^{h}	1.03	-0.41	48.2				
	^{VI}Fe(II) 2^{h}	0.96	0.89	35.9				

[a] Lorenztian half-width at half-maximum

[b] Reduced chi-squared goodness of fit value

[c] Average center shift

[d] Average quadrupole splitting, average hyperfine magnetic field

[f] Number of Voigt-based components used to model the hyperfine magnetic field

[g] Most probable hyperfine magnetic field value

[h] numbers refer to sites of the corresponding octahedral

3.4 Results

3.4.1 Chemical speciation

In the presence of ferrihydrite and lepidocrocite, dissolved sulfide was consumed within 30 minutes. In contrast, the reaction was slower when goethite was added and more than 5 hours were required to quantitatively remove the added dissolved sulfide (Fig. 3.1). The consumption of $S(-II)_{aq}$ was accompanied by the production of Fe(II) and MES (Fig. 3.1). In all cases, the concentration of dissolved Fe(II) represented only a minor fraction of $Fe(II)_{HCl}$ with a maximum concentration of 0.3 mmol L^{-1} (data not shown). In experiments with ferrihydrite and lepidocrocite, $Fe(II)_{HCl}$ concentrations reached almost instantaneously a level which remained practically constant during the first hour of reaction (Fig. 3.1). Production of $Fe(II)_{HCl}$ also followed $S(-II)_{aq}$ consumption in the experiments with goethite and, consequently, was slower compared to the reaction with ferrihydrite and lepidocrocite. It required The stoichiometric ratio between the concentration of Fe(II) produced until a constant $Fe(II)_{HCl}$ level had established and the $S(-II)_{aq}$ concentration consumed varied between the different starting materials (Table 3.3) ranging from 1.20 for ferrihydrite, 0.76 for lepidocrocite to 0.67 for goethite. Similar experiments performed with various initial concentrations of lepidocrocite demonstrated that ratios > 0.8 coincide with a significant fraction of excess Fe(II) not bound in the form of Fe(II) associated with sulphur (cf. Table 3 in Hellige et al. (2012)). Observations made by Wan et al (2014) imply that Fe(II) associated with surface polysulfide ($FeS_{n,s}$) can be also extracted with HCl. Hence $Fe(II)_{HCl}$ comprises FeS_s, $Fe(II)_{excess}$, and $FeS_{n,s}$.

Table 3.3 Concentrations of products during the reaction of H_2S with the three ferric (hydr)oxides after constant values were reached. Values for ferrihydrite and lepidocrocite correspond to t = 2 h, while those for goethite to t = 8 h

Mineral	$S(-II)_{ini}$	S °	$Fe(II)_{HCl}$	Excess Fe(II)	Fraction of excess Fe(II)	Protons consumed
	mmol L^{-1}	mmol L^{-1}	mmol L^{-1}	mmol L^{-1}	(%)	mmol L^{-1}
Ferrihydrite	7.5	5.1	9.0	4.2	46	1.2
Lepidocrocite	7.2	3.7	5.5	2.0	36	2.4
Goethite	6.7	1.5	4.5	-0.7	0	2.8

The results from that study further imply that the concentration of these surface Fe(II) sulphur species (FeS_s and $FeS_{n,s}$) can be estimated by the concentration difference between initially added sulfide and MES. We therefore calculated the amount of excess Fe(II) based on the S mass balance as

$$c(\text{excess-Fe(II)}) = c(Fe(II)_{HCl}) - F \cdot [c(FeS) + c(FeS_{n,s})]$$

$$= Fe(II)_{HCl,const} - F \cdot [c(S(-II)_{initial}) - c(MES_{const})], \qquad (1)$$

where $Fe(II)_{HCl,const}$ and MES_{const} are concentrations of $Fe(II)_{HCl}$ and MES after a constant concentration level was obtained, i. e. 2 h in case of ferrihydrite and about 5 hours, before the increase of $Fe(II)_{HCl}$ ceased.

lepidocrocite and 8 h in case of goethite. F is a correction factor that accounts for the generation of Fe(II) through reaction between Fe(III) and H_2S liberated from FeS_n species during the extraction. Based on the recovery tests of $Fe(II)_{HCl}$ in the presence of FeS_n species, F was set to be 2 for ferrihydrite, and 1 for lepidocrocite and goethite, respectively.

The largest fraction of Fe(II) in excess of FeS_s and $FeS_{n,s}$ was found for ferrihydrite (~ 46 % of HCl extractable Fe(II)). It was smaller for lepidocrocite (36 %) and even negative for goethite (Table 3.3). The negative value probably reflects the uncertainty inherent to the analytical methods so that the fraction of excess Fe(II) is assumed to be zero in case of goethite.

In the presence of ferrihydrite, the concentration of $Fe(II)_{HCl}$ achieved a maximum of almost 12 mmol L^{-1} at 48 hours. Even if one accounts for an overestimation of extractable Fe(II) due to interference with AVS during acidic extraction, a significant fraction of the initial amount of Fe(III) in ferrihydrite was reduced (Fig. 3.1A). After 48 hours, however, $Fe(II)_{HCl}$ and MES started to decrease for all three minerals. The decrease was more pronounced for $Fe(II)_{HCl}$ and most prominent in experiments with ferrihydrite (Fig. 3.1A).

Visually, all ferric suspensions turned black during the reaction with dissolved sulfide indicating formation of a solid FeS phase. After 2 weeks the black coloration of the suspensions disappeared for goethite and lepidocrocite while the ferrihydrite suspension remained black.

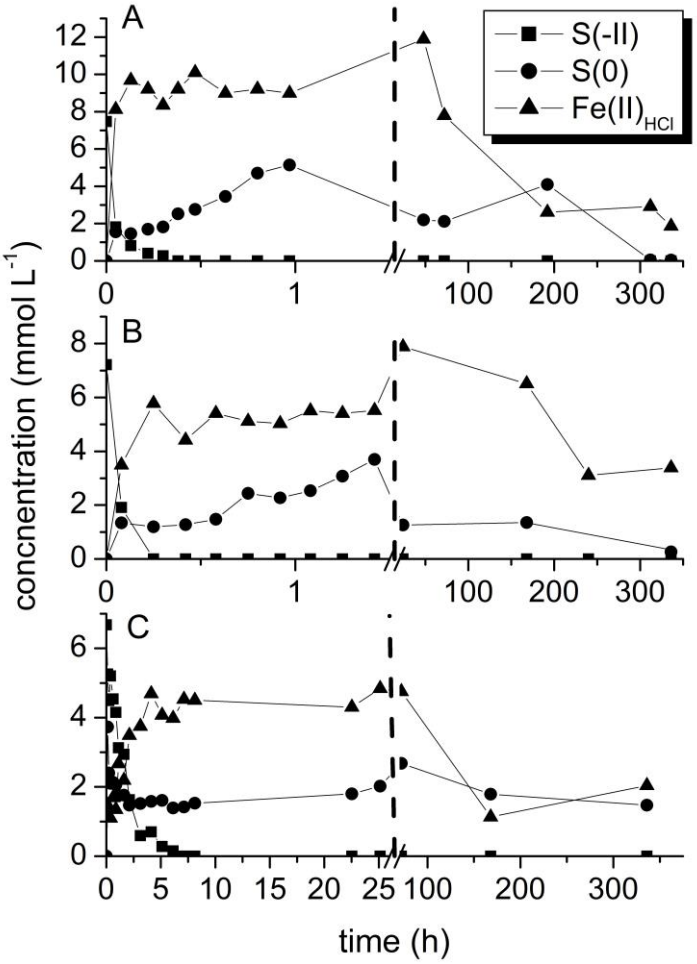

Fig. 3.1 Time evolution of sulphur and iron species during the reaction between dissolved sulfide and ferrihydrite (A), lepidocrocite (B), and goethite (C). Note the different time scale for goethite.

When constant concentration levels of MES and $Fe(II)_{HCL}$ were established, H^+ consumption was comparable for lepidocrocite and goethite with 2.4 mmol L^{-1} after 2 h and 2.8 mmol L^{-1} after 8 h, respectively (Fig. 3.2). Additional 0.8 mmol L^{-1} (lepidocrocite) and 0.4 mmol L^{-1} (goethite) of alkalinity were generated in the following 2 weeks. In the reaction with ferrihydrite, the amount of consumed H^+ was distinctly lower with only 1.2 mmol L^{-1} H^+ after 2 hours and additionally 0.4 mmol L^{-1} H^+ in the following 2 weeks. A drop in pH which could not be balanced by the pH-stat device (addition of HCl) occurred after 250 h in the experiment with ferrihydrite and lepidocrocite.

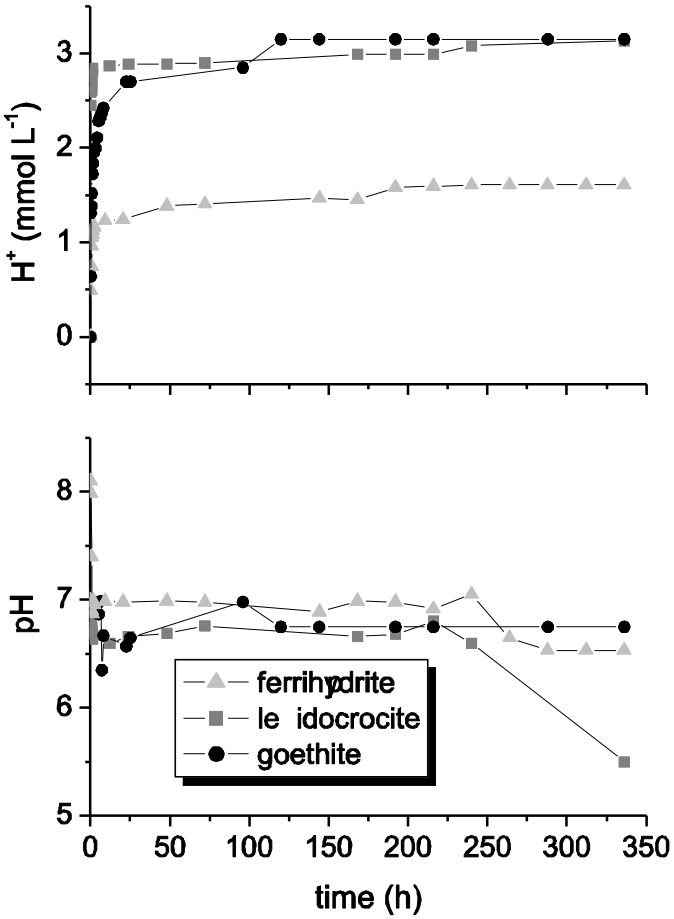

Fig. 3.2 pH progress (bottom) and H^+ consumption (top) during the reaction between ferrihydrite, lepidocrocite, and goethite with dissolved sulfide.

The three ferric (hydr)oxides showed the same chemical reaction pattern but the velocity of dissolved sulfide consumption was different. The reactivity was very high for lepidocrocite and ferrihydrite with the initial rate constant k_{obs} being in the same order of magnitude (~ $5 \cdot 10^{-3}$ L m^{-2} min^{-1}). It was significantly slower for goethite ($5 \cdot 10^{-4}$ L m^{-2} min^{-1}, cf. also Fig. 3.1). Initial rate constants k_{obs} were determined as pseudo first-order rate constant obtained from the concentration change of $c(S(-II)_{aq})$ with time divided by the surface area concentration of the ferric (hydr)oxides. Values for ferrihydrite and lepidocrocite bear some uncertainty due to the poor time resolution.

3.4.2 Spectroscopic and microscopic results

3.4.2.1 Mössbauer Spectroscopy

Mössbauer spectra revealed a dynamic transformation process with distinct differences between the three oxyhydroxides. The dominant signal in spectra from solids collected in experiments with lepidocrocite and goethite (Fig. 3.3 and Fig. 3.4) could be clearly attributed to the starting minerals. Six-line signals (sextets) with narrow line-widths were identified as lepidocrocite and goethite, respectively, based on model parameters that were consistent with an oxidation state of Fe(III) in a high-spin octahedral configuration similar to that in synthetic minerals with Fe(III) in its antiferromagnetic state.

In contrast to lepidocrocite and goethite, sextets were present after one week within spectra of solids from the original ferrihydrite experimental suspensions (Fig. 3.5). These sextets demonstrate abundance of iron in the Fe(III) oxidation state but they do not provide clear indication for the presence of ferrihydrite. The broad peaks and the large number of parameters (cf. Table 3.2) made it impossible to find a unique solution. The sextets represent iron which is magnetically ordered at this temperature and belong to a mixture of various minerals that may represent a combination of goethite, hematite, and magnetite as observed in TEM spectra (cf. below). Unfortunately, we could not collect enough material for the analysis of the first two samples of the ferrihydrite experiments taken after 1 hour and 24 hours (data not shown).

In spite of the large fraction of excess Fe(II) that was derived from wet chemical analyses in the presence of ferrihydrite and lepidocrocite in the initial phases of the experiment (eq. 1), no signals could be retrieved from the Mössbauer spectra that could be attributed to an Fe(II) containing phase.

After one week a second signal emerged in the form of a doublet in the presence of all ferric hydroxides. We exclude the possibility of this signal being an iron (hydr)oxide phase because crystalline iron (hydr)oxides, even paramagnetic ones, do not produce doublet signals at 4.2 K and instead produce sextet signals. However, diamagnetic iron sulfides such as pyrite and marcasite can remain as doublet signals when analysis temperature is 4.2K (Murad and Cashion, 2004). Pyrite and marcasite share the same

unit cell formula (FeS_2) and have low-spin octahedral Fe(II) configurations with paired d-orbital electrons that allow the minerals to remain paramagnetic at 4.2 K.

The abundance of FeS_2 was very high (almost 30 %) in ferrihydrite experiments after 1 week and slightly decreased or remained constant after 2 weeks (Table 3.2, Fig. 5). In the lepidocrocite experiments, the abundance was significantly smaller in the first week (1.8 %, Table 3.2, Fig. 3.3) compared to ferrihydrite but strongly increased to 6.6 % by the end of the second week. In the case of goethite, the signal seems to have decreased with time (Fig. 3.4). 8.4 % of the initially added goethite was transformed into FeS_2 after 1 week with only 2 % remaining after 2 weeks (Table 3.2). This observation, however, needs to be used with caution. Parts of the suspension of the sample taken after 2 weeks seem to have passed the filter during the filtration process so that the recovery of the solid material was probably incomplete in the goethite experiment. Based on these results 26.4 %, 6.6 %, and at least 2 % of the initially added ferrihydrite, lepidocrocite, and goethite, respectively, were converted into FeS_2 after two weeks (Table 3.2). From these values the concentration of pyrite Fe and consequently that of pyrite S can be derived, which was 6.3 mmol L^{-1} for ferrihydrite, 1.8 mmol L^{-1} for lepidocrocite and 0.9 mmol L^{-1} for goethite. This implies that the conversion efficiency of the initially added S(-II) in this time period varied strongly between the minerals. It was 85 % for ferrihydrite, 49 % for lepidocrocite and 13 % for goethite.

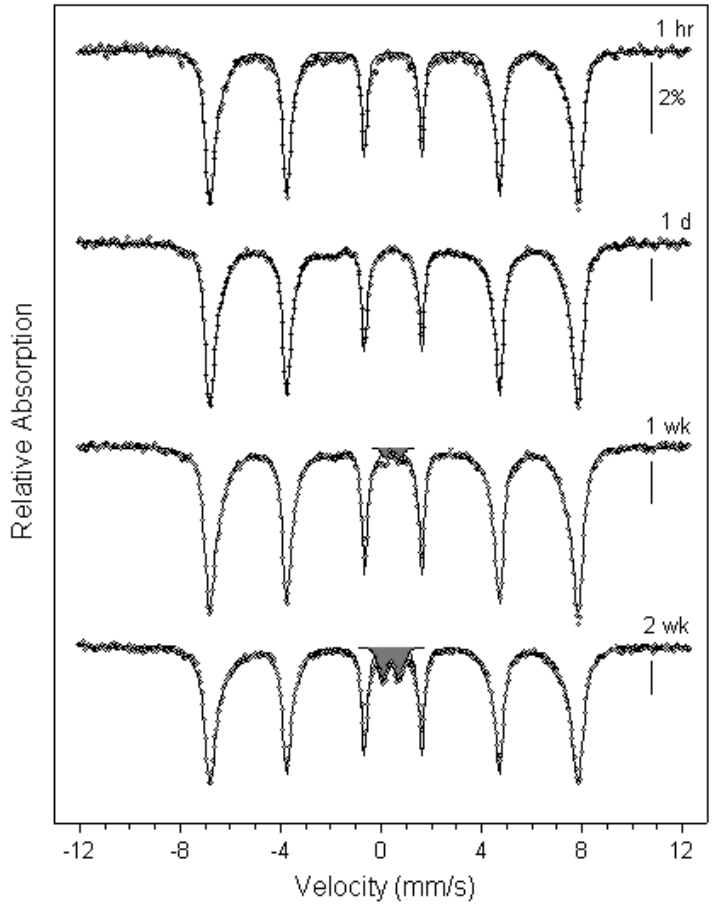

Fig. 3.3 Mössbauer spectra of lepidocrocite reacted with sulfide after 1 hour, 1 day, 1 week, and 2 weeks. White sextets correspond to lepidocrocite, and gray shaded to FeS_2. All spectra were collected at a temperature of 4.2 K. The scale bar represents 2% absorption for each spectrum. Solution conditions are listed in Table 3.1, and model parameters are listed in Table 3.3.

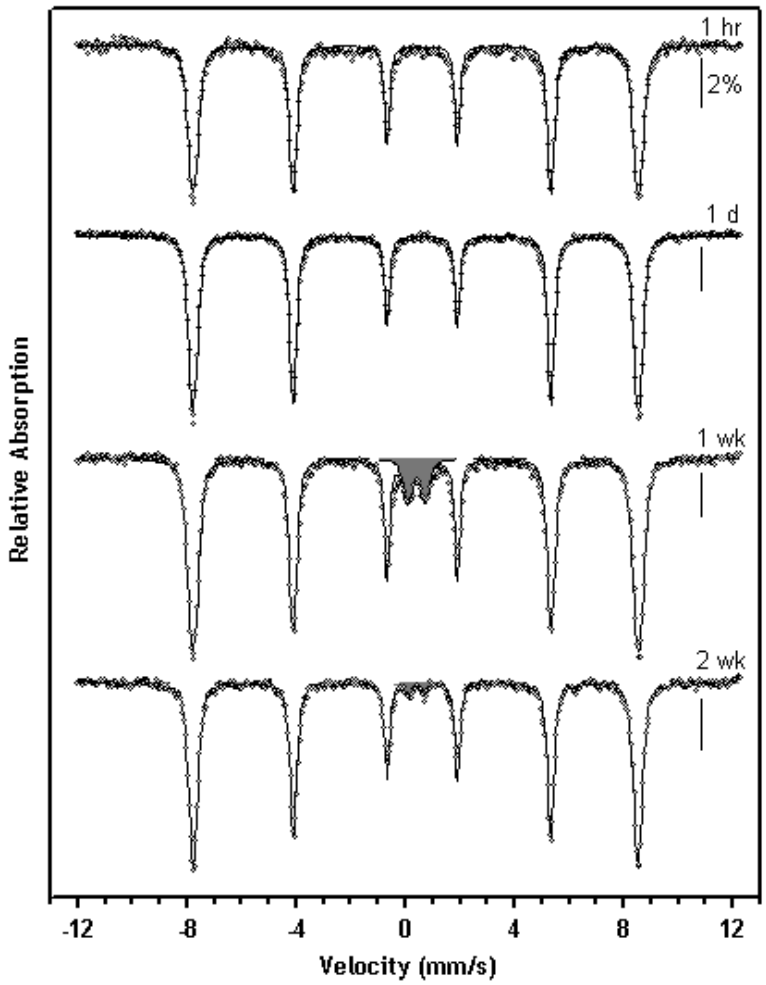

Fig. 3.4 Mössbauer spectra of goethite reacted with sulfide after 1 hour, 1 day, 1 week, and 2 weeks. White sextets correspond to goethite and gray shaded doublets to FeS_2. All spectra were collected at a temperature of 4.2 K. The scale bar represents 2% absorption for each spectrum. Solution conditions are listed in Table 1, and model parameters are listed in Table 3.

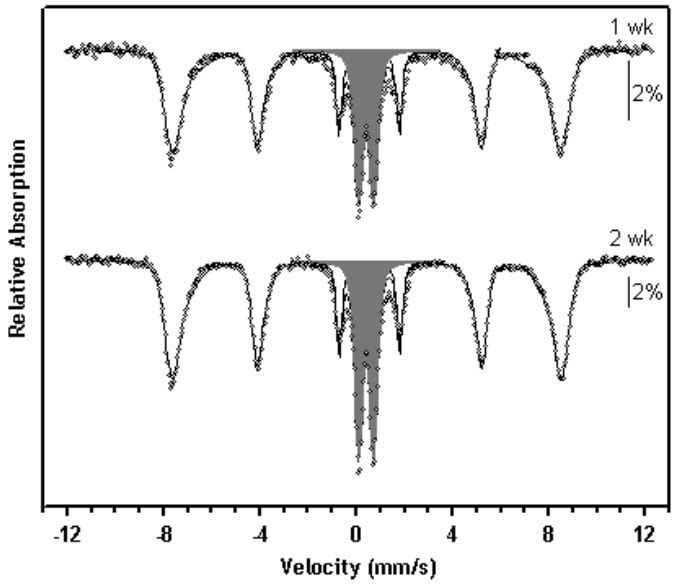

Fig.3.5 Mössbauer spectra of ferrihydrite reacted with sulfide after 1 week and 2 weeks. White sextets are bulk models for all Fe(III) (hydr)oxides present and may represent a combination of the goethite, hematite, and magnetite observed by TEM. Gray shaded doublets reflect signals from FeS_2. All spectra were collected at a temperature of 4.2 K. The scale bar represents 2% absorption for each spectrum. Solution conditions are listed in Table 3.1, and model parameters are listed in Table 3.3.

3.4.2.2 TEM Analysis

TEM analyses confirmed the dynamic transformation process occurring upon sulfidation of the various ferric (hydr)oxides. In particular, it revealed insight into the fate of sulfide during the reaction progress which was clearly different between the minerals.

TEM images display well-defined grains of ferrihydrite after 2 h of reaction with dissolved sulfide without any changes in either the morphology of the particles and or their electron diffraction patterns compared to the unreacted starting material. Hence, the almost complete reduction of Fe(III) in the initial phase, as implied by wet chemistry data, has not led to changes in the ferrihydrite structure detectable with TEM. Furthermore, the formation of other distinct different secondary phases was not observed. EDX mapping demonstrated that sulphur was evenly distributed and was probably adsorbed on the ferrihydrite surfaces (Fig. 3.6 d,e) as ferrous polysulfide associations (Wan et al., 2014).

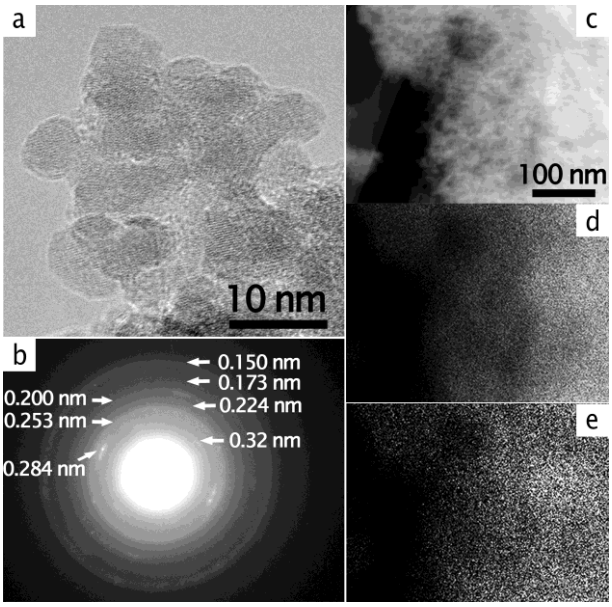

Fig. 3.6 High resolution TEM image (a) and electron diffraction pattern (b) of ferrihydrite after 2 hours reaction with dissolved sulfide. Dark-field STEM image (c) and EDX maps of iron [Fe Kα] (d) and sulphur [S Kα] distribution (e) show that sulphur was evenly distributed on the solid phase.

In contrast, the experiments performed with lepidocrocite revealed the formation of sulphur-rich rims around the lepidocrocite crystals that could be attributed to the nucleation of mackinawite by high resolution TEM images and electron diffraction (cf. Fig. 6 in Hellige et al., (2012)). Additionally, a thin layer of magnetite could be identified at the interface between the mackinawite and lepidocrocite structure which disappeared after 2 weeks of reaction (Hellige et al., 2012).

Goethite crystals were surrounded by a layer of mackinawite of variable thickness (Fig. 3.7, b,c) at the end of the first phase of the reaction (2 hours). In contrast to lepidocrocite, no evidence for a magnetite layer was found between the goethite core and the surrounding mackinawite layers. Greigite was not detectable in any of the experiments.

After two weeks of reaction, the appearance of particles retrieved from ferrihydrite experiments has changed completely. TEM images confirmed the complete transformation of ferrihydrite and the formation of new phases which is consistent with the chemical data and Mössbauer spectra. Table 3.4 shows the interplanar spacings (d-values) of the phases which can predominantly be attributed to the structures of magnetite, hematite and pyrite (Fig. 3.8 a,d,e). Only minor amounts of goethite were observed. In contrast to lepidocrocite and goethite, the black coloration of the suspension did not disappear towards the end of reaction which might be due to the very small size (50 – 100 nm, Fig. 3.8e) of the newly formed iron oxide particles.

Table 3.4 Interplanar spacings and corresponding lattice planes of the phases formed after 14 days of reaction of ferrihydrite with sulfide identified by electron diffraction and fast Fourier transformation of high resolution images.

pyrite		hematite		magnetite		goethite	
d_{hkl} [Å]	(hkl)	d_{hkl} [Å]	(hkl)	d_{hkl} [Å]	(hkl)	d_{hkl} [Å]	(hkl)
3.12	111	3.70	012	4.86	111	4.18	101
2.71	200	2.76	104	2.95	220	2.72	301
2.42	210	2.54	110	2.52	311	2.56	210
2.21	211	2.23	113	1.48	440	2.24	211/102
1.93	220	1.79	024			2.18	401
1.64	311	1.71	116				
1.47	312	1.46	214/300				
1.21	420						

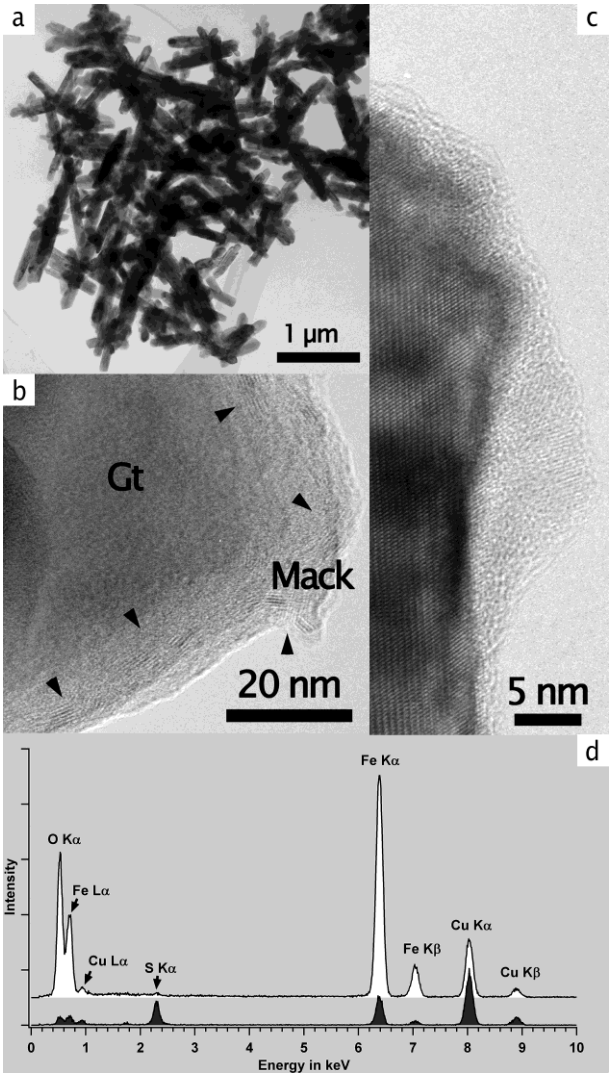

Fig. 3.7 Bright field TEM image (a) of the apparently pristine particle size and morphology of goethite after 2 hours of reaction. High resolution TEM images (b, c) reveal sulphur rich rims on goethite crystals. Lattice fringes in these rims are characteristic for mackinawite (FeS). EDX spectra (d) taken from the rims (black) and in the centre of goethite crystals (white) reveal the formation of iron sulfide with a Fe:S ratio close to 1:1 on the goethite surface.

In all samples collected from experiments after two weeks, electron dense particles were detected (Fig. 3.8a, Fig. 3.9a, cf. also Fig. 8d in Hellige et. al., (2012)). The morphology of the aggregated assemblages resembles quadric outlines (black squares) indicating an Ostwald ripening process to attain lower surface energy. EDX spectra revealed an Fe:S ratio of 1:2 in the black squares and electron diffraction identified

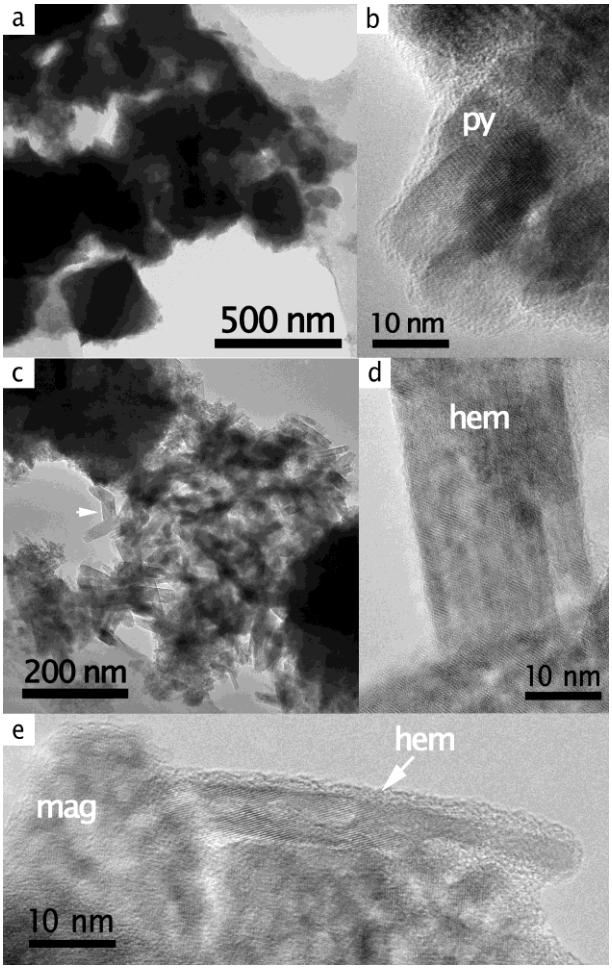

Fig. 3.8 Bright field (a, c) and high resolution (b, d, e) TEM images after 2 weeks of reaction between ferrihydrite and dissolved sulfide. Pyrite crystals are characterized by quadratic outlines and occur separated from ferric oxides (a, c). The aggregates consisted of agglomerated nanocrystalline domains (b). Ferrihydrite was completely transformed into hematite (arrow in c, d, e) and magnetite (e).

the occurrence of pyrite. All these features point towards the presence of anocrystalline pyrite domains that may have formed by oriented aggregation (Penn, 2004). These structures were not directly connected to the iron oxide crystals, suggesting that the primary particles formed by precipitation and not solid phase transformation.

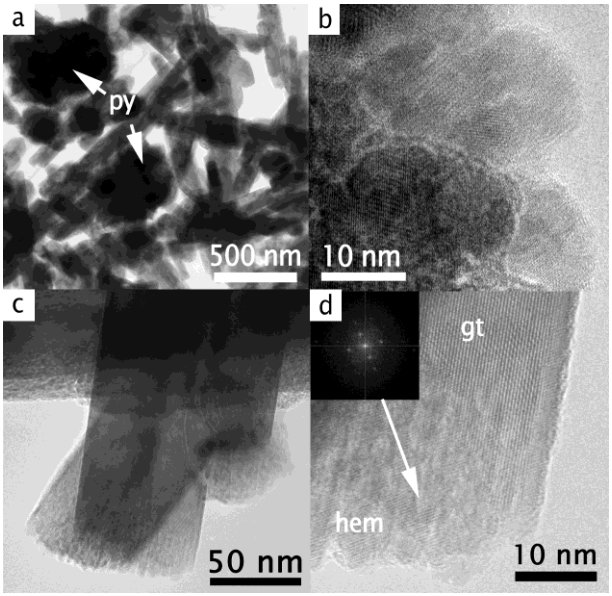

Fig.3.9 Bright field TEM image (a) showing the distribution of goethite and pyrite after 2 weeks reaction. The pyrite crystals consisted of nanocrystalline aggregates (b). Bright field TEM images (c, d) and FFT electron diffraction pattern (inset in d) revealed that minor amounts of goethite were transformed into hematite, preferably at the top of the acicular goethite crystals.

Additionally to pyrite, small amounts of hematite were detected in the goethite rims with a thickness of ~ 20 nm (Fig. 3.9d), preferably at the top of the acicular goethite crystals.

In conclusion, mineral transformations occurred in experiments with all three oxides during the second phase of the reaction. However, after 2 weeks of reaction the extent of these transformations and the composition of the solids differed. In particular, the formation of other iron oxides and pyrite was less pronounced in experiments with goethite than with lepidocrocite and ferrihydrite, whereas complete transformation into secondary minerals occurred in experiments with ferrihydrite.

3.5 Discussion

3.5.1 Formation of excess Fe(II)

Formation of non sulphur-associated excess Fe(II) is antagonistic to the formation of $FeS_{s.}$ Mackinawite is a very early product of the interaction between both, lepidocrocite and goethite and dissolved sulfide. A thin layer (~10-20 nm) of mackinawite was observed in the presence of lepidocrocite and goethite. FeS_s turned out to be the largest fraction (50 – 70 %) of surface sulphur species detected with cryostat XPS in a comparable experimental approach (Wan et al., 2014). In contrast, in experiments with ferrihydrite, in which the fraction of excess iron was highest, no mackinawite was detected. Hence, an inverse relationship seems to exist between the formation of mackinawite and excess Fe(II) within the first hours, which we relate to processes occurring at the mineral surface.

The reductive dissolution of ferric hydroxides is assumed to be preceded by a reversible surface complexation step (Dos Santos Afonso and Stumm, 1992)

$$>Fe_{III}OH + HS^- \leftrightarrow >Fe_{III}S^- + H_2O \quad (2),$$

which is followed by electron transfer

$$>Fe_{III}S^- \leftrightarrow >Fe_{II}S \quad (3)$$

and the release of an S radical

$$>Fe_{II}S + H_2O \leftrightarrow >Fe_{II}OH_2^+ + S^{\bullet -} \quad (4)$$

that readily reacts further. The rate limiting step is regarded to be the regeneration of a surface site. One possibility for the regeneration of a surface site is the detachment of Fe(II) (Dos Santos Afonso and Stumm, 1992)

$$>Fe_{II}OH_2^+ \rightarrow \text{new surface site} + Fe(II) + H_2O \quad (5)$$

The consumption rate of dissolved sulfide is different between the three hydroxides. The formation of Fe(II) occurs at a similar rate as the sulfide consumption in all cases (Fig. 3.1) indicating that the disappearance of dissolved sulfide from solution is not only due to sorption but is directly linked to the electron transfer reaction. Hence, the key to understand the formation of non sulphur-associated Fe(II) is related to the

regeneration mechanism of surface sites (eq. 5). At neutral pH, other pathways than release of Fe(II) into solution might be important: electron transfer into the bulk phase and surface precipitation of FeS_s.

Adsorbed Fe(II), which is equivalent to the surface complex $>Fe_{II}OH_2^+$ in eq. (5), is known to exchange electrons with the bulk phase of various ferric hydroxides. Hiemstra and van Riemsdijk (2007) postulate, based on modelling of charge densities arising from adsorption isotherms, that adsorption of Fe(II) to lepidocrocite requires complete surface oxidation via electron transfer to the bulk mineral,

$$>Fe_{II}OH_2^+ + Fe_{III}(bulk) \xrightarrow{k_{et}} >Fe_{III}OH + Fe_{II}(bulk) + H^+ \qquad (6)$$

Goethite and 2-line ferrihydrite revealed a much lower tendency for electron exchange and a larger fraction of adsorbed Fe(II). Pedersen et al. (2005) observed complete electron transfer between adsorbed Fe(II) and bulk ^{55}Fe(III) ferrihydrite within 2 days, while goethite and lepidocrocite reacted significantly lower. They measured characteristic reaction times ($1/k_{obs}$) for electron transfer ranging between 100 min for ferrihydrite and 23000 min for goethite. Rapid electron transfer was reported by Williams and Scherer (2004) to occur after 6 h equilibration between Fe(II) and bulk goethite and ferrihydrite. Silvester et al. (2005) reported considerable oxidation of Fe(II) upon adsorption onto 2-line ferrihydrite and goethite and its incorporation into the bulk oxide. Jang et al.(2008) observed electron transfer between Fe(II) and bulk goethite Fe(III) that reached equilibrium after 7 days with a characteristic reaction time of 1000 min based on measurements of natural abundance isotope fractionation upon adsorption of Fe(II). Interestingly, they could not retrieve the added Fe(II) and attributed this observation to the formation of structurally bound Fe(II), while other researchers were able to recover Fe(II) with dilute HCl from the bulk phase (Catalano et al., 2010; Handler et al., 2009; Williams and Scherer, 2004). Handler et al.,(2009), in a similar experimental approach, observed almost complete electron transfer between Fe(II) and bulk goethite within 30 days.

Note, that the electron transfer reported in the literature does not appear to create Mössbauer sensitive Fe(II) entities, which is in line with our observations. Attempts to follow the fate of ^{57}Fe(II) adsorbed onto 2-line ferrihydrite and goethite by Mössbauer spectroscopy failed (Silvester et al., 2005). The authors were not able to detect the Fe(II) character and interpreted this observation as a complete conversion of Fe(II)

into the host mineral by electron transfer between adsorbed $^{57}Fe(II)$ and the surrounding Fe(III) neigbours. Similar observations were made by Williams & Scherer (2004).

As this review shows there is clear evidence from the literature for electron transfer between adsorbed Fe(II) and bulk Fe(III) for all three minerals investigated in this study. It seems, however, that there are distinct differences in the reaction kinetics, with goethite being the slowest reactant and ferrihydrite being the fastest. Electron transfer with ferrihydrite proceeds on the time scale of the initial phase in this study, i. e. the first two hours.

Alternatively to bulk electron transfer, Fe(II) at the surface may be channeled into FeS_s. The rate of FeS_s formation is very fast with a characteristic reaction time $t_r = 1/k$ of about ~ 0.1 sec and a dependence on the concentration of total dissolved sulfide (Rickard, 1995). Based on the TEM images it is reasonable to assume growth of mackinawite directly on the host mineral ś surface

$$>Fe_{II}OH_2^+ + HS^- \xrightarrow{k_{FeS}} \text{new surface site} + FeS_{surf} + H_2O \qquad (7)$$

Hence, we can envision two competitive reactions for the regeneration of surface sites: bulk electron transfer that is mineral specific (eq. 6) and FeS_s growth that depends on the concentration of dissolved sulfide (eq. 7). These considerations explain the different extent of excess Fe(II) formation for the different iron (oxy)hydroxids and also provide a conclusive model for the relationship between the fraction of excess Fe(II) and the initial ratio of dissolved S(-II) concentration to surface-site concentration ($S(-II)_{aq}$: SS ratio) observed in Fig. 3.10 of Hellige et al. (2012). At high ratios reaction (7) is favourable. With decreasing ratios reaction (6) becomes more favorable. The extent of the reaction depends on the specific mineral (eq. 8) with k_{et} being the mineral specific pathway controlling parameter (eq. 8).

$$\frac{d\{>Fe_{II}OH_2^+\}}{dt} = \begin{cases} -k_{FeS} \cdot \{>Fe_{II}OH_2^+\} \cdot c(HS^-) & \text{high } S(-II)_{aq}\text{:SS ratio} \\ -k_{et} \cdot \{>Fe_{II}OH_2^+\} \cdot c(Fe_{III}(bulk)) & \text{low } S(-II)_{aq}\text{:SS ratio} \end{cases} \qquad (8)$$

This model allows us to reinterpret the shape of the fraction of excess Fe(II) data determined in experiments with lepidocrocite plotted as a function of $S(-II)_{aq}$: SS ratios in Fig. 10 of Hellige et al. (2012). The inflection point in this Figure reflects the $S(-II)_{aq}$:SS ratio at which the reaction rate for the formation of excess Fe(II) (i. e. electron transfer) exceeds that of FeS_s formation. The rapid electron transfer from Fe(II) to ferrihydrite reported by Pedersen et al. (2005) predicts that formation of FeS_s is rather impropable, in agreement with our TEM analyses which do not indicate mackinawite formation. In contrast, the electron transfer rate is low with goethite so that reaction (7) is favorable for this mineral and mackinawite forms at the crystal rims while excess Fe(II) formation is neglectable.

3.5.2 The role of excess Fe(II) as a driver of secondary phase formation

The most striking observation in this study is that the yield of pyrite in relation to the initially added sulfide varies significantly between the three ferric hydroxides and that the fraction of pyrite S after two weeks reaction time is related to formation of excess Fe(II) in the early stage of the reaction (Table 3.5).

Table 3.5 Relationship between fraction of excess Fe(II) after 2 h (lepidocrocite and ferrihydrite) or 8 h (goethite) reaction time and pyrite yield after 14 days.

	ferrihydrite	lepidocrocite	goethite
Fraction of excess Fe(II) after 2 – 8 h [% of $Fe(II)_{HCl}$]	46	36	0
Fraction of pyrite S after 14 days [% of initial S(-II)]	84	50	13

Spontaneous pyrite nucleation from aqueous solution is regarded to occur if a critical oversaturation is exceeded with regard to the activity product $a(Fe^{2+})\ a(H_2S)/a(H^+)^2$ which is reported to be 5.7×10^{-14} $mol^2\ L^{-2}$ at pH 7 (Harmandas et al., 1998; Rickard, 2012). It is argued that such a critical value is achieved already if the system is saturated with respect to FeS_s (Rickard, 2012). However, TEM images clearly demonstrate that there is no FeS left at the time when pyrite nanoparticles are precipitating. Further, dissolved sulfide was rapidly consumed to become

undetectable (< 10^{-6} mol L^{-1} after max 5 h in case of goethite). The maximum oversaturation possible based on this value and a measured dissolved Fe(II) concentration (0.3 mmol L^{-1}) is 2×10^{-11} mol^2 L^{-2} (no speciation of Fe(II) and no ionic strength considered), which is still three orders of magnitudes lower than the critical value. Hence, nucleation of pyrite from solution species seems improbable.

In our previous paper (Hellige et al., 2012) we have proposed a mechanism which explains the relationship between excess Fe(II) and pyrite formation. According to the mechanism, excess Fe(II) is a reductant for S° promoting the formation of pyrite through generation of polysulfides, which are regarded key precursors for the formation of pyrite (e. g. (Rickard and Luther, 2007))

$$2\ Fe^{2+}_{excess} + S_n + 4\ H_2O \leftrightarrow 2\ FeOOH + S_n^{2-} + 6\ H^+ \qquad (9)$$

Interestingly, no or only small amounts of dissolved polysulfides could be detected in comparable experiments while a substantial fraction of surface bound sulphur consisted of polysulfides (Wan et al., 2014). We therefore propose that dissolved polysulfides may react with surface bound Fe(II) to form surface bound precursors of pyrite.

HCl extractable Fe(II) as well as MES were significantly reduced or even disappeared in experiments with the three different iron oxyhydroxides after 14 days supporting the model proposed in reaction (9). Based on the stoichiometry of reaction 9, protons are generated which can explain the drop in pH in experiments with lepidocrocite and ferrihydrite (Fig. 3.2). Formation of surface-bound polysulfides gives rise to pyrite precipitation as suggested by the appearance of pyrite in Figs. 3.8a and 3.9a of this paper and Fig. 8d in Hellige et al (2012), implying that pyrite is not formed by solid phase transformation.

Besides the formation of pyrite, the unidentified fraction of excess Fe(II) might also trigger the transformation of ferrihydrite and lepidocrocite into iron (hydr)oxides with higher thermodynamic stability. Electron transfer between adsorbed Fe^{2+} and the bulk mineral is known to stimulate transformation of the receiving mineral (Cornell and Schwertmann, 2006). Indeed, secondary formation of iron oxyhydroxides occured in experiments with all three initial materials but at different rates and at different extent.

The most pronounced alterations happened with ferrihydrite. Selected area electron diffraction indicates that the ferrihydrite structure remained intact after 2 hours of reaction (Fig. 3.6). After one week, ferrihydrite transformed into a mixture of hematite, goethite and magnetite. Consumption of HCl was much lower compared to the other oxides (Fig. 3.2) which is a clear hint to the generation of protons along with the formation of the transformation products taking place already in a very early stage, e. g. during the formation of magnetite (for simplicity reasons we have used the stoichiometric formula $Fe(OH)_3$ for ferrihydrite in equation (10):

$$2\ Fe(OH)_3 + Fe^{2+} \rightarrow Fe_3O_4 + 2\ H_2O + 2\ H^+ \qquad (10)$$

Ferrihydrite has a similar anionic framework as hematite with the same stacking of close-packed anions. Liu et al. (2009) proposed that the nucleation and growth of hematite from ferrihydrite involved a combination of dehydration and rearrangement processes which are facilitated by the structural resemblance between these two minerals.

In contrast, goethite and magnetite are products related to Fe(II) driven reductive transformation (Cornell and Schwertmann, 2006). Pederson et al. (2005) observed complete ferrihydrite transformation into goethite at an aqueous Fe(II) concentration of 1 mmol L^{-1} within 2 days. They found, however, that lepidocrocite is the main product at a lower Fe(II) concentration of 0.2 mmol L^{-1}. Similarly, also the occurrence of magnetite seems to depend on aqueous Fe(II) concentration, with magnetite being generated from ferrihydrite at high concentrations (~ 2 mmol L^{-1}) only (Hansel et al., 2005). Pedersen et al. (2005) observed magnetite as a product from transformation of lepidocrocite at their highest experimental aqueous Fe(II) concentration of 1 mmol L^{-1}.

High concentrations of ferrous iron in solution also reflect a high degree of adsorbed Fe(II). Hence, the occurrence of goethite and magnetite as transformation products may be also related to the amount of excess Fe(II) so that this entity may drive transformation pathways in our systems. For example, magnetite forms as an intermediate layer between the lepidocrocite crystal and mackinawite surface coverage after reaction with sulfide (Hellige et al., 2012), while no magnetite is observed in experiments with goethite when no excess Fe(II) is produced.

Surprisingly, no transformation after reaction with aqueous Fe(II) has been reported for goethite although significant isotopic exchange between aqueous Fe(II) and solid phase Fe(III) could be observed (Handler et al., 2009; Jang et al., 2008; Pedersen et al., 2005). Handler et al. (2009) interpreted this effect in terms of conveyer-belt model according to which electron transfer occurs, but the new Fe(III) will lead to isostructural growth at separate goethite surface sites with now reduced Fe(II) being released back into solution. It remains speculative as to whether such a response to Fe(II) adsorption would also explain the reaction kinetics between sulfide and the goethite surface and thus the low formation rate of excess Fe(II). However, it becomes clear that no reductive transformation product should be expected in the goethite experiments. The traces of hematite observed at the top of acicular goethite crystals are probably due to a ripening process.

3.6 Conclusion

The results of this work give reason to the proposition of pathway for rapid pyrite formation that is based on three steps: i) sulfidation of ferric hydroxides, ii) generation of bulk electrons, and iii) generation of (surface bound) polysulfides by bulk electrons. These reactions are accompanied by a series of transformation steps. Depending on the iron hydroxide phase and the initial concentration of dissolved S(-II), different pathways of solid product formation appear on both, the ferric hydroxide side and the sulphur side, which implies a clear kinetic control of these reactions that are of high relevance for early diagenetic processes.

We propose that it is the rate of surface polysulfide generation (eq. 9) and subsequent reaction with precursors bound to the host mineral ́s surface that controls the overall rate of this sulfidation pathway. Pyrite formation pathways based on dissolution of solid FeS_n to aqueous FeS (FeS-pathway) and subsequent reactions with dissolved polysulfides in the absence of ferric oxides are comparatively slow (on the order of several months to years, e. g. Luther, (1991)). Hence, the sulfidation pathway needs to be considered in environments that operate on the time scale of days and weeks and that are subject to redox oscillations, such as tidal flats, wetlands, riparian soils, the sediment-water interface, or the capillary fringe in ground water systems. Ferrihydrite and lepidocrocite are characteristic for such environments with rapid redox recycling of Fe(II) (Cornell and Schwertmann, 2006). They present a high potential for excess Fe(II) formation and are therefore candidates to stimulate rapid formation of pyrite and transformation of the host ferric mineral in such environments. In contrast, the occurrence of goethite typically reflects matured environments that allowed for sufficient ripening time, although also goethite specimen of high reactivity are existing (e. g. van der Zee et al., (2003)).

We have demonstrated that dissolved sulfide interacts with ferric hydroxides in two ways. It generates Fe(II) (respectively excess electrons) driving transformations of these minerals and it is a sulfide source for FeS_s formation. The extent of FeS_s and/or Fe(II) formation, however, seems to depend on the ratio between dissolved sulfide and the amount of surface sites (SS) available (Hellige et al., 2012).

At low $S(-II)_{aq}$:SS ratios, the concentration of dissolved sulfide is low relative to the concentration of reactive surface sites, which matches conditions in environments that are often abundant in ferric hydroxides and in which sulfide may be continually supplied e. g. through microbial reduction or diffusion. From these considerations a geochemical window can be derived that supports the occurrence of the sulfidation pathway (Fig. 3.10).

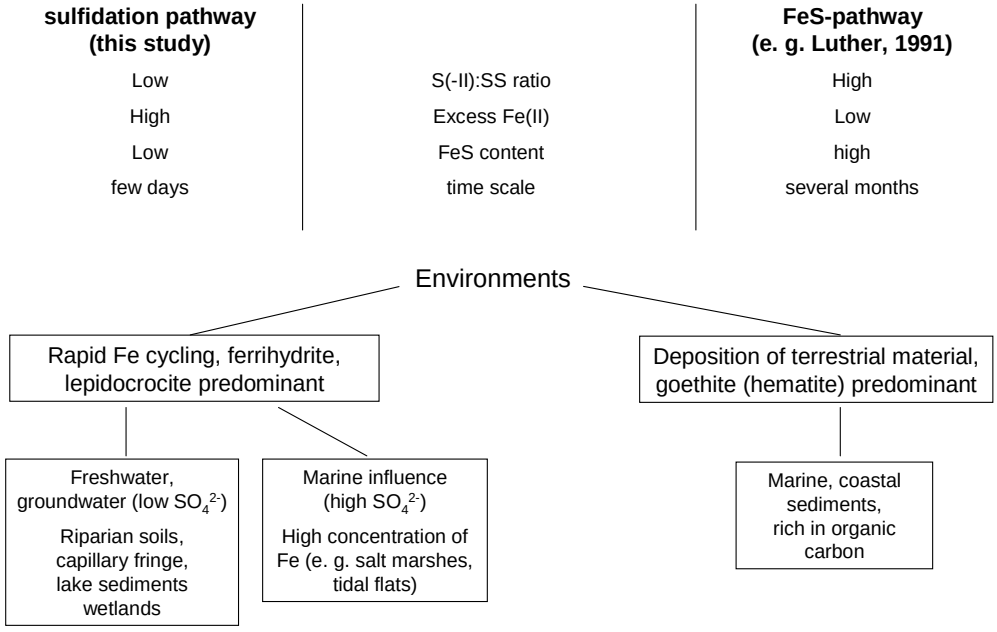

Fig. 3.10 Scheme for the classification of environments according to their potential for rapid pyrite formation.

Rapid pyrite formation (on a time scale of days) has been observed in such environments (Howarth, 1979; Otero and Macias, 2002). Pyrite formation was attributed to direct precipitation of pyrite with Fe^{2+} and polysulfides (Giblin, 1988; Giblin and Howarth, 1984), the polysulfides being assumed to be products of a not specified oxidation of sulfide. Similar to our experiments (except the first couple of hours), concentrations of dissolved sulfide were low (1- 20 μmol L^{-1}) probably due to consumption by ferric iron. Polysulfides were not measured in these studies. In a study on reflooding a formerly drained coastal wetland, Burton et al. (2011) observed decoupling of pyrite and AVS/greigite formation and could not relate its formation to the classical pathway via mackinawite. In the light of our study pyrite formation in

such systems occurred under conditions where dissolved sulfide is produced but maintained at low concentrations by high amounts of reactive ferric (hydr)oxides and therefore allows for a high fraction of excess Fe(II).

In contrast, high $S(-II)_{aq}$:SS ratios reflect conditions in marine systems (or specific sulfate-rich terrestrial environments) with a high supply of organic material to stimulate sulfate reduction on the one hand. According to the results derived in the present work, the formation of excess Fe(II) and its rapid conversion into pyrite would be suppressed by the fast formation of FeS_s if the reactivity of the iron minerals towards sulfide is low (e. g. (Canfield et al., 1992)). Such conditions exist where the reoxidation of Fe(II) to generate low crystallinity Fe(III) phases is impeded and the iron mineralogy is controlled by deposition of specimen of higher crystallinity, such as goethite (and probably also hematite although we did not study this mineral). We propose that the anomalous accumulation of acid volatile sulfide at 40 cm depth of a fjord in the presence of low dissolved sulfide concentrations reflects such conditions (Gagnon et al., 1995). Similar observations were made at the sulfidation front at a depth of ~ 300 cm depth in a Black Sea sediment (Jørgensen et al., 2004), where AVS accumulated upon reaction of sulfide with reactive iron. It is reasonable to assume that "reactive iron" at this depth is not a high surface-area material so that reaction pathway (7) may be faster than electron transfer to the bulk mineral (reaction (6)) under these conditions.

This short discussion cannot encompass and revisit the entire body of pyrite formation studies but it underpins that the specific reactivity of iron minerals towards sulfide needs to be considered when discussing the formation of pyrite and of other secondary minerals.

Our study has emphasized the role of an adsorption step preceding the entire sulfidation mechanism. It has been demonstrated that the reactivity of iron minerals can be significantly affected by interfering adsorbates. Phosphate even inhibited reductive dissolution of ferric (hydr)oxides (Biber et al., 1994). Hence, the role of important constituents of natural waters such as DOC or Si in affecting the sulfidation reaction needs to be tested in order to refine our understanding of the response of

natural systems rich in these compounds on the interaction between ferric (hydr)oxides and dissolved sulfide.

An interesting novel observation is the decoupling of reaction times during the interaction between sulfide and ferric hydroxides. Generation of excess Fe(II), which we identified as a requirement for pyrite formation, occurs within hours, while the formation of pyrite takes place within days. This phenomenon may be regarded as a process of charging the ferric minerals with electrons prior to consumption along with the pyrite formation process. Under conditions, where redox fluctuations occur on a time scale shorter than that of the formation of pyrite (e. g. tidal fluctuations), excess Fe(II) may thus exert some reactivity towards other oxidants than elemental sulphur (e. g. humic acids) and transfer electrons. Conceptually, electron transfer from sulfide to the bulk ferric mineral may thus be regarded as the build-up of electric capacity in a dynamic redox system, the role of which for other electron transfer processes being far from understood.

Acknowledgements

This research was funded by the Deutsche Forschungsgemeinschaft (DFG) and part of the priority program 580 “Electron Transfer Processes in Anoxic Aquifers” (PE 438/11-2). Kilian Pollok was supported by grant 03G0718A from the R&D programme Geotechnologien. We thank Stefan Haderlein and Andreas Kappler, University of Tübingen for using their Mössbauer spectroscopic instrument. Christian Schröder is acknowledged for the fruitful discussions. We also thank the staff members of the Department of Hydrology, University of Bayreuth for help and support.

3.7 References

Biber, M. V., dos Santos Afonso, M., and Stumm, W., 1994. The coordination chemistry of weathering: IV. Inhibition of the dissolution of oxide minerals. *Geochimica et Cosmochimica Acta* **58**, 1999-2010.

Bonneville, S., Behrends, T., and Van Cappellen, P., 2009. Solubility and dissimilatory reduction kinetics of iron (III) oxyhydroxides: a linear free energy relationship. *Geochimica et Cosmochimica Acta* **73**, 5273-5282.

Burton, E. D., Bush, R. T., Johnston, S. G., Sullivan, L. A., and Keene, A. F., 2011. Sulfur biogeochemical cycling and novel Fe–S mineralization pathways in a tidally re-flooded wetland. *Geochimica et Cosmochimica Acta* **75**, 3434-3451.

Canfield, D. E., Raiswell, R., and Bottrell, S. H., 1992. The reactivity of sedimentary iron minerals toward sulfide. *American Journal of Science* **292**, 659-683.

Catalano, J. G., Fenter, P., Park, C., Zhang, Z., and Rosso, K. M., 2010. Structure and oxidation state of hematite surfaces reacted with aqueous Fe (II) at acidic and neutral pH. *Geochimica et Cosmochimica Acta* **74**, 1498-1512.

Cornell, R. M. and Schwertmann, U., 2006. *The iron oxides: structure, properties, reactions, occurrences and uses*. John Wiley & Sons.

Dos Santos Afonso, M. and Stumm, W., 1992. Reductive dissolution of iron(III) (hydr)oxides by hydrogen sulfide. *Langmuir* **8**, 1671-1675.

Einsele, W., 1936. Über die Beziehungen des Eisenkreislaufes zum Phosphatkreislauf im Eutrophen See. *Archiv fur Hydrobiologie* **29**, 664-686.

Ferdelman, T. G., Church, T. M., and Luther, G. W., 1991. Sulfur enrichment of humic substances in a Delaware salt marsh sediment core. *Geochimica et Cosmochimica Acta* **55**, 979-988.

Fischer, W. R., 1987. Standard potentials (Eo) of iron (III) oxides under reducing conditions. *Zeitschrift für Pflanzenernährung und Bodenkunde* **150**, 286-289.

Fonselius, S., Dyrssen, D., and Yhlen, B., 1999. *Determination of hydrogen sulphide*.

Gagnon, C., Mucci, A., and Pelletier, É., 1995. Anomalous accumulation of acid-volatile sulphides (AVS) in a coastal marine sediment, Saguenay Fjord, Canada. *Geochimica et Cosmochimica Acta* **59**, 2663-2675.

Giblin, A. E., 1988. Pyrite formation in marshes during early diagenesis. *Geomicrobiology Journal* **6**, 77-97.

Giblin, A. E. and Howarth, R. W., 1984. Porewater evidence for a dynamic sedimentary iron cycle in salt marshes1. *Limnology and Oceanography* **29**, 47-63.

Gorski, C. and Scherer, M., 2011. Fe2+ sorption at the Fe oxide-water interface: A revised conceptual framework. *Aquatic Redox Chemistry* **1071**, 477-517.

Gorski, C. A. and Scherer, M. M., 2009. Influence of magnetite stoichiometry on FeII uptake and nitrobenzene reduction. *Environmental Science & Technology* **43**, 3675-3680.

Haderlein, S. B. and Pecher, K., 1998. Pollutant reduction in heterogeneous Fe (II)-Fe (III) systems. In: Sparks, D. L. and Grundl, T. Eds.), *Kinetics and Mechanisms of Reactions at the Mineral/Water Interface*. ACS Symposium Series. 715. 342-357.

Handler, R. M., Beard, B. L., Johnson, C. M., and Scherer, M. M., 2009. Atom exchange between aqueous Fe (II) and goethite: An Fe isotope tracer study. *Environmental Science & Technology* **43**, 1102-1107.

Hansel, C. M., Benner, S. G., and Fendorf, S., 2005. Competing Fe (II)-induced mineralization pathways of ferrihydrite. *Environmental Science & Technology* **39**, 7147-7153.

Harmandas, N. G., Navarro Fernandez, E., and Koutsoukos, P. G., 1998. Crystal Growth of Pyrite in Aqueous Solutions. Inhibition by Organophosphorus Compounds. *Langmuir* **14**, 1250-1255.

Hellige, K., 2011. The Reactivity of Ferric (Hydr)oxides towards Dissolved Sulphide. *Dissertation Thesis*, Fakultät für Biologie, Chemie und Geowissenschaften, Universität Bayreuth. 126pp.

Hellige, K., Pollok, K., Larese-Casanova, P., Behrends, T., and Peiffer, S., 2012. Pathways of ferrous iron mineral formation upon sulfidation of lepidocrocite surfaces. *Geochimica et Cosmochimica Acta* **81**, 69-81.

Hiemstra, T. and van Riemsdijk, W. H., 2007. Adsorption and surface oxidation of Fe(II) on metal (hydr)oxides. *Geochim. Cosmochim. Acta* **71**, 5913-5933.

Howarth, R. W., 1979. Pyrite: its rapid formation in a salt marsh and its importance in ecosystem metabolism. *Science* **203**, 49-51.

Jang, J.-H., Mathur, R., Liermann, L. J., Ruebush, S., and Brantley, S. L., 2008. An iron isotope signature related to electron transfer between aqueous ferrous iron and goethite. *Chemical Geology* **250**, 40-48.

Jørgensen, B. B., Böttcher, M. E., Lüschen, H., Neretin, L. N., and Volkov, I. I., 2004. Anaerobic methane oxidation and a deep H 2 S sink generate isotopically heavy sulfides in Black Sea sediments. *Geochimica et Cosmochimica Acta* **68**, 2095-2118.

Larese-Casanova, P. and Scherer, M. M., 2007. Fe (II) sorption on hematite: New insights based on spectroscopic measurements. *Environmental Science & Technology* **41**, 471-477.

Liu, H., Guo, H., Li, P., and Wei, Y., 2009. Transformation from δ-FeOOH to hematite in the presence of trace Fe (II). *Journal of Physics and Chemistry of Solids* **70**, 186-191.

Luther, G. W., 1991. pyrite synthesis via polysulfide compounds. *Geochimica et Cosmochimica Acta*, 2839-2849.

Murad, E. and Cashion, J., 2004. *Mössbauer spectroscopy of environmental materials and their industrial utilization*. Kluwer Academic Publishers.

Otero, X. L. and Macias, F., 2002. Variation with depth and season in metal sulfides in salt marsh soils. *Biogeochemistry* **61**, 247-268.

Pedersen, H. D., Postma, D., Jakobsen, R., and Larsen, O., 2005. Fast transformation of iron oxyhydroxides by the catalytic action of aqueous Fe (II). *Geochimica et Cosmochimica Acta* **69**, 3967-3977.

Peiffer, S. and Gade, W., 2007a. Reactivity of ferric oxides toward H2S at low pH. *Environmental Science & Technology* **41**, 3159-3164.

Peiffer, S. and Gade, W., 2007b. Reactivity of ferric oxides toward H_2S at low pH *Environ. Sci. Technol.* **41**, 3159-3164.

Penn, R. L., 2004. Kinetics of oriented aggregation. *The Journal of Physical Chemistry B* **108**, 12707-12712.

Postma, D., 1993. The reactivity of iron oxides in sediments: a kinetic approach. *Geochimica et Cosmochimica Acta* **57**, 5027-5034.

Poulton, S. W., Krom, M. D., and Raiswell, R., 2004. A revised scheme for the reactivity of iron (oxyhydr)oxide minerals towards dissolved sulfide. *Geochimica et Cosmochimica Acta* **68**, 3703-3715.

Pyzik, A. J. and Sommer, S. E., 1981. Sedimentary iron monosulfides: Kinetics and mechanism of formation. *Geochimica et Cosmochimica Acta* **45**, 687-698.

Raiswell, R. and Canfield, D. E., 2012. The iron biogeochemical cycle past and present. *Geochemical Perspectives* **1**, 1-2.

Rickard, D., 1995. Kinetics of FeS precipitation: Part 1. Competing reaction mechanisms. *Geochimica et Cosmochimica Acta* **59**, 4367-4379.

Rickard, D., 2012. *Sulfidic sediments and sedimentary rocks*. Newnes.

Rickard, D. and Luther, G. W., 2007. Chemistry of iron sulfides. *Chemical Reviews* **107**, 514-562.

Rickard, D. T., 1974. Kinetics and mechanism of the sulfidation of goethite. *American Journal of Science* **274**, 941-952.

Rickard, D. T., 1975. Kinetics and mechanism of pyrite formation at low temperatures. *American Journal of Science* **275**, 636-652.

Roden, E. E., 2003. Fe (III) oxide reactivity toward biological versus chemical reduction. *Environmental Science & Technology* **37**, 1319-1324.

Schwertmann, U. and Cornell, R. M., 2008. *Iron oxides in the laboratory*. Wiley-Vch.

Silvester, E., Charlet, L., Tournassat, C., Gehin, A., GrenÈche, J.-M., and Liger, E., 2005. Redox potential measurements and Mössbauer spectrometry of Fe II adsorbed onto Fe III (oxyhydr) oxides. *Geochimica et Cosmochimica Acta* **69**, 4801-4815.

Tamura, H., Goto, K., Yotsuyanagi, T., and Nagayama, M., 1974. Spectrophotometric determination of iron (II) with 1, 10-phenanthroline in the presence of large amounts of iron (III). *Talanta* **21**, 314-318.

Thamdrup, B., 2000. Bacterial manganese and iron reduction in aquatic sediments, *Advances in microbial ecology*. Springer.

van der Zee, C., Roberts, D. R., Rancourt, D. G., and Slomp, C. P., 2003. Nanogoethite is the dominant reactive oxyhydroxide phase in lake and marine sediments. *Geology* **31**, 993-996.

Wan, M., Shchukarev, A., Lohmayer, R., Planer-Friedrich, B., and Peiffer, S., 2014. Occurrence of Surface Polysulfides during the Interaction between Ferric (Hydr)Oxides and Aqueous Sulfide. *Environmental Science & Technology* **48**, 5076-5084.

Williams, A. G. and Scherer, M. M., 2004. Spectroscopic evidence for Fe (II)-Fe (III) electron transfer at the iron oxide-water interface. *Environmental Science & Technology* **38**, 4782-4790.

4. Fe/S ratio controls pathway and kinetics of pyrite formation during Fe(III)-S(-II) interaction

Moli Wan[1,*], Christian Schröder[2], Stefan Peiffer[1]

[1] BayCEER, Department of Hydrology, University of Bayreuth, D-95440, Bayreuth, Germany

[2] Biologcial and Environmental Sciences, School of Natural Sciences, University of Stirling, Stirling FK9 4LA, Scotland, UK

[*] Corresponding author. Phone ++49-921-553500, Fax ++49-921-552366, moli.wan@uni-bayreuth.de

Manuscript in preparation. Planned submission to *Geochimica et Cosmochimica Acta*

4.1 Abstract

The formation of pyrite has been extensively studied because of its abundance in many anoxic environments. Yet the pathway and kinetics of pyrite formation are still under controversy. We investigated the pyrite formation during the anoxic reaction between high reactive ferric hydroxides and aqueous sulfide, which were performed in the anoxic glove box at neutral pH. The initial molar ratios of Fe/S were adjusted to be 'high' with Fe concentrations being in excess of sulfide (HR) and 'low' with excess sulfide to Fe in ferric hydroxides (LR). Approximately the same surface area was applied in all HR runs in order to compare the mineral reactivity of ferric hydroxides Electron transfer between aqueous sulfide and ferric hydroxides in the first 2 hours led to a formation of ferrous iron and oxidized sulfur which can be extracted by methanol (MES). Metastable FeS formed in all of the experiments. Pyrite formed at a different rate in HR and LR runs although the MES and ferrous iron concentration were rather similar. Pyrite occurred within 48 hours and crested after 1 week in all HR runs. By contrast, pyrite started to form only after 2 months in LR runs. The mineral reactivity of ferric hydroxides having a strong positive influence on sulfide oxidation, affected little on pyrite formation in HR runs. The correlation between pyrite formation rate and Fe/S ratio and the comparison of the pyrite formation rate with the model of Rickard (1975) suggested different pyrite formation pathways in the HR and LR runs. We hypothesize a novel polysulfide pathway that ferrous iron generated during the interaction of ferric and sulfide interaction can bound directly with surface polysulfides to precipitate pyrite rapidly. The reaction is competitive with respect to FeS precipitation and is significantly withdrawn by decreasing Fe/S ratio. In LR runs pyrite formation follows the model of Rickard (1975) and is kinetically controlled by the dissolution of FeS. Hence, The Fe/S ratio can perform as an indicator for rapid pyrite formation during early diagenesis in the anaerobic/suboxic sediments.

Key words: rapid pyrite formation, pathway, polysulfide, reactive ferrous iron, iron-sulfur interaction, ferric hydroxides, Mössbauer spectroscopy

4.2 Introduction

The formation of pyrite has been extensively studied because of its abundance in many anoxic environments such as marine and river sediments, groundwater aquifers, and peat lands, and hence its importance in both iron and sulfur cycling. It forms over a wide pH interval, ranging from acidic to alkaline conditions (Luther, 1991; Price and Shieh, 1979; Wilkin and Barnes, 1996). It is generally thought that sulfide reacting with iron-containing minerals forms metastable iron sulfide minerals before eventually transforming into pyrite in the presence of different sulfur sources (Benning et al., 2000; Berner, 1970; Hellige et al., 2012; Luther, 1991; Rickard, 1997; Rickard and Luther, 1997; Schoonen and Barnes, 1991b; Schoonen, 2004). Several studies investigated the transformation from iron sulfide to pyrite, starting with different sulfur species under different conditions. It has been verified that the transformation occurs in solutions containing thiosulfate and zero-valent sulfur such as elemental sulfur and polysulfides (Luther, 1991; Price and Shieh, 1979; Schoonen and Barnes, 1991b; Wilkin and Barnes, 1996). Besides, hydrogen sulfide/bisulfide was suggested to sulfidate FeS to form pyrite (Rickard, 1997; Rickard and Luther, 1997; Schoonen, 2004).

A wide spectrum of sulfur species is involved in the transformation of metastable iron sulfide to pyrite, whereby the kinetics and pathways of the transformation appear to be different with different sulfur species. In a homogenous polysulfide solution at neutral pH and ambient temperature, pyrite formation occurred only after 4 months aging of FeS which precipitated from ferrous iron and aqueous sulfide solution (Luther, 1991). By contrast, solid phase transformation of freeze-dried mackinawite to pyrite under H_2S atmosphere appeared to occur within 1 day (Butler and Rickard, 2000; Rickard, 1997). The rapid formation was later explained in terms of activation of pyrite formation by the occurrence of oxidized sulfur species associated with the dried mackinawite (Benning et al., 2000). Rapid pyrite formation was observed during the interaction between ferric iron and aqueous sulfide/polysulfides. Occurrence of pyrite was observed within 2 days under acidic conditions (Berner, 1964; Luther, 1991; Price and Shieh, 1979) and within 14 days at neutral pH (Hellige et al., 2012). In a Transmission Electron Microscopy (TEM) study, Hellige et al. (2012) observed the coverage of lepidocrocite crystals by a rim of an amorphous phase rich in Fe and S

containing local nano-mackinawite structure after two hours of reaction and complete consumption of aqueous sulfide. The amorphous phase dissolved after several days followed by the precipitation of pyrite nano phases dislocated from the lepidocrocite surface. In an X-ray photoelectron spectroscopy study performed under comparable experimental conditions, Wan et al. (2014) were able to demonstrate that a large amount of polysulfide species were associated with the ferric (hydr)oxide's surface, while aqueous polysulfide species make up only a minor fraction. Of particular importance was disulfide, which - not yet bound as pyrite - seemed to be the main surface polysulfide species. It was suggested that surface polysulfide species, especially surface disulfide, could bind to Fe(II) to form a non-crystalline FeS_2 precursor to trigger the formation of pyrite.

It appears that the rate of pyrite formation upon sulfidation of ferric hydroxides depends on the mineral type (Peiffer et al., 2015) and the Fe/S molar ratio (Hellige et al., 2012). It was proposed that the extent of pyrite formation is ruled by two factors: 1) the ratio between concentrations of added sulphide and available mineral-specific surface area, and 2) the capability of the iron(hydr)oxide to conduct electrons to trigger formation of pyrite precursor compounds (Peiffer et al., 2015).

Such experimental observations are matched by field data. In natural sediments with abundant hydrogen sulfide and/or elemental sulfur, metastable iron sulfide dominates with only a minor fraction of pyrite (Burton et al., 2006; Kraal et al., 2013). By contrast, in a fairly oxidized marine sediment from Santa Catalina Basin where sulfide concentration are usually undetectable, pyrite instead of iron monosulfides turn out to be the major mineral in the surface sediments (Howarth, 1979; Johnston et al., 2014; Kaplan et al., 1963).

In this study we are aiming to resolve the fate of ferrous iron generated during ferric iron-sulfide interaction and its role on the secondary iron (sulfide) minerals, especially pyrite formation in the presence of different sulfur species such as sulfide and surface and/or aqueous polysulfides. To these ends, ferric hydroxides were reacted with aqueous sulfide at neutral pH in an anoxic glove box, and different Fe to S ratios were applied in order to vary the reaction conditions. ^{57}Fe sensitive Mössbauer spectroscopy was applied to analyze the solid phases. Hellige et al (2012) also used

Mössbauer spectroscopy but were not able to observe intermediate Fe-S species, only the end product pyrite. They assumed that the intermediate products had been oxidized during sampling transport and/or the amount of intermediate was too low to be visible in Mössbauer spectra. We therefore optimized our measurement procedures by using ^{57}Fe enriched materials and applying a non-delay measurement.

4.3 Materials and methods:

The experiments were performed in a glove box system (Glovebox system, Innovative Technology, USA) with a working atmosphere of N_2 (99.99%). The oxygen level was in a range of 0-1 ppm. All solutions and organic solvents were purged with N_2 (99.99%) for 1 h to remove oxygen prior to transferring into the glove box. All commercial reagents except methanol (HPLC grade) are analytical grade. Sodium sulfide (Na_2S) and methyl trifluoromethanesulfonate (triflate, $CF_3SO_2OCH_3$) were purchased from Sigma-Aldrich, Germany; zinc acetate (ZnAc), iron(II) chloride tetrahydrate ($FeCl_2 \cdot 4H_2O$) and iron(III) nitrate nonahydrate ($Fe(NO_3)_3 \cdot 9H_2O$) from Merck, Germany; methanol (HPLC grade) from Geyer, Germany; and piperazine-N,N′-bis(2-ethanesulfonic acid) (PIPES, $C_8H_{18}N_2O_6S_2$) from VWR , Germany.

4.3.1 Ferric hydroxides

Synthetic ferric hydroxides were prepared after Schwertmann and Cornell (2008) as previously described in detail (Wan et al., 2014). In brief, to synthesize goethite, 100 mL $Fe(NO_3)_3$ (c = 1 mol L^{-1}) and 180 mL KOH (c = 5 mol L^{-1}) were mixed rapidly in a 2 L polyethylene flask. The suspension was diluted to 2 L with distilled water and kept at 70 ℃ for 60 h. To synthesize lepidocrocite, 200 mL $FeCl_2$ (c = 0.06 mol L^{-1}) solution with pH 6.8 was oxidized by air pumped through the solution with a flow rate of 100 mL min^{-1}. The pH was maintained at 6.8 by addition of NaOH (c = 0.5 mol L^{-1}) with a pH-stat device (Titrino, Metrohm). The oxidation was carried out at room temperature with sufficient stirring. In order to enhance the signal of minor Fe-bearing phases in the Mössbauer spectra, we enriched the ^{57}Fe isotope tenfold in the ferric hydroxides used for Mössbauer analysis. The ^{57}Fe enriched ferric hydroxides were synthesized after the same protocol mentioned above, with a modification of reagent preparation: 80 mL commercial Fe salt solution was mixed with 20 mL corresponding ^{57}Fe salt prior to synthesis. $^{57}Fe(NO_3)_3$ was prepared by dissolution of pure ^{57}Fe metal powder in 20 mL HNO_3 (c = 1 mol L^{-1}) in air. $^{57}Fe(Cl)_2$ was prepared by dissolution of pure ^{57}Fe metal powder in 20 mL hot HCl (c = 2 mol L^{-1}, 60 ^{o}C) in the glove box.

The synthetic ferric hydroxides were washed with deionized water (18.2MΩ), freeze dried and characterized with X-ray diffractometry (XRD), scanning electron microscopy (SEM), ^{57}Fe-enriched ferric hydroxides were also characterized with

Mössbauer spectroscopy . All three methods depicted pure goethite and lepidocrocite, except that ^{57}Fe-enriched lepidocrocite contained 4 % goethite. SEM showed acicular goethite crystals with a length of 600 nm to 1 µm and lath-like lepidocrocite crystals with length in the *c*-direction of around 200 nm.

Multi-point BET (Brunauer, Emmett and Teller) gas adsorption with N_2 (Gemini 2375 analyzer) gave a surface area of goethite with 39.33 $m^2\ g^{-1}$ and lepidocrocite with 70.24 $m^2\ g^{-1}$.

4.3.2 Experimental set-up:

The experiments were performed in a 4-port reactor and followed the set-up described in previous studies (Hellige et al., 2012; Wan et al., 2014). In brief, a 450 mL aqueous sulfide solution (Na_2S) was adjusted to pH 7.0 in the glove box by addition of HCl (c = 1 mol L^{-1}), to which 50 mL of a suspension containing a preselected amount of synthetic ferric hydroxides (goethite or lepidocrocite) was added. The pH was kept constant at pH = 7.0 ± 0.1 with HCl (c= 0.1 mol L^{-1}) using a pH-Stat device. The solution was gently stirred with a teflon-coated magnetic stirring bar during the whole experiment. The initial conditions of the various experimental runs are listed in Table 4.1. The sulfide concentration was adjusted prior to the addition of ferric hydroxides, and the total iron concentration was determined after mixing of the sulfide containg solution with the ferric hydroxides. The initial molar ratios of Fe/S were adjusted to be 'high' with Fe concentrations being in excess of sulfide (HR) and 'low' with excess sulfide to Fe in ferric hydroxides (LR). Approximately the same concentration of surface area was applied in all HR runs in order to compare the mineral reactivity of ferric hydroxides (Table 4.1). All runs were conducted at ambient temperature (around 22 ^oC) except Runs 8 and 9, which started at ambient temperature and ended at approx. 33^oC after 168 h due to an unexpected heating during a warm summer period. A blank experiment running for 168 h in the 4-port reactor with aqueous sulfide at pH 7 yielded a linear H_2S degassing rate of 0.014 mmol $L^{-1}\ h^{-1}$ (R^2 = 0.914).

In order to prevent degassing of hydrogen sulfide, long-term aging experiments were performed in serum bottles sealed with thick Butyl-septa and aluminium caps through which only trace amounts of sulfide escaped during sampling. The pH was checked

regularly and if necessary adjusted by addition of HCl and/or NaOH (c = 0.1 mol L^{-1}). The suspensions were shaken by hand for several minutes every day. Runs 37 and 38 with lepidocrocite and 8 mmol L^{-1} sulfide each were performed in PIPES buffer (pH 7, c=50 mmol L^{-1}). The aqueous phase was sampled regularly to determine iron and sulfur species. Samples for Mössbauer spectroscopy were only taken from the experiments with ^{57}Fe-enriched ferric hydroxides.

Three HR runs were performed with the only purpose to detect proton consumption during the reaction between sulfide and the ferric hydroxides. To this end H^+ consumption was recorded by the pH-Stat device and no aqueous samples were taken.

Table 4.1 Initial conditions for all runs. pH was kept at 7.0 ±0.1

Run ID	Name	Runtime	c(Fe(TOT))	SS[a] Fe(TOT)	c(S(-II)$_{ini}$)
		h	mmol L^{-1}		
1	HR_Gt	3	40.0	0.88	7.9
2	HR_Gt	3	40.1	0.88	8.0
3	HR_Gt	3	41.7	0.92	6.6
4	HR_Gt	3	39.2	0.86	4.4
5	HR_Gt	3	39.1	0.86	6.0
6	HR_Gt	168	38.6	0.85	10.6
7	HR_Gt	168	35.8	0.79	9.6
8	HR_Gt[b]	168	37.8	0.83	7.8
9	HR_Gt[b]	168	39.1	0.86	8.3
10	HR_Gt[c]	168	41.6	0.93	8.1
11	HR_Gt[c]	168	39.1	0.87	9.7
14	LR_Gt	216	3.1	0.07	8.3
15	LR_Gt	3600	3.8	0.08	13.9
16	LR_Gt	3600	4.0	0.09	14.2
17	LR_Gt	3600	4.0	0.09	14.9
18	LR_Gt[c]	3600	3.4	0.08	14.9
23	HR_Lp	2.4	22.5	0.89	8.0
24	HR_Lp	264	25.0	0.98	7.2
25	HR_Lp	168	22.1	0.87	8.9
26	HR_Lp	168	22.5	0.89	8.0
27	HR_Lp	168	22.0	0.87	7.8
28	HR_Lp[c]	168	15.8	0.63	8.0
29	HR_Lp[c]	48	15.8	0.63	7.9
30	HR_Lp[c]	96	19.2	0.77	8.8
32	LR_Lp	168	4.3	0.17	8.2
33	LR_Lp	168	4.3	0.17	8.1
34	LR_Lp	168	4.5	0.18	7.4
35	LR_Lp	168	0.7	0.03	7.0
36	LR_Lp	168	3.1	0.12	6.1
37	LR_Lp[c d]	3312	3.8	0.15	7.9
38	LR_Lp[c d]	3312	4.2	0.17	7.8
39	LR_Lp	3768	4.1	0.16	17.2
40	LR_Lp	3768	3.5	0.14	16.5
41	LR_Lp	3768	3.4	0.14	20.3
42	LR_Lp[c]	3768	3.8	0.15	17.4

[a] concentration of surface site was calculated based on a value of 6.3 x 10^{-6} mol m^{-2} for both ferric hydroxides (Peiffer and Gade, 2007)

[b] higher temperature (approx. 33 °C) at the end of experiment

[c] ^{57}Fe-enriched ferric hydroxides were applied, mineral phases in these runs were characterized by Mössbauer spectroscopy

[d] with 50 mmol L^{-1} PIPES buffer

4.4 Sampling and analysis

4.4.1 Wet chemical analysis

Sampling and analytical procedures were performed according to previous studies (Hellige et al., 2012; Wan et al., 2014) with additional evaluation of the effect of low pH on the ferrous iron extraction process. Samples were filtered (0.2 µm, Nylon) and the aqueous phase was analyzed for aqueous Fe(II) ($Fe(II)_{aq}$), aqueous sulfide ($S(-II)_{aq}$), aqueous polysulfide (S_n^{2-}), thiosulfate ($S_2O_3^{2-}$) and sulfate (SO_4^{2-}). Unfiltered samples were analyzed for acid extractable Fe(II) ($Fe(II)_{HCl}$), total iron concentration (Fe(TOT)) and for methanol extractable sulfur (MES).

Iron species were determined photometrically using the phenanthroline method (Tamura et al., 1974) after specific pre-treatment steps. The total Fe content (Fe(TOT)) was measured as at least triplicates after dissolution of 500 µL of unfiltered samples in 500 µL hot HCl (c = 12 mol L^{-1}, T = 60 ℃) for 1 week. $Fe(II)_{aq}$ was analyzed after addition of 500 µL HCl (c = 1 mol L^{-1}) into 500 µL filtered samples. $Fe(II)_{HCl}$ was extracted by addition of 500 µL unfiltered samples into 500 µL HCl (c = 1 mol L^{-1}) and filtered after 15 min. During the acidic extraction step metastable iron sulfide (mainly FeS, c.f. eq 1) will release H_2S, which may generate ferrous iron upon reaction with ferric hydroxides and thus lead to overestimation of $Fe(II)_{HCl}$ during the acidic extraction. Therefore, test experiments were carried out to quantify the effect of acidic FeS extraction in the presence of ferric hydroxides on the yield of $Fe(II)_{HCl}$. The FeS was precipitated by adding $FeCl_2$ (c = 2 mol L^{-1}) slowly into Na_2S containing solution (c = 2 mol L^{-1}). After overnight equilibration, aliquots of the FeS suspension were injected into the ferric (hydr)oxide suspension. Then HCl (c = 1 mol L^{-1}) was added and allowed to react for 60 min. to extract $Fe(II)_{HCl}$ from the mixture. Samples were taken and filtered after 1 min, 15 min, 30 min and 60 min. Reference runs indicated a complete recovery of $Fe(II)_{HCl}$ after 15 min (103 % ± 6 %). $Fe(II)_{HCl}$ remained constant in the presence of goethite, but increased over time in the presence of lepidocrocite. A mean FeS recovery of 97 % ± 3 % and 119 % ± 4 % was retrieved after 15 min in the experiments with goethite and lepidocrocite, respectively. Hence, the $Fe(II)_{HCl}$ seems to be completely recovered in the experiments with goethite, while being overestimated with lepidocrocite. The $Fe(II)_{HCl}$ concentration was estimated by

dividing the measured $Fe(II)_{HCl}$ concentration by the FeS recovery factor (0.97 and 1.19 for goethite and lepidocrocite, respectively). Solid phase bound Fe(II) ($Fe(II)_{sol}$) (except pyrite-Fe) was then calculated as the difference between the corrected $Fe(II)_{HCl}$ concentration and the measured concentration of $Fe(II)_{aq}$.

$S(-II)_{aq}$ was determined photometrically after filtration and fixation with ZnAc (c = 0.1 mol L^{-1}) using the methylene blue method (Fonselius et al., 1999) . Methanol extractable sulfur (MES) was extracted after pre-treatment of the suspension with zinc acetate (ZnAc) to precipitate free sulfide, following a procedure modified after Kamyshny et al. (2009). Prior to the extraction step, 250 µL of ZnAc (c = 0.1 mol L^{-1}) were added to 500 µL unfiltered sample. After 10 min, 6 mL methanol were injected into the suspension. The samples were shaken for 3 h and then filtered (0.2 µm). The filtrates were analyzed for zero-valent sulfur using HPLC as described in Wan et al. (2014). MES comprised all zero-valent sulfur which is in the form of elemental sulfur or associated with aqueous polysulfide (Kamyshny et al., 2009) and surface polysulfide (Wan et al., 2014).

Aqueous polysulfide species were transformed into more stable organic polysulfanes prior to the measurement due to their instability, (Kamyshny et al., 2006). 200 µL of the filtered samples and 8 µL triflate were added simultaneously into 1200 µL methanol previously buffered with 100 µL phosphate buffer (c = 50 mmol L^{-1}, pH 7) and shaken intensively for 10 s as described in the previous studies (Kamyshny et al., 2006; Wan et al., 2014). The obtained organic polysulfanes were determined with HPLC. The total amount of aqueous polysulfides (S_n^{2-}(aq)) was calculated as the sum of the individual polysulfide fractions (S_2^{2-} (aq) to S_8^{2-} (aq)) as described by Wan et al (2014).

SO_4^{2-} was determined turbidimetrically based on $BaSO_4$ precipitation as described by Tabatabai (1974). $S_2O_3^{2-}$ was determined by ion-pair chromatography following the methods described by Steudel et al. (1987). Both species were below the detection limit in all runs (detection limits were 6 µmol L^{-1} and 28 µmol L^{-1}, respectively).

The samples for photometric measurements were stored in a dark cool room (4 ^{o}C) and measured within one day. The samples for HPLC measurement were stored in a refrigerator (-18^{o}C) and measured within one week after preparation.

4.4.2 Mössbauer Spectroscopy

Solid phase samples were collected at certain time steps for Mössbauer spectroscopy analysis (see Table 4.1). The time steps were carefully selected according to our results from wet chemical analysis and the TEM results from Hellige et al. (2012). In the HR runs samples for high resolution analysis were taken after sulfide was consumed (1.5 h in the experiments with goethite and 15 min with lepidocrocite), after a period were stable transient concentrations had established (3 h with goethite, 2 h with lepidocrocite), during a period when MES decreased (48 h, 72 h with both minerals) and at the end of the experiments (168 h with both minerals). In the LR runs, samples were taken after 72 h and 168 h, and after every following month.

To prepare samples of the solid fraction for Mössbauer spectroscopy analysis, 20 mL of the suspension enriched with ^{57}Fe were sampled and filtered through cellulose membrane filter paper (Ø 13 mm and 0.45 µm pore size) inside the glove box until the filter was clogged. The filter with solid fraction on top was sealed between two layers of Kapton tape after the small amount of remaining liquid had been carefully removed. The samples were placed in a sealed bottle to avoid contact with air during transportation from the glove box to the spectrometer and measured without further delay. The spectra were collected with a WissEl Mössbauer transmission spectrometer, using a ^{57}Co in Rh matrix γ-ray source mounted on a constant acceleration drive system. Samples were cooled in a Janis closed-cycle Helium gas cryostat that allowed measurements at 140 K, 77 K, 4.2 K as well as room temperature. During measurement, the samples were kept at vacuum or in a low pressure He atmosphere to avoid oxidation. Spectra were calibrated against a spectrum of alpha-Fe(0) foil at room temperature. Data acquisition times were usually about 24 h per spectrum. Spectral fitting was carried out using Recoil software (University of Ottawa, Canada) with the Voigt-based fitting routine. The concentration of each iron mineral phase detected by Mössbauer spectroscopy was calculated by multiplying the total Fe concentration (Fe(TOT)) with the respective fitted spectral area representing the relative fraction of individual mineral phases (supporting information Table S4.1).

4.5 Results

4.5.1 Chemical speciation

In all runs, consumption of aqueous sulfide ($S(-II)_{aq}$) and built-up of sulfur and ferrous iron species were observed in the first few hours. Different reaction patterns appeared thereafter.

H^+ consumption was faster in the experiments with lepidocrocite (Fig. 4.1). H^+ consumption increased initially and achieved a constant level of around 2.2- 2.4 mmol L^{-1} after 2 h in the HR_Gt run, and of around 3.1 mmol L^{-1} after already 15 min in the HR_Lp run. We did not record the H^+ consumption after 24 h in the HR_Gt run. In the HR_Lp run, H^+ consumption started to increase again after 24 h steadily to 9.6-11.4 mmol L^{-1}.

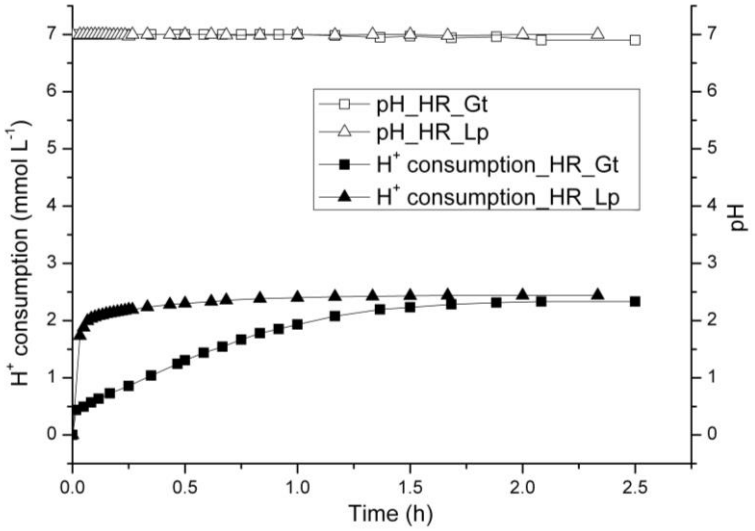

Fig. 4.1 pH value and H^+ consumption at the first 2.5 h in the high Fe/S ratio with goethite and lepidocrocite

In the HR runs with goethite (HR_Gt), most of the $S(-II)_{aq}$ was consumed after 1.5 h. The concentration remained lower than 0.05 mmol L^{-1}, then decreased to 0.003 mmol L^{-1} after 24 or 48 h (Fig. 4.2, Run 7 & Run 9). Methanol extractable sulfur (MES) and solid phase bound Fe(II) ($Fe(II)_{sol}$) built up along with the consumption of $S(-II)_{aq}$ in the first 1.5 h, and remained relatively constant for the next several hours. Both species started to decrease after 4 h (Run 9) or after 24 h (Run 7) with a faster

decrease in Run 9 at a higher reaction temperature. The concentration of aqueous Fe(II) ($Fe(II)_{aq}$) was around 0.02 mmol L^{-1} in the first 24 h (Run 9) or 72 h (Run 7) and increased to around 0.5 mmol L^{-1} after 72 h. S_n^{2-} was detectable only in the first 15 min with a total concentration of 0.03 mmol L^{-1} (data not shown).

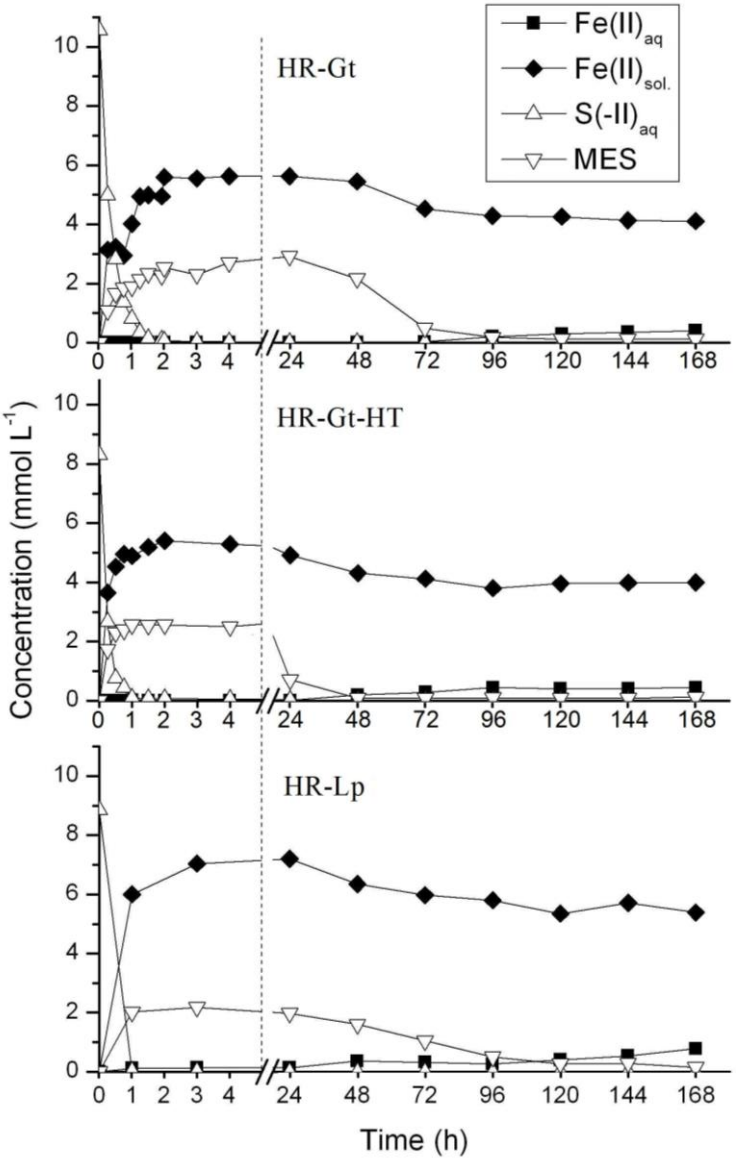

Fig. 4.2 Iron and sulfur speciation in the HR runs

The reaction in the HR runs with lepidocrocite (HR_Lp) showed a similar pattern but with a faster consumption of $S(-II)_{aq}$ and corresponding built-up of Fe(II) and MES. $S(-II)_{aq}$ was almost consumed after 15 min in Run 24. In Run 25 we started to sample

only after 1 h (Fig. 4.2). $S(-II)_{aq}$ decreased to 0.017 mmol L^{-1} while MES and $Fe(II)_{sol}$ increased to around 2.0 mmol L^{-1} and 6.0 mmol L^{-1} within 1 h and then slowly to 2.2 mmol L^{-1} and 7.0 mmol L^{-1} after 3 h, respectively (Fig. 4.1). After 24 h the concentration of both species decreased while that of $Fe(II)_{aq}$ started to increase from 0.12 mmol L^{-1} to 0.9 mmol L^{-1} after 168 h. More ferrous iron was generated in the HR_Lp run (Run 25) than in the HR_Gt runs (Run 7 & 9). The concentration difference was 1.6 mmol L^{-1} for $Fe(II)_{sol.}$ and 0.1 mmol L^{-1} for $Fe(II)_{aq}$ in the experiments with Lp and Gt, respectively. The difference changed after 168 h to 1.3 mmol L^{-1} for $Fe(II)_{sol}$ and 0.4 mmol L^{-1} for $Fe(II)_{aq}$.

In the short-term LR experiments, which ran for 168 h, it seems that most of the ferric iron was consumed during the first several hours. After 3 h, $Fe(II)_{HCl}$ concentrations reached almost the initial Fe(III) concentrations with 2.9 mmol L^{-1} in the run with goethite (Run 14) and 4.2 mmol L^{-1} in the run with lepidocrocite (Run 33). As $Fe(II)_{aq}$ concentration remained 0.006-0.010 mmol L^{-1} in all of the LR runs (data not shown), $Fe(II)_{HCl}$ comprises only solid phase Fe(II). At the same time, MES achieved a concentration at ~1.5 mmol L^{-1} in both LR_Gt and LR_Lp runs. Both species remained virtually constant thereafter. $S(-II)_{aq}$ decreased after 3 h to 2.3 mmol L^{-1} in LR_Gt run and 0.5 mmol L^{-1} in LR_Lp run, and continued to decrease with a slower rate. S_n^{2-} concentration rose to 0.5 mmol L^{-1} after 15min and then dropped to 0.03 mmol L^{-1} at the end of the experiments.

In the long term LR experiments with a high concentration of inital $S(-II)_{aq}$ (13.9-20.3 mmol L^{-1}) running for more than 3600 h (e.g. Run 18 & Run 42), MES, S_n^{2-} and $Fe(II)_{HCl}$ were the dominating species generated in the presence of a large amount of residual $S(-II)_{aq}$ (>10 mmol L^{-1}). MES and S_n^{2-} were relatively constant at ~1.6 mmol L^{-1} and ~0.2 mmol L^{-1}, respectively (data not shown). The concentration of $Fe(II)_{sol.}$ showed slight variations in Run 42 but a steady decrease after 2160 h in Run 18 (Fig. 4.4). In the LR experiment with a lower concentration of initial sulfide (7.9 mmol L^{-1}) (Run 37 and 38), the concentration of $Fe(II)_{sol.}$ remained unchanged with around 3.4 mmol L^{-1} until 2160 h and then decreased to 1.8 mmol L^{-1} after 3312 h (Fig. 4.4). Aqueous $S(II)_{aq}$ showed the same tendency. Residual $S(-II)_{aq}$ concentration remained at a constant level of 0.5 mmol L^{-1} until 2160 h and then decreased to 0.05 mmol L^{-1}

after 3312 h (data not shown). $Fe(II)_{aq}$ concentration remained undetectable during the entire reaction time in all of the LR runs (detection limit was 0.007 mmol L^{-1}).

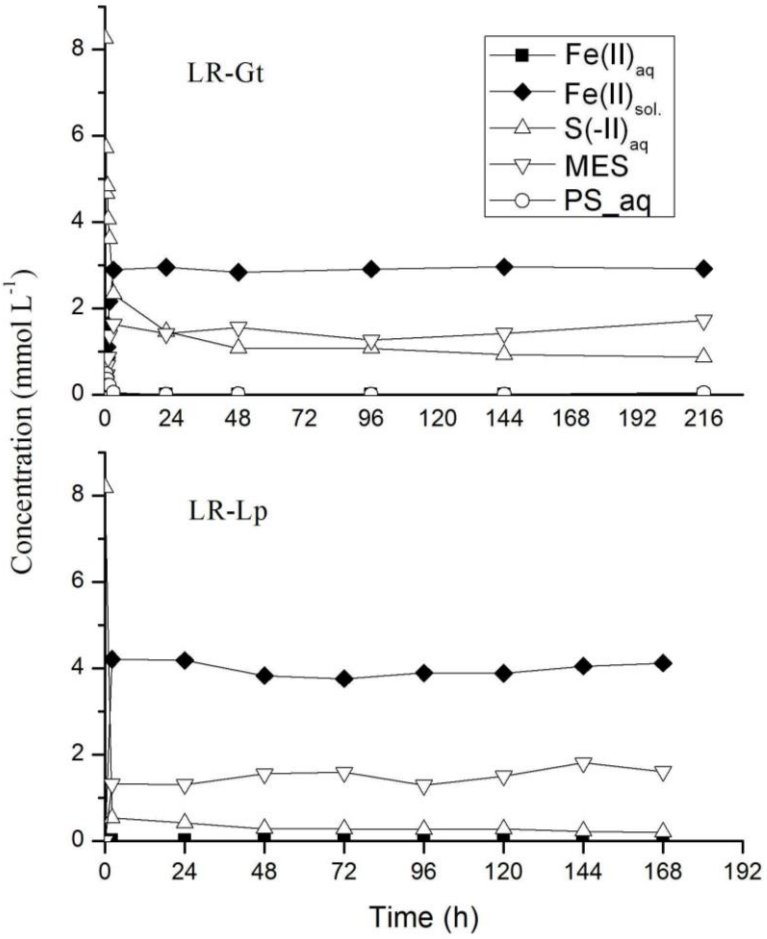

Fig.4.3 Iron and sulfur species in the short-term LR runs within 168 h.

In summary, two different reaction patterns were observed. HR runs were quite dynamic within the first 168 h and can therefore be divided into three phases: 1. Consumption of $S(-II)_{aq}$ and build-up of MES and $Fe(II)_{sol.}$; 2. Consumption of MES and $Fe(II)_{sol.}$; 3. Build-up of $Fe(II)_{aq}$ pool. In contrast, in LR runs the system seems to have reached a steady-state after the initial consumption of $S(-II)_{aq}$ and formation of MES and $Fe(II)_{sol}$ in the presence of high levels of residual aqueous sulfide. The system remained at this state until consumption of $Fe(II)_{sol.}$ occurred after 2160 h in the LR_Gt run with a high concentration of initial sulfide (e.g. Run 18) and in the LR_Lp run with a lower concentration of initial sulfide (e.g. Run 37 and 38). No significant change regarding $Fe(II)_{sol.}$ concentration was observed in the LR_Lp runs

with high concentration of initial sulfide (e.g. Run 39 – Run 41). $Fe(II)_{aq}$ in all LR runs remained negligible.

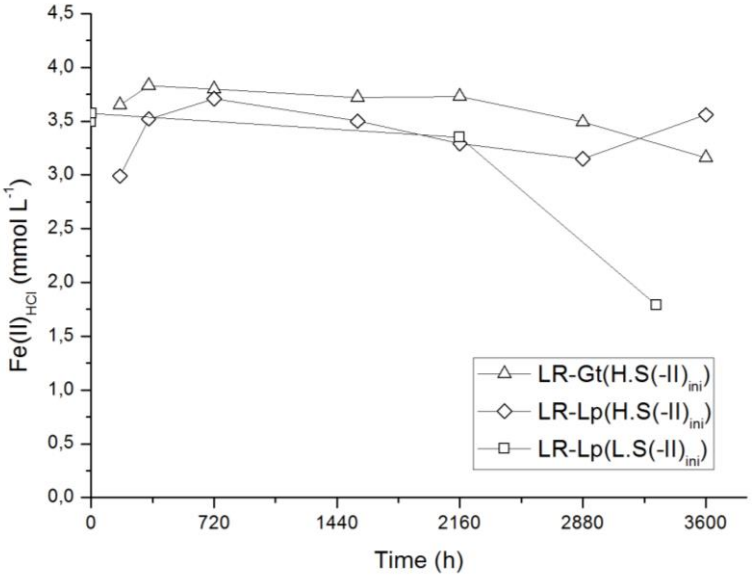

Fig. 4.4 $Fe(II)_{sol.}$ concentration in the long-term LR runs.

4.5.2 Mössbauer spectroscopy

We used Mössbauer spectra collected at a sample temperature of ~5 K to identify and quantify Fe-bearing phases in the solid state. At this temperature the ferric hydroxides are fully magnetically ordered and the resulting six-line subspectra can be easily distinguished from pyrite, which is diamagnetic and displays a two-line subspectrum. Lepidocrocite, in particular, has a magnetic ordering of 77 K above which its subspectrum is a paramagnetic two-line pattern with parameters overlapping those of pyrite, making accurate differentiation more difficult.

The Mössbauer spectra reveal the formation of an additional phase other than Lp, Gt and pyrite in all of the runs shortly after the beginning of the reaction. This phase presents as an asymmetric six-line pattern and appears as a minor phase in the HR runs (Fig. 4.5), and as the dominant or exclusive phase in LR runs (Fig. 4.6-4.7). We propose that this phase represents an intermediate Fe-sulfide phase. This attribution is made based on i) TEM observations by Hellige et al. (2012) who observed a phase rich in Fe and S at the surface of lepidocrocite after a reaction with sulfide; ii) the presence of surface polysulfides and the possibility of Fe-polysulfide association as

discussed in Wan et al. (2014); and iii) the fact that the phase appears with consistent Mössbauer parameters throughout our experiments. Mössbauer parameters reported.

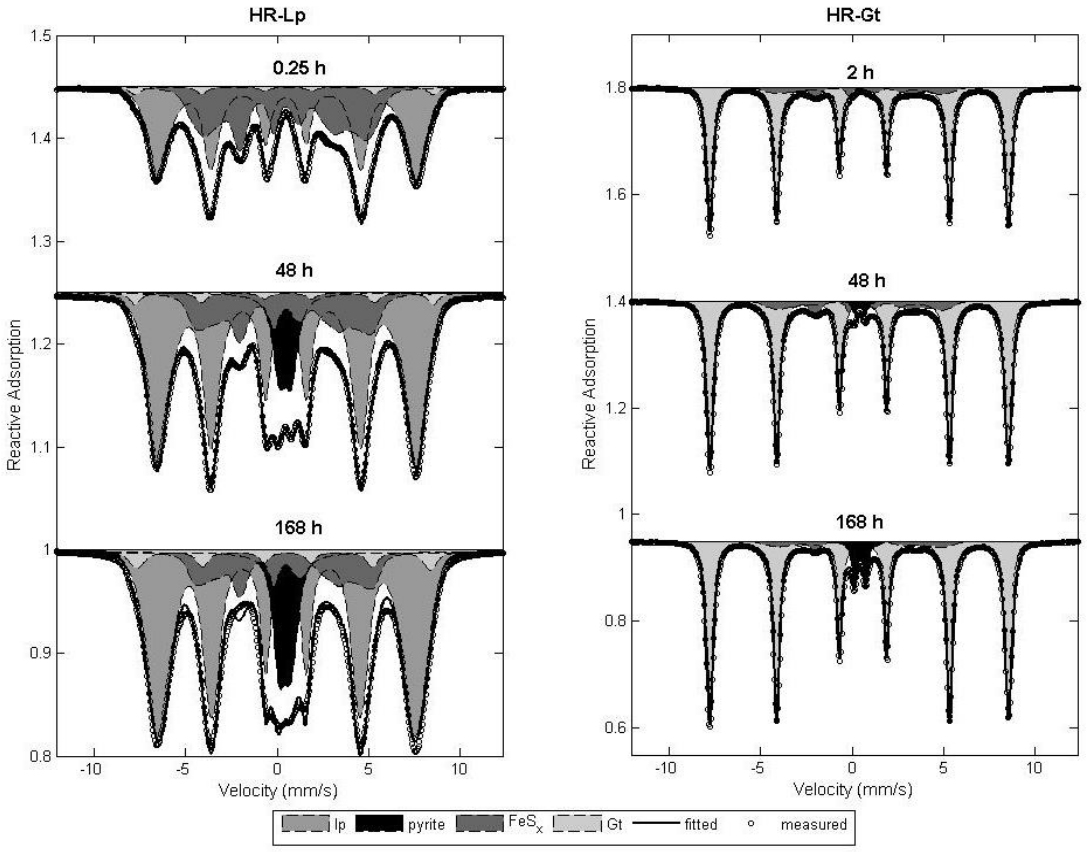

Fig. 4.5 Representive Mössbauer spectra of HR runs. Corresponding parameters were listed in Table 4.2.

for mackinawite previously (e.g. (Bertaut et al., 1965; Morice et al., 1969; Mullet et al., 2002; Vaughan and Ridout, 1971) are conflicting with each other and are not consistent with our results in all cases. We are trying to resolve this conflict in more detail in a separate manuscript (Schröder et al., in prep.). In this study we will refer to this phase as FeS_x with $x \geq 1$ and acknowledge that it may comprise mackinawite as well as other Fe sulfide intermediates.

In HR runs, FeS_x occurred within the first two hours in which no pyrite formation could be observed. After 48 h, pyrite is present in addition to FeS_x. After 168 h, the amount of pyrite has increased significantly while the amount of FeS_x has decreased. It appears that much more Fe(III) of the Lp had reacted to form FeS_x and eventually pyrite. This difference is, however, only relative and caused by the higher Fe:S ratio

(Table 4.1) in the HR_Gt experiments, which was chosen to compensate for the lower specific surface area of Gt compared to Lp.

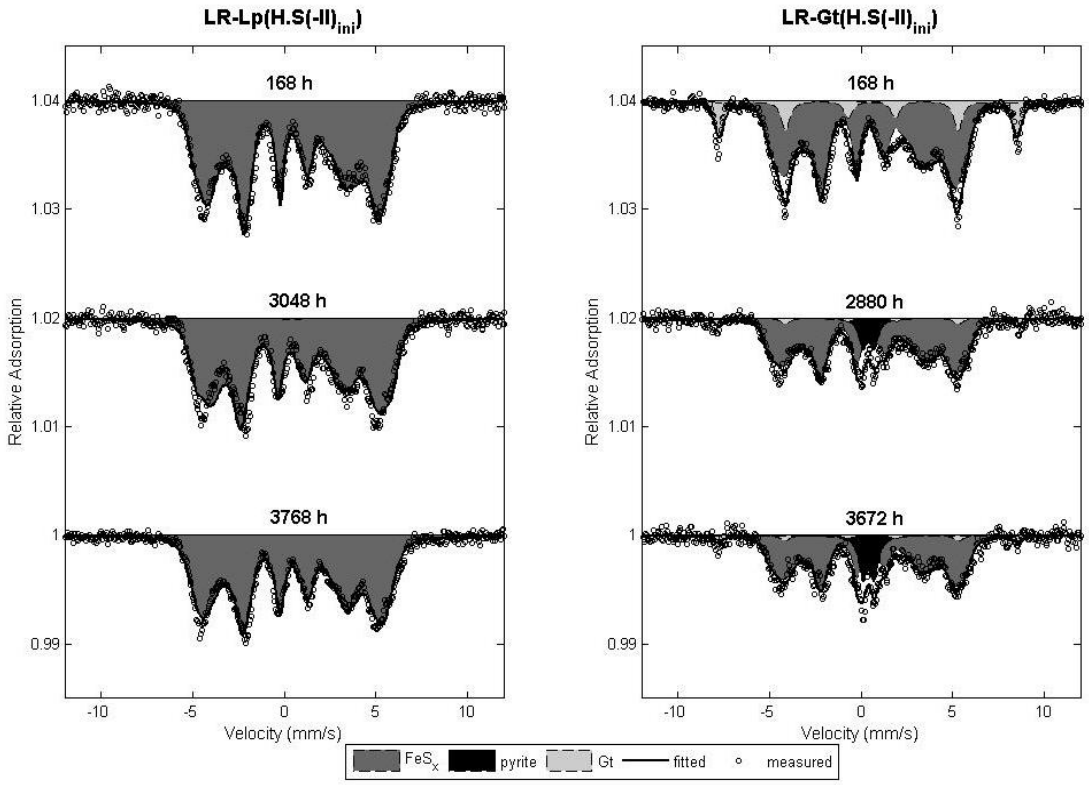

Fig. 4.6 Representive Mössbauer spectra of long-term LR runs (left: Lp; right: Gt) in the precence of high concentration of remaining aqueous sulfide. Corresponding parameters were listed in Table 4.2.

In the LR runs with high concentration of initial $S(II)_{aq}$, Lp is completely consumed and transformed into FeS_x after 72 h. This phase remains almost unchanged until the end of the experiment after 3768 h when still no pyrite formation can be observed (Fig. 4.6). The major phase in the Gt run is also FeS_x but there are some marked differences. First, Gt is not completely consumed after 168 h, and a residual amount of Gt remains until the end of the experiment after 3672 h. Secondly, pyrite formed after 2880 h. In the LR_Lp run with lower concentration of initial aqueous sulfide, all Lp was again converted into FeS_x afte 72 h. However, in this case most of FeS_x has been converted into pyrite and greigite after 3312 h (Fig. 4.7).

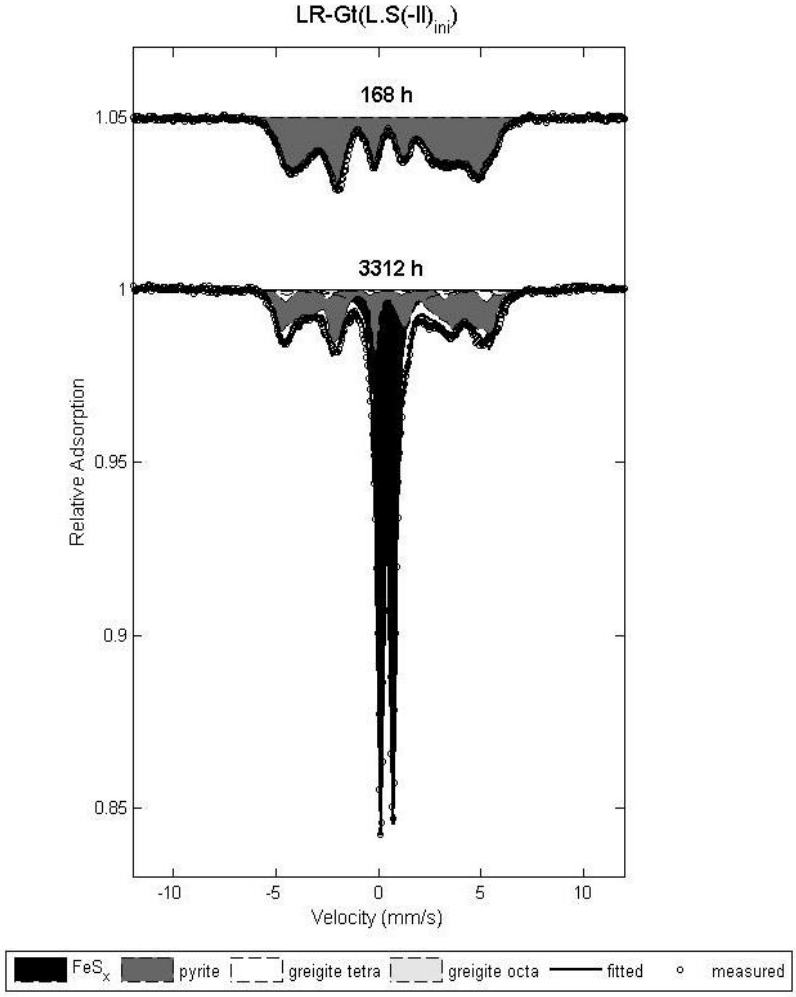

Fig. 4.7 Mössbauer spectra of long-term LR_Lp run in the presence of low concentration of remaining aqueous sulfide. Corresponding parameters were listed in Table 4.2.

Table 4.2 Model parameters for 4.2 K Mössbauer spectra of ^{57}Fe hydroxides reacted with sulfide

	Δ (mm/s)	ΔE_Q (mm/s)	H (T)
Lepidocrocite	0.49	0.03	43.5
Goethite	0.48	-0.11	50.5
FeS_x	0.48	-0.02	27.8
Greigite tetra	0.37	0	30.4
Greigite oct	0.71	-0.015	32.0
pyrite	0.42	0.60	

In all of the runs, pyrite formation occurred at the time points where $Fe(II)_{HCl}$ and/or MES started to decrease, which indicates a relationship between consumption of MES and $Fe(II)_{HCl}$ and pyrite formation. We therefore examined the concentration of MES and Fe(II) bound with pyrite in selected runs with goethite (HR run). Fe(II) bound with pyrite was extracted with hot concentrated HCl (c=12 mol L^{-1}). Prior to the extraction, ferric (hydr)oxides and weak acid extractable $Fe(II)_{HCl}$ were carefully removed with cold HCl (c=9 mmol L^{-1}) (detailed extraction procedures c.f. supporting information). The determination of pyrite in this way is semi-quantitative because some small particles of pyrite may dissolve during the pre-treatment process. It appeared, albeit with uncertainty, that the increase of pyrite concentration indeed corresponded to the consumption of MES (SI 4.1).

4.6 Discussion

4.6.1 Kinetics of pyrite formation

In this subchapter we are going to examine the kinetics of pyrite formation and to evaluate the importance of parameters controlling pyrite formation in different runs.

Pyrite was observed in several studies the interaction between ferric iron and sulfide (Hellige et al., 2012; Peiffer et al., 2015; Price and Shieh, 1979). Elemental sulfur, polysulfides (associated to the surface) and solid-phase ferrous iron species are key initial products (Hellige et al., 2012; Peiffer et al., 2015; Price and Shieh, 1979; Wan et al., 2014) which are regarded to be essential for pyrite formation (refe.). In our study, MES (oxidized sulfur comprising elemental sulfur and polysulfide) as well as $Fe(II)_{HCl}$ reached their maximum concentration after a completion of sulfide reduction (within 3 h, Fig. 4.2 and Fig. 4.3). For instance, MES concentration was in a range of 1-2.5 mmol L^{-1}, and ferrous iron was 4-7 mmol L^{-1}. MB spectra indicated that especially in HR runs the decrease in MES and ferrous iron occurring after 24-48 h corresponds to pyrite formation. Although the concentrations of MES and ferrous iron in LR runs were similar to those that in HR runs, pyrite formation was significantly delayed in these experiments. The formation rate in LR runs was much slower than in HR runs, in which pyrite concentration reached a maximum within 1 week (Fig. 4.8).

The separated analytical methods (wet chemical analysis and MB spectroscopy) showed a strong relationship between MES decrease and pyrite formation. And the additional examination in concentration of MES and Fe(II) bound with pyrite at different time steps in HR runs revealed a negative correlation (SI 4.1, and Fig. 4.9) although the extraction procedures of Fe(II) bound with pyrite was underneath an inevitable uncertainty. Therefore the pyrite formation rate can be derived using the following relationship (eq 1):

$$R = \frac{\Delta c_{FeS_{2,py}}}{\Delta t} = -\frac{\Delta c_{MES}}{\Delta t} \qquad (1)$$

where R denotes pyrite formation rate, $\Delta c_{FeS_{2,py}}$ and Δc_{MES} denote change of concentration of pyrite and MES, respectively.

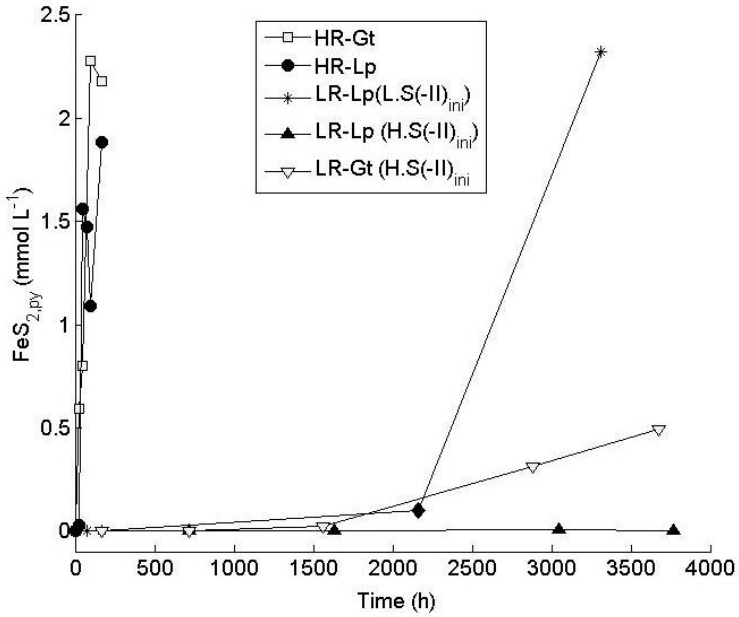

Fig. 4.8 Pyrite concentration measured with Mössbauer spectroscopy. The diamond point at 2160 h in LR_Lp run with low initial $S(-II)_{aq}$ (L. $S(-II)_{ini}$) means that pyrite was calculated according to the wet chemical analyais.

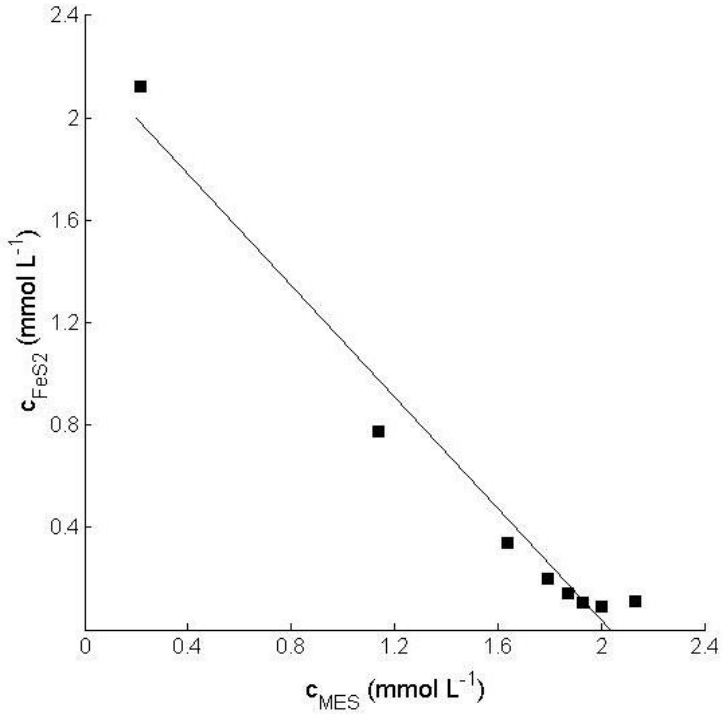

Fig. 4.9 Representive plot of the concentration of MES and Fe(II) bound with pyrite at each individual time step in HR run.

The consumption rate of MES in HR runs appeared to be pseudo first-order with respect to the maximum concentration of MES during the first phase of the reaction (within the first 3 h) (Fig. 4.10). The slopes obtained from the logarithmic plot of MES consumption (Fig. 4.10) have a mean value of 6×10^{-6} s^{-1} for both the HR_Gt (Run 6&7) and the HR_Lp (Run 2,3&5) run at room temperature and 2×10^{-5} s^{-1} for the HR_Gt run (Run 8&9) at high temperature. It seems that, at room temperature, the reactivity of iron hydroxides has little effect on the pyrite formation rate in the HR_Gt run and HR_Lp run. Higher reaction temperature leads to a faster MES consumption and thus faster pyrite formation. An increase in temperature was also reported to accelerate pyrite synthesis from FeS and different sulfur sources (Luther, 1991; Rickard, 1997).

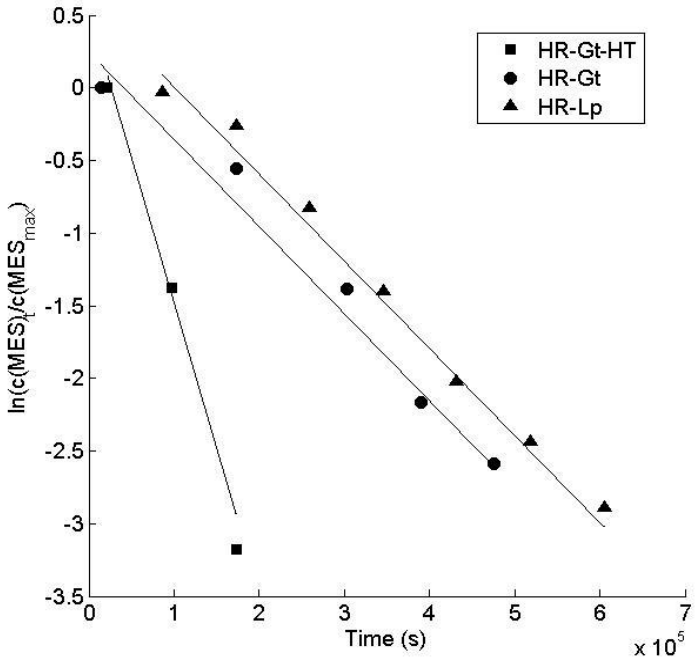

Fig. 4.10 Plot of logarithm of MES consumption versus time for HR runs.

The slopes derived from Fig. 4.10 can be interpreted as observed reaction rate constant k_{obs} for the formation of pyrite from MES (eq 2),

$$R_{py} = -k_{obs} \cdot c_{MES_{max}} \qquad (2)$$

which can be compared with the rate constant derived for the polysulfide pathway. The polysulfide pathway is based on pyrite synthesis in a suspension containing elemental sulfur, aqueous sulfide and FeS and predicted that pyrite formation depended on the FeS and polysulfide (Rickard, 1975), which can be rapidly form during the reaction between elemental sulfur and aqueous sulfide (eq 3a) (Kamyshny et al., 2006). Pyrite formation rate via the polysulfide pathway (eq 3b) is second order with respect to the surface area of FeS and first order with respect to elemental sulfur and aqueous sulfide activity (eq 4).

$$HS^- + (n-1)/8\ S_8 = H^+ + S_n^{2-} \quad (3a)$$

$$FeS + S_n^{2-} = FeS_{2,py} + S_{n-1}^{2-} \quad (3b)$$

$$R_{py} = k_{py} \cdot (A_{FeS})^2 \cdot A_{S^0} \cdot \{S(-II)_{aq}\} \cdot \{H^+\} \quad (4)$$

where R_{py} denotes pyrite formation rate; k_{py} denotes the rate constant); A_{FeS} and A_{S^0} denote the surface area of FeS and elemental sulfur, respectively; $\{S(-II)_{aq}\}$ and $\{H^+\}$ denote the activity of aqueous sulfide and proton, respectively.

k_{py} was derived from the dataset in Rickard (1975) was 1.5×10^{-13} cm^6 mol^{-1} L^{-1} s^{-1}. It seemed, however, that this value is erroneous because of the incorrect unit. We have therefore recalculated the rate constant using the original data from Rickard (1975) (calculation process c.f. supporting information). The recalculated k_{py} is with an order of 10^4 L^5 mol^{-5} $s^{-1}$with a consideration of concentration instead of surface area (eq 5).

$$R_{py} = k_{py} \cdot (c_{FeS})^2 \cdot c_{S^0} \cdot c_{S(-II)_{aq}} \cdot c_{H^+} \quad (5)$$

In our experiments the pH was kept constantly at 7 and $S(-II)_{aq}$ was negligible, the concentration of which was < 0.3 mmol L^{-1} after 3 h). Moreover, the decrease of $Fe(II)_{HCl}$ was around 1-2 mmol L^{-1} and compared with the total $Fe(II)_{HCl}$ (5-7 mmol L^{-1}), it is reasonable to assume that $Fe(II)_{HCl}$ concentration remained a magnitude order of 10^{-4} mol L^{-1}. Using these values we can roughly calculate the first order rate constant k_{py} with respect to MES, having an magnitude order of 10^{-13} s^{-1} with a presumption that $S(-II)_{aq}$ concentration was constantly with an magnitude order of 10^{-4} mol L^{-1}.The obtained first order rate constant k_{py} is 7 orders of magnitude smaller

compared with k_{obs}, indicating that pyrite formation rate in our HR runs is significantly faster than that obtained by Rickard (1975).

Pyrite formation rates runs were faster than predicted by the model proposed in Rickard (1975) not only in HR runs but also in LR runs. Fig. 4.11 displays pyrite concentrations predicted by the polysulfide pathway (eq 4) with concentrations of $Fe(II)_{HCl}$, MES and $S(II)_{aq}$ as measured in the LR runs. Only in the LR_Lp run with rather high initial $S(-II)_{aq}$ concentration (c=20 mmol L^{-1}) the predicted pyrite concentration matches the measured one.

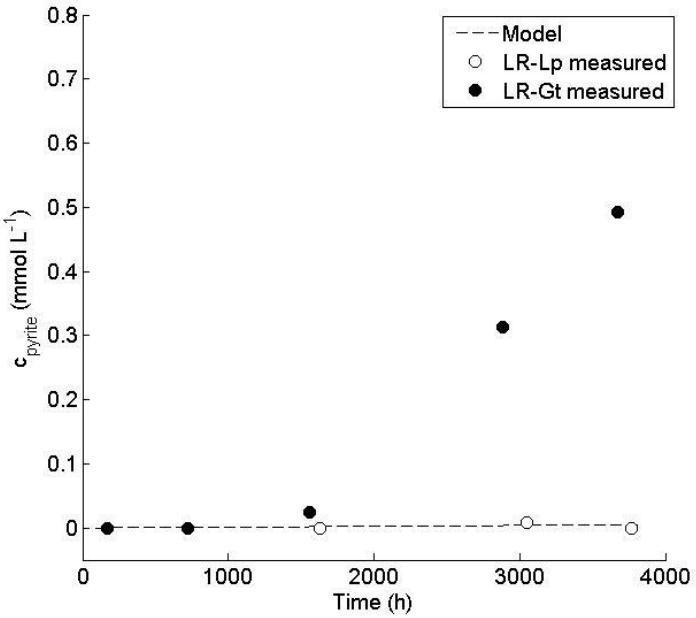

Fig. 4.11 Measured $FeS_{2,py}$ concentration in LR_Gt and LR_Lp with high concentration of initial $S(II)_{aq}$ compared to predicted $FeS_{2,py}$ concentration forming via the polysulfide pathway (eq 3).

Overall, pyrite formation in our experiments is significantly faster than that predicted by Rickard's polysulfide model (Rickard, 1975), particularly in the HR runs where only trace amounts of $S(-II)_{aq}$ remained in the system after 3 h.The pyrite formation rates achieved a maximum at a given ratio of surface sites of goethite and lepidocrocite to sulfide (>0.06 in our study), up to which the rate significantly orders of magnitude slowed (Fig. 4.12). Interestingly, this threshold ratio (>0.06) revealed the presence of residual ferric hydroxides during pyrite formation, which gives a hint

that pyrite formation was linked to mineral reactivity and/or the surface species or surface complexes at the ferric hydroxides' surfaceWe have observed that mineral reactivity

of lepidocrocite and goethite had little effect on pyrite formation. It seems, therefore, that the surface species or surface complexes of ferric hydroxides played an indisputable role. .

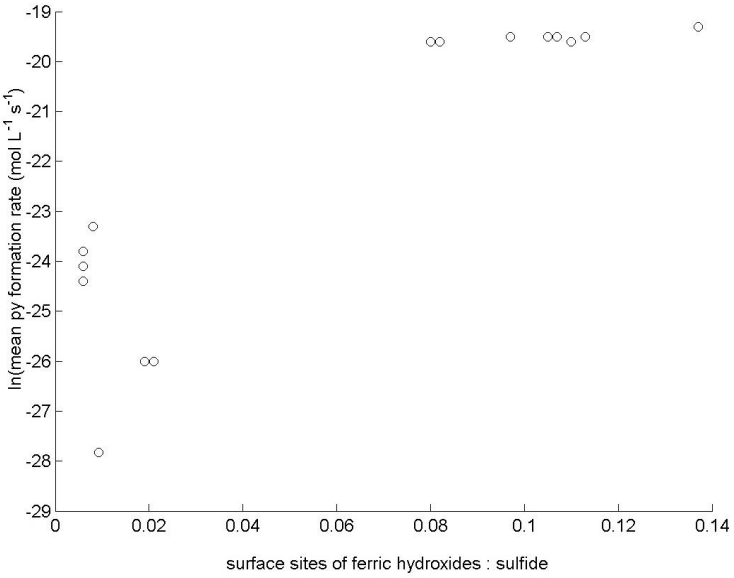

Fig. 4.12 The relationship between logarithm of the mean pyrite formation rate and the molar ratio of surface sites of ferric hydroxides to sulfide.

4.6.2 Ferrous iron species interface pyrite formation

Since Rickard's model (1975) cannot well explain the kinetics of pyrite formation in our experiments, we are considering alternatively that pyrite can nucleate and grow in the presence of essential ferrous iron and disulfide species. The fundamental reaction for pyrite formation was simply the reverse form of pyrite dissolution. (eq 6) (Rickard, 2012) .

$$Fe^{2+} + S_2^{2-} = FeS_2 \qquad (6)$$

It should be noticed that the equation 6 is another form of polysulfide pathway of Rickard's model, only that Fe^{2+} was supplied by the dissolution of FeS (discussed below). The rate-limiting processes of pyrite nucleation/grow are regarded to be the production of reactive sulfur species and of reactive ferrous iron (Luther, 1991;

Rickard, 2012; Schoonen and Barnes, 1991a). With the presence of both essential ferrous iron and disulfide, pyrite formation is kinetically controlled by the degree of supersaturation and an achievement of a critical supersaturation readily initiate a spontaneous pyrite nucleation (Harmandas et al., 1998; Rickard, 2012; Schoonen and Barnes, 1991a). The supersaturation ratio of pyrite (Ω_{py}) was calculated by concentration of both reactive ferrous iron and disulfide. Hence, the question arises whether and how both sulfur and ferrous iron species do interfere in the pyrite formation process.

It can be inferred from companion experiments that the concentration of polysulfide species, i.e. S_2^{2-} was rather high in our experiments. Wan et al (2014) observed that up to 100 % of the oxidized sulfur occurred in a form of polysulfides bound to mineral surface under identical experimental conditions. Up to 34 % of these surface bound polysulfides were S_2^{2-}. Also in the LR runs occurrence of disulfide was observed at the mineral surface (Wan et al., 2014) and in the solution could form rapidly during the rapid equilibrium between aqueous sulfide and elemental sulfur according to the study of Kamyshny (2006).

Since S_2^{2-} formation was fast (within 3 h as a pool of MES), and its concentration was relatively high, we propose that the rate of pyrite formation is controlled by the supply of Fe(II). Metastable iron monosulfide as FeS has been long suggested as a precursor for pyrite formation (Luther, 1991; Schoonen and Barnes, 1991a, b). However, Fe(II) is not necessarily produced by the dissolution of FeS (Rickard, 2012) (eq 7).

$$FeS + H^+ \rightleftharpoons Fe^{2+} + HS^- \qquad (7)$$

Rather, any iron compound which is able to supply Fe(II) can potentially contribute to pyrite formation(Rickard, 2012) . It is interesting to note that significant amounts of HCl extractable Fe(II) could be identified in previous studies (Hellige et al., 2012; Peiffer et al., 2015; Poulton, 2003; Poulton et al., 2004) that appeared not be bound to FeS (excess Fe(II), (Hellige et al., 2012)).

We are therefore going back to examine the Fe(II) generation during the interaction between aqueous sulfide and ferric hydroxides. It is noticed that a surface species ($>Fe^{II}OH_2^+$) could release Fe^{2+} (8d) after a series of processes regarding surface

complexation (eq 8a), electron transfer (eq 8b) and reactive sulfur radical release (8c) (Dos Santos Afonso and Stumm, 1992).

$$> Fe^{III}OH + HS^- \rightarrow > Fe^{III}SH + OH^- \qquad (8a)$$

$$> Fe^{III}SH \rightarrow > Fe^{II}S^{\cdot}H \qquad (8b)$$

$$> Fe^{II}S^{\cdot}H + H_2O \rightarrow > Fe^{II}OH_2^+ + S^{\cdot -} \qquad (8c)$$

$$> Fe^{II}OH_2^+ \rightarrow new\ surface\ site + Fe^{2+} + H_2O \qquad (8d)$$

Fe^{2+} can be trapped for FeS precipitation in the presence of aqueous sulfide, as observed in most of studies regarding pyrite formation (Benning et al., 2000; Hellige et al., 2012; Luther, 1991; Peiffer et al., 2015; Poulton, 2003; Price and Shieh, 1979; Schoonen and Barnes, 1991b; Schoonen, 2004). However, when establishing an electron balance, it appeared that a substantial fraction of the generated Fe(II) could not be attributed to FeS. It was proposed that this excess Fe(II) is adsorbed or associated with the surface (Hellige et al., 2012; Peiffer et al., 2015; Poulton, 2003; Poulton et al., 2004). The competition between excess Fe(II) and FeS formation is proposed to be ruled by two factors: 1) the ratio between added sulphide and available surface area of the ferric hydroxides, and 2) the capability of the iron(hydr)oxide to conduct electrons from surface bound $>Fe^{II}OH_2^+$ to bulk Fe(III) and to accommodate structural Fe(II) which depends on the kinetics of electron transfer between $>Fe^{II}OH_2^+$ and the bulk mineral, i.e. mineral reactivity . With increasing initial sulfide concentration, precipitation of FeS is kinetically favoured. The concentration of $>Fe^{II}OH_2^+$ decreases upon precipitation of FeS (eq 7) and finally disappears under conditions where sulfide is in huge excess to ferric hydroxides, which is the case in our LR runs.

According to this model, the surface species $>Fe^{II}OH_2^+$ generated during the initial interaction between sulfide and ferric hydroxides is reactive and able to induce the electron transfer and trigger the formation of secondary mineral such as magnetite (Hellige et al., 2012; Peiffer et al., 2015) and therefore can supply Fe^{2+} for pyrite formation. Since a large amount of polysulfde species, particularly S_2^{2-} were associated at the mineral surface (Wan et al., 2014) and the polysulfide species have different reactivities decreasing in the sequence $S_5^{2-} > S_4^{2-} > HS^- > HS_2^-$ at near neutral

to slight alkaline pH (c.f. LUTHER, 1990) .The ion reactivity sequence gives a hint that long-chain polysulfides have a higher tendency to react with iron. We therefore propose that after sulfide oxidation at the mineral surface, $>Fe^{II}OH_2^+$ sequesters the polysulfides to form a ferrous iron polysulfide Fe-S_n complex (eq 9),

$$> Fe^{II}OH_2^+ + S_n^{2-} \rightarrow Fe{-}S_n + H_2O \qquad (9)$$

although the Fe-S_2 complex may form more slowly than FeS (eq 7) due to the lower ion reactivity. These complexes are located at the surface and should be mixed with FeS precipitation, either as an amorphous phase or as mackinawite. The chemical properties of ferrous iron in the iron polysulfide complexes and FeS may be different, leading to the asymmetric six-line in the Mössbauer spectra.

It is reasonable to assume that the concentration of surface sites is high relative to aqueous sulfide concentration in the HR runs. Hence, also the concentration of $>Fe^{II}OH_2^+$ is high and through that the tendency to form surface bound Fe-S_n especially Fe-S_2 complexes is high. The presence of Fe-S_n complexes can be proved by our previous and present chemical, microscopic and spectrometric methods. TEM studies showed an amorphous phase at the surface of ferric hydroxides (Hellige et al., 2012; Peiffer et al., 2015). The Mössbauer spectra demonstrated an asymmetric six-line after 3 h implying a presence of compounds other than mackinwite. Combined with wet chemical analysis it is suggested that almost all of the intermediate products located at the surface of ferric hydroxides in HR runs (Hellige et al., 2012; Peiffer et al., 2015; Wan et al., 2014), and ferrous iron generated was generally in excess to that bound with FeS (Hellige et al., 2012; Peiffer et al., 2015). The rest of the $Fe(II)_{HCl}$ ("excess Fe(II)") is able to transfer electrons into the ferric hydroxides bulk (Hellige et al., 2012; Peiffer et al., 2015), or direct bound with polysulfides species due to their higher ion reactivity (Luther, 1990). Other possibility is that electrons go through the bulk and reduce either ferric iron or S^o to form polysulfide (Hellige et al., 2012; Peiffer et al., 2015), which again served for pyrite formation. Nevertheless, whether or not complexes form in between, the accumulation of $>Fe^{II}OH_2^+$ and polysulfide species at the mineral surface served as the sources for pyrite formation. A calculation showed Ω_{py} with an order of 10^{19} in the presence of surface species excess Fe(II) and surface polysulfides (calculation process see supporting information), which is huge

compared with that of 10^{14} required for spontaneous pyrite nucleation (Harmandas et al., 1998; Rickard, 2012)and therefore lead to a rapid pyrite nucleation near the ferric hydroxides surface after 24-48 h, depending on the reaction temperature. The precipitation of FeS prior to pyrite formation cannot be avoided, because once achieving Ω_{py}, the system tend to saturated with FeS as well, and nucleation rate of FeS is significantly faster than that of pyrite (Schoonen and Barnes, 1991a).

The pyrite nucleation triggered the collapse of mixed phases at the surface of ferric hydroxides and appeared to induce FeS dissolution after 72 h (c.f. TEM observation in Heillige et al.(2012)). The polysulfide and ferrous iron at the surface $>Fe^{II}OH_2^+$ were significantly decreased and allowed a new surface sites generated along with pyrite nucleation. And the new surface sites are readily to adsorb residual HS^- adsorption (eq 8a) and activate a sulfide oxidation (eq 8b-8c) at the surface after 24-48h. The concentration of residual HS^- was low (<0.05 mmol L^{-1}) and should equilibrate with FeS. The consumption of subtle HS^- would induce the dissolution of FeS (eq 7) and also release Fe^{2+} as for pyrite formation or to the solution (Fig. 4.2, after 48 h). The total reaction can be described as following equation (10).

$$2H_2O + 2FeS + 2FeOOH = \ FeS_2 + \ Fe^{2+} + 6OH^- \qquad (10)$$

In LR runs, pyrite formation was significantly slower compared with that in HR runs, although the concentration of generated $Fe(II)_{HCl}$ and MES were similar with that in HR runs (e.g. $Fe(II)_{HCl}$ concentrations were 3-4 mmol L^{-1} in compared with 5-7mmol L^{-1} in HR runs). As mentioned above, the generated ferrous iron, which is not bound with sulfide as FeS, served as pyrite formation. And sulfide is able to outcompete with the formation of excess Fe(II) in precipitation FeS with ferrous iron(Peiffer et al., 2015). In LR runs, all of the generated ferrous iron was preferentially trapped by aqueous sulfide to precipitate FeS. And correspondingly, the reactive Fe(II) required for pyrite formation was only produced by the dissolution of FeS (eq 7). With the presence of polysulfide species, pyrite formation is kinetically controlled by the dissolution of FeS. The concentration of $Fe(II)_{aq}$ calculated via the equation derived by Rickard (2006) was around 4.2×10^{-15} mol L^{-1} and 1.3×10^{-13} mol L^{-1} at neutral pH in the presence of c.a. 15 mmol L^{-1} (e.g. Run 42) and 0.5 mmol L^{-1} (e.g. Run 37) residual sulfide, respectively. And the corresponding Ω_{py} was in an order of 10^{-6} and

10^{-8} in the presence of 0.2 mmol L^{-1} aqueous polysulfide (the calculation was with an assumption of all polysulfides to be disulfide, calculation process see supporting information). These values were far from that of 10^{14} required for spontaneous pyrite nucleation. Therefore, the pyrite formations were slower in both cases than that in HR runs. And higher Ω_{py} in Run 37 yielded a faster pyrite nucleation (Fig. 4.8).

Interestingly, in the LR_Gt in the presence of high residual sulfide (e.g. Run 18) where the Fe/S ratio is similar with LR_Lp (Run 42), pyrite formed faster (Fig. 4.8). This phenomenon can be again linked to the availability of excess Fe(II) but in a small regime. Mössbauer spectroscopy confirmed a small amount of goethite still remained in the system, albeit decreasing along with time. The presence of goethite provided a reactive surface to allow a high Ω_{py} in a very small regime. Hence, pyrite nucleation occurred near the goethite surface. Once pyrite nuclei formed, the crystal grows was relatively fast (Schoonen and Barnes, 1991a).

4.7 Conclusion and implication

The sulfidation of ferric hydroxides leads to a build-up of both ferrous iron and zero-valent sulfur (either polysulfides or elemental sulfur), both of which are essential for pyrite formation. The generated ferrous iron, aside from precipitation of FeS in the presence of aqueous sulfide, could associate at the surface bound with surface polysulfide species and leads to an rapid pyrite formation within 24-48 h. Compared with normal polysulfide pathway that Fe(II) is mainly originated from FeS dissolution, this novel pyrite formation takes advantage of the presence of excess Fe(II) at the surface and allow fast pyrite nucleation near the surface of ferric hydroxides (Fig. 4.13). The formation of excess Fe(II) is competitive with FeS precipitation (Peiffer et al., 2015). The concentration of Fe(II) for pyrite formation is therefore highly depended on the initial ratio of Fe/S. In the low Fe/S ratio experiments, all generated Fe(II) was precipitated as FeS. Pyrite formation follows the normal polysulfide pathway and therefore kinetically controlled by the dissolution of FeS in the presence of abundant sulfide/polysulfide.

There are several implications concerning the molar Fe/S ratio affecting the kinetics and pathway of pyrite formation during ferric iron and sulfide interaction. The most important of which is that Fe/S ratio may perform as an indicator for rapid pyrite formation during early diagenesis in the anaerobic/suboxic sediments where reactive ferric iron as ferrihydrite, lepidocrociite and goethite present. Johnston et al. (2014) studied iron and sulfur cycling in a re-flooded wetlands and found that abundant ferrous iron present in both pore water as well as reactive ferric iron in the near-surface sediment. Furthermore, aqueous sulfide is depleted in the pore water due to an insufficient sulfate reduction. Hence, high Fe/S ratio is expected in this floodplain and rapid pyrite formation is expected to occur via novel polysulfide pathway. Here, aqueous sulfide generated via sulfate reduction reacted with ferric iron and trigger pyrite formation within days to weeks, leading to absence of FeS and abundance of pyrite in the near-surface sediment (c.f. Fig. 7 in Johnston et al. (2014)). By contrast, sulfide-rich sediments where ferrous iron is depleted in the pore water reflecting a low Fe/S ratio system, pyrite formation was constrained and FeS was usually preserved and dominated in the near-surface sediments (Kraal et al., 2013).

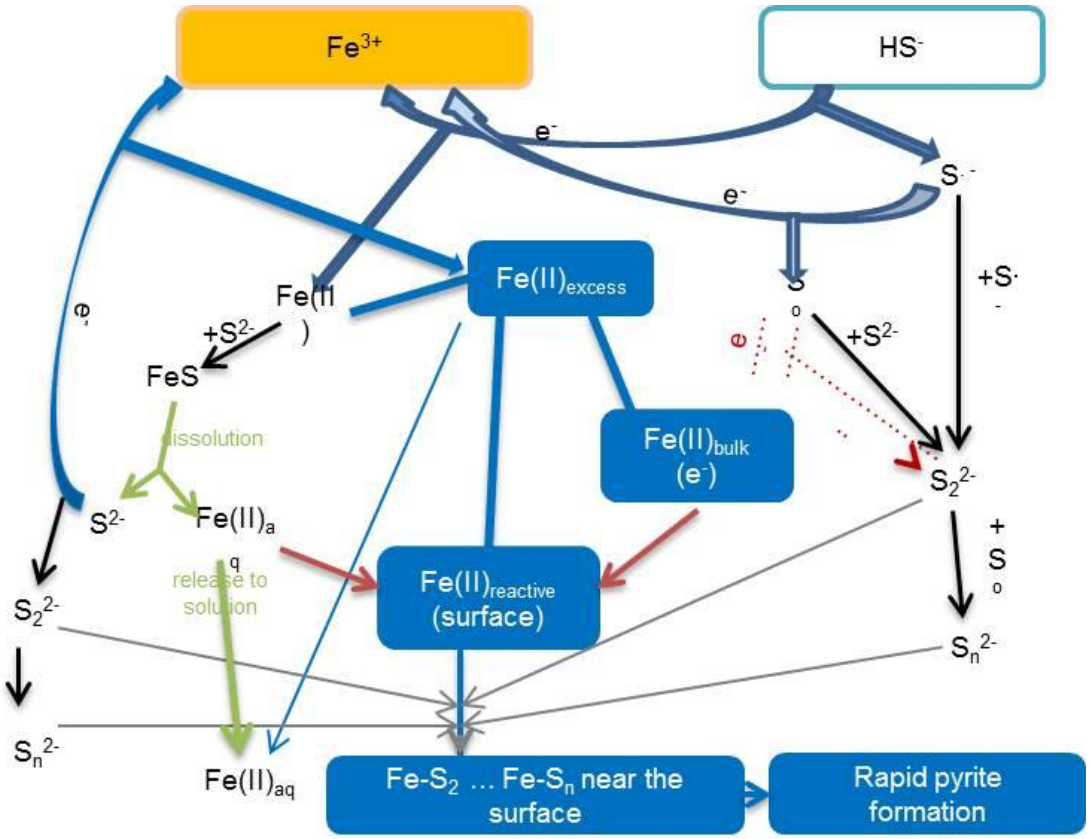

Fig. 4.13 Novel polysulfide pathway near the surface of ferric hydroxides. The iron supply for rapid pyrite formation was marked in red. The initial electron transfer (dark fat arrows) between sulfide and ferric iron generates ferrous iron and $S^o/S^{\cdot-}$. A fraction of ferrous iron was in the form of excess Fe(II) (marked in red), which can either transfer electrons into the bulk ferric hydroxides and later on reduce S^o to form polysulfide (dot line and arrow) or stayed at the surface readily bound with surface polysulfide to form pyrite. The pyrite nucleation leads to a decrease of $Fe(II)_{excess}$, which induced FeS dissolution (green thin arrows) and a second electron transfer (pinky fat arrows) between sulfide and ferric iron, resulting in excess Fe(II) (pinky fat arrows) and polysulfide (black arrows) generation. The increase of $Fe(II)_{aq}$ was originated from FeS dissolution (green arrows) or release of excess Fe(II) (red arrow).

Acknowledgements

This study was financially supported by the German Research Foundation (DFG) for the research group “etrap” (electron transfer processes in anoxic aquifers) (FOR 580, PE 438/11-3 und Z)

The authors declare no competing of financial interest.

4.8 References

Benning, L.G., Wilkin, R.T., Barnes, H., 2000. Reaction pathways in the Fe–S system below 100 C. *Chemical Geology* **167**, 25-51.

Berner, R.A., 1964. Iron sulfides formed from aqueous solution at low temperatures and atmospheric pressure. The *Journal of Geology*, 293-306.

Berner, R.A., 1970. Sedimentary pyrite formation. *American Journal of Science* **268**, 1-23.

Bertaut, E., Burlet, P., Chappert, J., 1965. Sur l'absence d'ordre magnetique dans la forme quadratique de FeS. *Solid State Communications* **3**, 335-338.

Burton, E.D., Bush, R.T., Sullivan, L.A., 2006. Sedimentary iron geochemistry in acidic waterways associated with coastal lowland acid sulfate soils. *Geochimica et Cosmochimica Acta* **70**, 5455-5468.

Butler, I.B., Rickard, D., 2000. Framboidal pyrite formation via the oxidation of iron (II) monosulfide by hydrogen sulphide. *Geochimica et Cosmochimica Acta* **64**, 2665-2672.

Dos Santos Afonso, M., Stumm, W., 1992. Reductive dissolution of iron(III) (hydr)oxides by hydrogen sulfide. *Langmuir* **8**, 1671-1675.

Fonselius, S., Dyrssen, D., Yhlen, B., 1999. Determination of hydrogen sulphide.

Harmandas, N.G., Navarro Fernandez, E., Koutsoukos, P.G., 1998. Crystal Growth of Pyrite in Aqueous Solutions. Inhibition by Organophosphorus Compounds. *Langmuir* **14**, 1250-1255.

Hellige, K., Pollok, K., Larese-Casanova, P., Behrends, T., Peiffer, S., 2012. Pathways of ferrous iron mineral formation upon sulfidation of lepidocrocite surfaces. *Geochimica et Cosmochimica Acta* **81**, 69-81.

Howarth, R.W., 1979. Pyrite: its rapid formation in a salt marsh and its importance in ecosystem metabolism. Science **203**, 49-51.

Johnston, S.G., Burton, E.D., Aaso, T., Tuckerman, G., 2014. Sulfur, iron and carbon cycling following hydrological restoration of acidic freshwater wetlands. *Chemical Geology* **371**, 9-26.

Kamyshny, A., Borkenstein, C.G., Ferdelman, T.G., 2009. Protocol for Quantitative Detection of Elemental Sulfur and Polysulfide Zero-Valent Sulfur Distribution in Natural Aquatic Samples. *Geostandards and Geoanalytical Research* **33**, 415-435.

Kamyshny, A., Ekeltchik, I., Gun, J., Lev, O., 2006. Method for the determination of inorganic polysulfide distribution in aquatic systems. *Analytical Chemistry* **78**, 2631-2639.

Kaplan, I.R., Emery, K.O., Rittenbebg, S.C., 1963. The distribution and isotopic abundance of sulphur in recent marine sediments off southern California. *Geochimica et Cosmochimica Acta* **27**, 297-331.

Kraal, P., Burton, E.D., Bush, R.T., 2013. Iron monosulfide accumulation and pyrite formation in eutrophic estuarine sediments. *Geochimica et Cosmochimica Acta* **122**, 75-88.

Luther, G.W., 1990. The frontier-molecular-orbital theory approach in geochemical processes. In Aquatic Chemical Kinetics; Stumm, W., Ed.; Wiley: New York. 173-198.

Luther, G.W., 1991. pyrite synthesis via polysulfide compounds. *Geochimica et Cosmochimica Acta*, 2839-2849.

Morice, J., Rees, L., Rickard, D., 1969. Mössbauer studies of iron sulphides. *Journal of Inorganic and Nuclear Chemistry* **31**, 3797-3802.

Mullet, M., Boursiquot, S., Abdelmoula, M., Génin, J.-M., Ehrhardt, J.-J., 2002. Surface chemistry and structural properties of mackinawite prepared by reaction of sulfide ions with metallic iron. *Geochimica et Cosmochimica Acta* **66**, 829-836.

Peiffer, S., Behrends, T., Hellige, K., Larese-Casanova, P., Wan, M., Pollok, K., 2015. Pyrite formation and mineral transformation pathways upon sulfidation of ferric hydroxides depend on mineral type and sulphide concentration. *Chemical Geology* **400**, 44-55.

Peiffer, S., Gade, W., 2007. Reactivity of ferric oxides toward H2S at low pH. *Environmen*tal *Science & Technology* **41**, 3159-3164.

Poulton, S.W., 2003. Sulfide oxidation and iron dissolution kinetics during the reaction of dissolved sulfide with ferrihydrite. *Chemical Geology* **202**, 79-94.

Poulton, S.W., Krom, M.D., Raiswell, R., 2004. A revised scheme for the reactivity of iron (oxyhydr)oxide minerals towards dissolved sulfide. *Geochimica et Cosmochimica Acta* **68**, 3703-3715.

Price, F.T., Shieh, Y., 1979. Fractionation of sulfur isotopes during laboratory synthesis of pyrite at low temperatures. *Chemical Geology* **27**, 245-253.

Rickard, D., 1997. Kinetics of pyrite formation by the H2S oxidation of iron(II) monosulfide in aqueous solutions between 25-125 °C: the rate equation. *Geochimica et Cosmochimica Acta*, 115-134.

Rickard, D., 2006. The solubility of FeS. *Geochimica et Cosmochimica Acta* **70**, 5779-5789.

Rickard, D., 2012. Sulfidic sediments and sedimentary rocks. **Newnes**.

Rickard, D., Luther, G.W., 1997. Kinetics of pyrite formation by the H2S oxidation of iron (II) monosulfide in aqueous solutions between 25 and 125 °C: The mechanism. *Geochimica et Cosmochimica* Acta **61**, 135-147.

Rickard, D.T., 1975. Kinetics and mechanism of pyrite formation at low temperatures. *American Journal of Science* **275**, 636-652.

Schoonen, M., Barnes, H., 1991a. Reactions forming pyrite and marcasite from solution: I. Nucleation of FeS2 below 100 °C. *Geochimica et Cosmochimica Acta* **55**, *1495-1504.*

Schoonen, M., Barnes, H., 1991b. Reactions forming pyrite and marcasite from solution: II. Via FeS precursors below 100 C. *Geochimica et Cosmochimica Acta* **55**, 1505-1514.

Schoonen, M.A., 2004. Mechanisms of sedimentary pyrite formation. *SPECIAL PAPERS-GEOLOGICAL SOCIETY OF AMERICA*, 117-134.

Schröder, C., Wan, M., Peiffer, S., in prep. Electromagnetic properties of mackinawite: Removing inconsistencies between density functional theory and Mössbauer spectroscopy.

Schwertmann, U., Cornell, R.M., 2008. Iron oxides in the laboratory. **Wiley-Vch**.

Steudel, R., Holdt, G., Göbel, T., Hazeu, W., 1987. Chromatographic Separation of Higher Polythionates SnO 62-(n= 3… 22) and Their Detection in Cultures of Thiobacillus ferroxidans; Molecular Composition of Bacterial Sulfur Secretions. *Angewandte Chemie International Edition in English* **26**, 151-153.

Tabatabai, M., 1974. A rapid method for determination of sulfate in water samples. *Environmental Letters* **7**, 237-243.

Tamura, H., Goto, K., Yotsuyanagi, T., Nagayama, M., 1974. Spectrophotometric determination of iron (II) with 1, 10-phenanthroline in the presence of large amounts of iron (III). *Talanta* **21**, 314-318.

Vaughan, D., Ridout, M., 1971. Mössbauer studies of some sulphide minerals. *Journal of Inorganic and Nuclear Chemistry* **33**, 741-746.

Wan, M., Shchukarev, A., Lohmayer, R., Planer-Friedrich, B., Peiffer, S., 2014. Occurrence of Surface Polysulfides during the Interaction between Ferric (Hydr)Oxides and Aqueous Sulfide. *Environmental Science & Technology* **48**, 5076-5084.

Wilkin, R., Barnes, H., 1996. Pyrite formation by reactions of iron monosulfides with dissolved inorganic and organic sulfur species. *Geochimica et Cosmochimica Acta* **60**, 4167-4179.

4.9 Supporting Information

Fe/S ratio controls pathway and kinetics of pyrite formation during Fe(III)-S(-II) interaction

Moli Wan[1], Christian Schröder[2], Stefan Peiffer[1]

[1] BayCEER, Department of Hydrology, University of Bayreuth, D-95440, Bayreuth, Germany

[2] Biologcial and Environmental Sciences, School of Natural Sciences, University of Stirling, Stirling FK9 4LA, Scotland, UK

* Corresponding author. Phone ++49-921-553500, Fax ++49-921-552366, moli.wan@uni-bayreuth.de

9 pages, 1 figure and 3 tables are presented in this supplementary file.

Table S4.1 Area concentration of iron mineral in the Mössbauer spectra in Fig 4.5, 4.6 and 4.7

	Time	Pyrite	lepidocrocite	goethite	FeS	greigite
	h			%		
HR_Lp	0.25	0	56.82	3.63	39.55	0
	48	9.87	67.64	3.17	19.32	0
	168	11.91	63.10	5.82	19.17	0
HR_Gt	2	0.00	0.00	89.52	10.48	0
	48	2.17	0.00	86.89	10.93	0
	168	5.90	0.00	87.36	6.74	0
LR_Lp(H.S(-II)$_{ini}$)	168	0	0	0	100	0
	3048	0.24	0	0	99.76	0
	3768	0	0	0	100	0
LR_Gt(H.S(-II)$_{ini}$)	168	0	0	18.07	81.70	0
	2880	9.20	0	6	84.80	0
	3672	14.50	0	0	79.70	0
LR_Lp(L.S(-II)$_{ini}$)	168	0	0	0	100	0
	3312	58.07	0	0	36.07	5.85

pyrite extraction with concentrated hydrochloride acid

Fe(II) which is strongly bound sulfide, such as pyrite cannot be easily dissolved in 1 mol L^{-1} HCl, such Fe(II) species ($Fe(II)_{py}$) were therefore extracted by concentrated HCl (c = 12 mol L^{-1}) in two HR runs with goethite (Run 7 and Run 9). In 1mL unfiltered samples 3 mL HCl (c = 12 mol L^{-1}), the mixture was shaken and carefully observed in order to make sure that all of the ferric hydroxides were dissolved. This process took usually 16 h. Then mixture was centrifuged, the supernatant was carefully removed, the residual was washed three times by adding deionized water and centrifuging, decanting the supernatant. The residual was dissolved by 1 mL hot HCl (c = 12 mol L^{-1}) at 60 ℃ for 1 week. Then the concentration was measured using method described in the manuscript(Tamura et al., 1974). As nano pyrite cystal may be dissolved in cold concentrated HCl, this measurement was therefore only semi-quantitative.

The representative data of $Fe(II)_{py}$ concentration along with MES concentration in the HR_Gt runs (Run 7 and Run 9) was depicted in the figure SI 4.1.

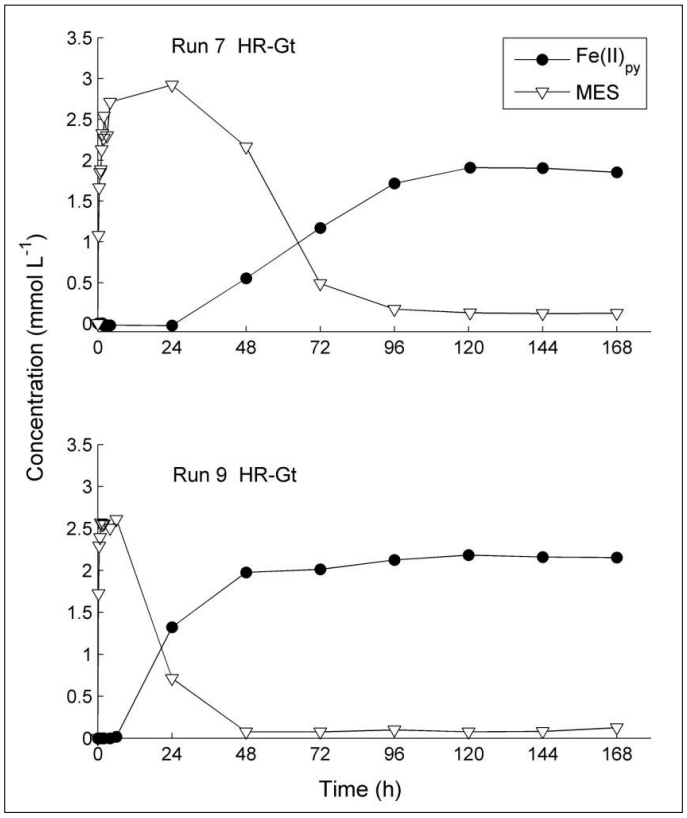

SI 4.1 $Fe(II)_{py}$ and MES concentration in selected HR_Gt runs.

Recalculation of rate constant with respect to pyrite formation using the original data from Rickard (1975)

To simply the calculation process we applied concentration instead of ion activities to calculate the rate constant k_{py} (eq 1)

$$R_{py} = k_{py} \cdot (c_{FeS})^2 \cdot c_{S^0} \cdot c_{S(-II)_{aq}} \cdot c_{H^+} \qquad (1)$$

The results are showed in Table S4.2.

Table S4.2 recalculation of rate constants k_{py} from original dataset from Rickard (1975). Recalculated data are in an italic typeface.

Run	R_{py}	$P(H_2S)^a$	*c(S(-II)$_{aq}$)^b*	$c(H^+)$	$\{S(-II)_{aq}\}^c$	*c(FeS)^d*	SA^e. FeS	*c(S^o)^f*	SA. S^o	T	k_{py}
	mol L^{-1} s^{-1}	atm	mol L^{-1}	mol L^{-1}	-	mol L^{-1}	cm^2	mol L^{-1}	cm^2	K	L^5 mol^{-5} s^{-1}
401	8.3×10^{-7}	1	*9.87*	1×10^{-7}	2×10^{-1}	*4.09* $\times10^{-2}$	1.6×10^{5}	*3.13* $\times10^{-1}$	1.4×10^{3}	313	*7.94* $\times10^{4}$
402	4.8×10^{-7}	0.5	*4.93*	1×10^{-7}	1×10^{-1}	*4.09* $\times10^{-2}$	1.6×10^{5}	*3.13* $\times10^{-1}$	1.4×10^{3}	313	*9.18* $\times10^{4}$
403	2.3×10^{-7}	0.25	*2.47*	1×10^{-7}	5×10^{-2}	*4.09* $\times10^{-2}$	1.6×10^{5}	*3.13* $\times10^{-1}$	1.4×10^{3}	313	*8.8* $\times10^{4}$
404	9.5×10^{-7}	0.1	*0.99*	1×10^{-7}	2×10^{-2}	*4.09* $\times10^{-2}$	1.6×10^{5}	*3.13* $\times10^{-1}$	1.4×10^{3}	313	*9.08* $\times10^{4}$
405	4.9×10^{-7}	0.05	*0.49*	1×10^{-7}	1×10^{-2}	*4.09* $\times10^{-2}$	1.6×10^{5}	*3.13* $\times10^{-1}$	1.4×10^{3}	313	*9.37* $\times10^{4}$
502	4.8×10^{-7}	1	*9.87*	1×10^{-7}	2×10^{-1}	*4.09* $\times10^{-2}$	1.6×10^{5}	*1.56* $\times10^{-1}$	7×10^{2}	313	*9.18* $\times10^{4}$
503	1.9×10^{-7}	1	*9.87*	1×10^{-7}	2×10^{-1}	*4.09* $\times10^{-2}$	1.6×10^{5}	*7.81* $\times10^{-2}$	3.5×10^{2}	313	*7.27* $\times10^{4}$
504	5.4×10^{-8}	1	*9.87*	1×10^{-7}	2×10^{-1}	*4.09* $\times10^{-2}$	1.6×10^{5}	*3.13* $\times10^{-2}$	1.4×10^{2}	313	*5.16* $\times10^{4}$
602	1.5×10^{-7}	1	*9.87*	1×10^{-7}	2×10^{-1}	*2.10* $\times10^{-2}$	8.2×10^{5}	*3.13* $\times10^{-1}$	1.4×10^{3}	313	*5.46* $\times10^{4}$
603	4.8×10^{-8}	1	*9.87*	1×10^{-7}	2×10^{-1}	*1.05* $\times10^{-2}$	4.1×10^{5}	*3.13* $\times10^{-1}$	1.4×10^{3}	313	*6.99* $\times10^{4}$
604	2×10^{-6}	1	*9.87*	1×10^{-7}	2×10^{-1}	*6.39* $\times10^{-2}$	2.5×10^{5}	*3.13* $\times10^{-1}$	1.4×10^{3}	313	*7.83* $\times10^{4}$
702	7×10^{-7}	1	*9.87*	3.16×10^{-7}	5×10^{-1}	*4.09* $\times10^{-2}$	1.6×10^{5}	*3.13* $\times10^{-1}$	1.4×10^{3}	313	*2.68* $\times10^{4}$
703	6.4×10^{-7}	1	*9.87*	1×10^{-7}	1.1	*4.09* $\times10^{-2}$	1.6×10^{5}	*3.13* $\times10^{-1}$	1.4×10^{3}	313	*1.11* $\times10^{4}$
802	4.5×10^{-6}	1	*9.87*	1×10^{-7}	2×10^{-1}	*4.09* $\times10^{-2}$	1.6×10^{5}	*3.13* $\times10^{-1}$	1.4×10^{3}	323	*4.30* $\times10^{4}$
803	4.2×10^{-7}	1	*9.87*	1×10^{-7}	2×10^{-1}	*4.09* $\times10^{-2}$	1.6×10^{5}	*3.13* $\times10^{-1}$	1.4×10^{3}	305	*4.02* $\times10^{4}$
804	1.2×10^{-7}	1	*9.87*	1×10^{-7}	2×10^{-1}	*4.09* $\times10^{-2}$	1.6×10^{5}	*3.13* $\times10^{-1}$	1.4×10^{3}	293	*1.15* $\times10^{4}$

[a] partial pressure of hydrogen sulfide gas

[b] concentration of total aqueous sulfide, calculated followed Henry's law $p=k \cdot c$ with $k = 0.10$ mol L^{-1} bar^{-1} (Sander)

[c] reactivity of total aqueous sulfide, not used in the recalculation

[d] concentration of FeS calculated using the surface area of 4.4×10^5 cm^2 g^{-1} and 0.1 L solution (Rickard, 1975)

[e] initial surface area of FeS

[f] concentration of S^o calculated with the surface are of 1.4×10^3 cm^2 g^{-1} and 0.1 L solution (Rickard, 1975)

Supersaturation ratio of pyrite in LR runs with presence of high aqueous sulfide

Supersaturation ratio (Ω_{py}) was calculated using the following equation (Harmandas et al., 1998):

$$\Omega_{py} = \frac{\{Fe^{2+}\} \cdot \{S_2^{2-}\}}{K_{sp}} \qquad (2)$$

where braces denote the activities of the corresponding ions and K_{sp} is the thermodynamic solubility product of pyrite (8.511×10^{-26} mol^2).

In order to simplify the calculation, we applied ions concentration instead of activities and apply the highest concentration of aqueous polysulfides to present disulfide (0.5 mmol L^{-1}) . The ferrous iron was under the detection limit in the LR runs, the concentration was therefore calculated via FeS solubility (Rickard, 2006):

$$\log c_{Fe(II)} = \log K_{FeS} + \log K_{sp} - \log\{H_2S\} - 2pH \qquad (3)$$

where $c_{Fe(II)}$ denotes total concentration of Fe^{2+}, k_{FeS} (log k_{FeS} = -5.7) and k_{sp} (log k_{sp} = 3.5) denote two different solubility product of mackinawite. Braces denotes activity of H_2S was replaced by concentration during calculation.

The calculation showed at pH 7 in the presence of around 20 mmol L^{-1} aqueous sulfide, the total Fe^{2+} was with the order of 10^{-15} mol L^{-1}. And the supersaturation ratio of pyrite was therefore with an order of 10^{-7}.

Table S4.3 supersaturation ratio Ω_{py} with respect to pyrite in the solution (LR runs) and near the ferric hydroxides' surface

Run No.	Run description	Fe(II)	$S(-II)_{aq}$	S_n^{2-} [b]	pH	Ω_{py}
42	LR_Lp($H.S(-II)_{ini}$)	4.21×10^{-15} [a]	1.5×10^{-2}	5×10^{-4} [b]	7	1.24×10^{7}
37	LR_Lp($L.S(-II)_{ini}$)	1.26×10^{-13} [a]	5×10^{-4}	5×10^{-4} [b]	7	3.71×10^{8}
7	HR_Gt	5.5×10^{-3} [c]	n. [d]	2.8×10^{-3} [e]	7	9.05×10^{18}
25	HR_Lp	7×10^{-3} [c]	n.	2×10^{-3} [e]	7	8.22×10^{18}

[a] Fe(II) concentration calculated via equation 3 after Rickard (2006)

[b] the maximum queous polysulfide concentration. We assume 30 % of which to be disulfide(Wan et al., 2014)

[c] measured acid extractable Fe(II), assumed 10% of which to be Fe(II) supply for rapid pyrite formation near the surface of ferric hydroxides

[d] concentration negligible

[e] measured MES. Most of which is in a form of surface polysulfide according to the previous study and we assume 30 % of MES to be disulfide(Wan et al., 2014).

References

Harmandas, N. G., Navarro Fernandez, E., and Koutsoukos, P. G., 1998. Crystal Growth of Pyrite in Aqueous Solutions. Inhibition by Organophosphorus Compounds. *Langmuir* **14**, 1250-1255.

Rickard, D., 2006. The solubility of FeS. *Geochimica et Cosmochimica Acta* **70**, 5779-5789.

Rickard, D. T., 1975. Kinetics and mechanism of pyrite formation at low temperatures. *American Journal of Science* **275**, 636-652.

Sander, R., "Henry's Law Constants" in **NIST Chemistry WebBook, NIST Standard Reference Database Number 69**, Eds. P.J. Linstrom and W.G. Mallard, National Institute of Standards and Technology, Gaithersburg MD, 20899, http://webbook.nist.gov.

Tamura, H., Goto, K., Yotsuyanagi, T., and Nagayama, M., 1974. Spectrophotometric determination of iron (II) with 1, 10-phenanthroline in the presence of large amounts of iron (III). *Talanta* **21**, 314-318.

Wan, M., Shchukarev, A., Lohmayer, R., Planer-Friedrich, B., and Peiffer, S., 2014. Occurrence of Surface Polysulfides during the Interaction between Ferric (Hydr)Oxides and Aqueous Sulfide. *Environmental Science & Technology* **48**, 5076-5084.

5. Electromagnetic Properties of FeS Phases: Insights from Mössbauer Spectroscopy

Christian Schröder[1,*], Moli Wan[2], Stefan Peiffer[2]

[1] Biological and Environmental Sciences, School of Natural Sciences, University of Stirling, Stirling FK9 4LA, Scotland, UK

[2] Department of Hydrology, University of Bayreuth, 95440 Bayreuth, Germany

[*] Corresponding author. Phone: +44-(0)1786-467809, Fax: +44-(0)1786-467843, christian.schroeder@stir.ac.uk

Manuscript ready to submit to Physics and Chemistry of Minerals

5.1 Abstract

Despite its importance in low-temperature aqueous environments, identification and characterization of mackinawite with standard mineralogical tools remain challenging, mostly due to the small particle size at a nano range and the sensibility towards oxidation. Here, we applied Mössbauer spectroscopy to compare four FeS samples prepared after different synthesis protocols. The cryogenic measurement at around 5 K was selected to study their electromagnetic property. FeS precipitated freshly from a homogeneous ferrous iron and sulfide solution showed a single line. Whereas a dry-aging of the same sample in the anoxic glove box for 1 month lead to a secondary asymmetric six-line occurrence aside from the presence of single line. The FeS prepared from interaction between ferric hydroxide and aqueous sulfide at neutral pH showed only the asymmetric six-line. Varying the initial ratio of ferric iron to sulfide seemed no significant effect on the FeS phase. The single line may result from the instance of cubic valence electron distribution and/or cubic lattice site symmetry, which indicates the FeS precipitation from homogeneous ferrous iron and aqueous sulfide to be cubic FeS. The appearance of asymmetric six line implies either an intermediate spin state (spin state =1) or the presence of impurities or vacancies in the lattices, which indicated no stoichiometric 1:1 FeS generation during reaction between ferric iron and sulfide. A clear transformation occurred between different FeS phases. This study therefore calls for more investigations on FeS synthesized after standard protocols with modern characterization methods.

5.2 Introduction

Iron(II) monosulfide, FeS, is widespread in low-temperature aqueous environments. As a metastable phase it plays an important part in pyrite formation pathways in soils and sediments, and hence participates in many (bio)geochemical processes (e.g. (Rickard and Luther, 2007) and references therein). Stoichiometric FeS occurs in three different mineral forms: As mackinawite, FeS_m; troilite, FeS_t; and cubic FeS, FeS_c. While cubic FeS occurs as a corrosion product of steel and troilite is common in meteorites, only mackinawite has been reported as widespread in natural low-temperature aqueous environments. Mackinawite has likely been available since the Hadean eon (Hazen, 2013), and might have played a role in the origin of life (Russell and Hall, 1997). It has also shown potential for industrial applications in microbial fuel cells (Nakamura et al., 2010) and it has been proposed to be a possible superconductor (Kwon et al., 2011), prompting an interest in its electromagnetic properties.

Despite its significance, and although it has been studied for several decades already, identification and characterization of mackinawite with standard mineralogical tools remain challenging, mostly because it generally occurs in the form of nanosized particles. ^{57}Fe Mössbauer spectroscopy probes hyperfine interactions at the Fe nucleus and does not require any long-range ordering (Gütlich and Schröder, 2012). It should be well-suited to the investigation of mackinawite's electromagnetic properties. However, Mössbauer results are conflicting with calculated results on Fe spin states and the closely related magnetic properties of mackinawite. Rickard and Luther (2007) prescribe a High Spin (HS) state to Fe in mackinawite, whereas Vaughan and Ridout (1971) and Mullet et al. (2002) designate it as Low Spin (LS) on the basis of Mössbauer observations. Density Functional Theory (DFT) calculations have led to opposing conclusions with regard to the magnetic moment of Fe in mackinawite. Devey et al. (2008) calculated a non-magnetic stable ground state, it should have a substantial magnetic moment according to Subedi et al. (2008). Unpaired electrons are necessary for a magnetic moment to arise, and consideration of the accompanying spin is challenging with DFT (Jacob and Reiher, 2012). Mössbauer spectroscopy should be able to provide clarity, yet reported Mössbauer results are similarly confusing. They show the absence of magnetic ordering even when samples were

cooled down to below 4.2 K (Bertaut et al., 1965; Vaughan and Ridout, 1971) as well as magnetic ordering already at room temperature (Morice et al., 1969), while Mullet et al. (2002) observed a mix of phases in spectra obtained at ~11 K with some showing magnetic ordering and others not.

In order to gain a better understanding of these inconsistencies and converge on an interpretation of Fe spin states in and magnetic properties of mackinawite, we used Mössbauer spectroscopy to investigate FeS phases formed under a variety of experimental conditions. For each of these experimental setups, previous studies had assumed the FeS to be mackinawite but this designation had not been confirmed independently in each case. Our investigations provide a better knowledge of which spectral features are reflecting properties of true mackinawite and which reflect different mineral forms of FeS or mineral mixtures. With that knowledge, Mössbauer spectroscopy will be a valuable tool to identify mackinawite in natural samples and to inform DFT calculations upon its electromagnetic properties. In the following we refer to FeS if the mineralogical form is unclear and otherwise to the mineral names, i.e. mackinawite, cubic FeS, or troilite.

5.3 Materials and methods

5.3.1 Mineral synthesis and sample preparation

Mineral synthesis and sample preparation for Mössbauer analysis were performed in anoxic glove box systems with a working atmosphere of N_2 (99.99%) (Unilab Glovebox, M. Braun, and Jacomex Glovebox, Jacomex) because of mackinawite's sensitivity towards oxygen. All solutions were prepared inside a glove box with deionized water (18 MΩ), which had been purged with N_2 for 1 h prior to transferring into the glove box. All chemicals were analytical grade.

5.3.2 Filtered FeS precipitate from Fe(II) and S(-II) solution

The reagent solutions were prepared in crimp bottles sealed with septa and aluminum caps. The pre-weighed chemicals ($FeCl_2 \cdot 4H_2O$ and Na_2S, repectively) were each dissolved in a 100 mL deionized water to obtain a Fe or S concentration of 2 mol L^{-1}. The Fe(II) solution was then slowly injected into the S(-II) solution with a syringe. A black precipitate appeared immediately. The solution in the crimp bottle was stirred gently with a teflon-coated magnetic stirring bar during the whole reaction. After all the Fe(II) solution was injected, the precipitate was left in the bottle for another 24 h. A sample was directly filtered (Ø 13 mm, 0.45 µm, cellulose filter paper) from the suspension and measured immediately.

5.3.3 Freeze-dried FeS

Another sample was prepared following the same procedure, collected via centrifuging, decanting the supernatant, washing with deionized water and centrifuging again. The black precipitate was freeze-dried, stored in the sealed crimp vial under N_2 atmosphere, and measured after 1 month of storage.

5.3.4 FeS from interaction between Fe(III) and S(-II) with different Fe/S ratios

The sample preparation from Fe(III) and S(-II) interaction followed the experimental set-up described by Wan et al. (2014). In brief, 450 mL S(-II) solution (approx. 8 mmol L^{-1} Na_2S solution) was adjusted to pH 7.0 by addition of HCl (c = 1 mol L^{-1}) in a closed reaction vessel and 50 mL of suspension containing a preselected amount of synthetic lepidocrocite was added. The pH was kept constant at pH = 7.00 ± 0.05 with HCl (c= 0.1 mol L^{-1}) using a pH-Stat device (Titrino, Metrohm). The suspension was gently stirred with a teflon-coated magnetic stirring bar during the whole experiment.

Initial molar ratios of Fe/S were adjusted to be 'high' (Fe/S = 2.8) in order to obtain excess lepidocrocite after complete S(-II) consumption, and 'low' (Fe/S = 0.5) in order to obtain excess S(-II). The samples were taken by filtration (Ø 13 mm, 0.45 µm, cellulose filter paper) after 3 h in the experiment with high Fe/S ratio and after 72 h in the experiment with low Fe/S ratio. Samples were measured immediately.

5.3.5 Mössbauer spectroscopy

Filters with solid fraction on top were sealed between two layers of oxygen-proof Kapton tape inside a glove box after small amounts of excess liquid had been carefully removed. The samples were placed in a sealed bottle to avoid contact with air during transportation from the glove box to the spectrometer and measured without delay. The Mössbauer spectrometers sample chamber was pre-cooled to ~ 5 K and flushed with helium gas upon opening. The entered sample was frozen immediately upon entering, the sample chamber was sealed airtight and pumped to remove any oxygen that might have entered the chamber. Mössbauer spectra were collected with a WissEl Mössbauer transmission spectrometer, using a 57Co in Rh matrix γ-ray source mounted on a constant acceleration drive system. Samples were cooled in a Janis closed-cycle Helium gas cryostat and measured ~5 K. During measurement, the samples were kept at vacuum or in a low pressure He atmosphere to avoid oxidation. Spectra were calibrated against a spectrum of alpha-Fe(0) foil at room temperature. Spectral fitting was carried out using Recoil software (University of Ottawa, Canada) with the Voigt-based fitting routine.

5.4 Results and discussion

Figure 5.1 shows the Mössbauer spectra obtained from the different FeS samples as well as a spectrum of lepidocrocite. Mössbauer parameters are listed in Table 5.1. The spectrum of the wet-filtered FeS is a single line. A single line subspectrum also appears at the same position in the freeze-dried FeS sample, accompanied by a six-line subspectrum. While the single line subspectrum is absent in the Mössbauer spectra of the remaining FeS samples, the six-line subspectrum appears exclusively in the FeS sample derived from interaction between Fe(III) and S(-II) at Fe/S = 0.5, and accompanies the lepidocrocite subspectrum in the FeS sample derived from interaction between Fe(III) and S(-II) at Fe/S = 2.8.

Both the single line subspectrum and the six-line subspectrum represent FeS because the wet-filtered material has been synthesized following one of the common protocols for FeS synthesis (e.g. (Rickard et al., 2006)), and Hellige et al. (2012) identified mackinawite on the basis of 5 Å d-spacings observed with Transmission Electron Microscopy (TEM) in experiments sulfidizing lepidocrocite identical to ours. Do the single line and the six-line subspectrum stem from the same mineral but reflect differences in particle size or the degree of crystallinity or purity, or do these subspectra actually represent two different mineral forms of FeS?

In the first case, the wet-filtered precipitate may be of such a small particle size that magnetic ordering is precluded even at liquid helium temperature (superparamagnetism). Particle sizes may have grown during the freeze-drying process, allowing magnetic ordering to take place in a fraction of the particles. Another option is that magnetic ordering occurs because of a lowered symmetry as a result of the inclusion of other elements such as oxygen into the crystal structure. We cannot totally exclude oxidation during the freeze-drying process, and the sulfidation of lepidocrocite, γ-FeOOH, might also have introduced oxygen into the crystal structure.

In the second case, single line and six-line subspectra representing two different mineral forms of FeS, we know of three different mineral forms: mackinawite, troilite, and cubic FeS. Troilite can be excluded due to its mismatch in the spectra in all of our samples (Hafneb and Kalvius, 1966). There are no Mössbauer data for cubic FeS

available from the literature. Both single line and six-line spectra have been reported for mackinawite but it may be disputed whether these authors actually measured mackinawite or another form of FeS they were not aware of.

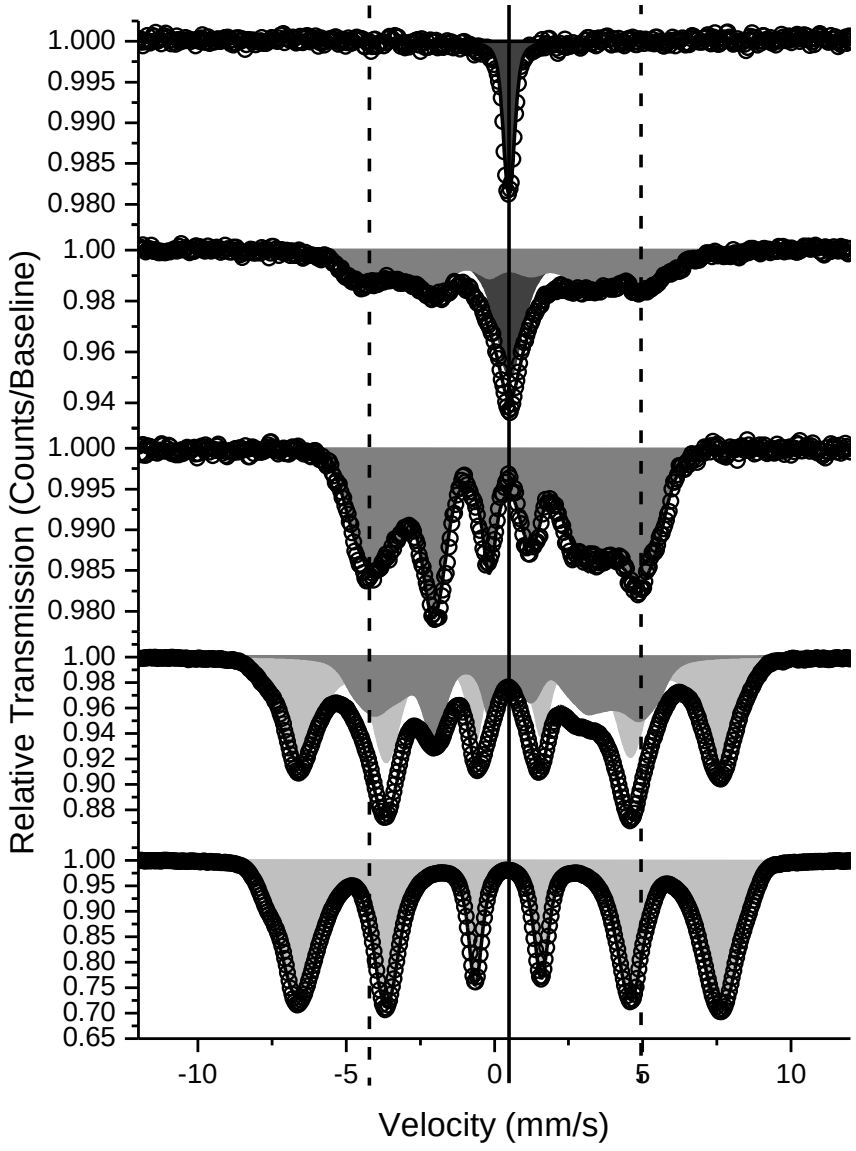

Figure 5.2 Mössbauer spectra collected at sample temperatures of ~5 K from (from top) wet-filtered FeS; freeze—dried FeS; FeS from interaction between Fe(III) and S(-II), Fe/S = 0.5; FeS from interaction between Fe(III) and S(-II), Fe/S = 2.8; and lepidocrocite. The black solid line marks the position of the single line subspectrum (dark grey) representing FeS and the dashed black lines mark the outer two lines of the six-line subsepctrum (grey) representing FeS. The subspectrum representing lepidocrocite is shaded in light grey.

Table 5.1 Mössbauer Parameters used to fit the samples

Phase	No. of lines	δ mm/s	ΔE_Q mm/s	B_{hf} T	Area ratio %
		Wet-filtered FeS			
FeS	1	0.49	-	-	100
		Freeze-dried FeS			
FeS	1	0.51	-	-	37
FeS	6	[0.47][a]	[-0.09]	[27.2]	63
		FeS from interaction between Fe(III) and S(-II), FeS = 0.5			
FeS	6	0.47	-0.09	27.2	100
		FeS from interaction between Fe(III) and S(-II), FeS = 2.8			
FeS	6	[0.47]	[-0.09]	[27.2]	38
γ-FeOOH	6	[0.50]	[0.06]	[43.6]	62
		Lepidocrocite			
γ-FeOOH	6	0.50	0.06	43.6	100

[a] numbers in spare brackets were not varied during the spectral fitting process

In the second case, single line and six-line subspectra representing two different mineral forms of FeS, we know of three different mineral forms: mackinawite, troilite, and cubic FeS. Troilite can be excluded due to its mismatch in the spectra in all of our samples (Hafneb and Kalvius, 1966). There are no Mössbauer data for cubic FeS available from the literature. Both single line and six-line spectra have been reported for mackinawite but it may be disputed whether these authors actually measured mackinawite or another form of FeS they were not aware of.

A single absorption line has been reported by Bertaut et al. (1965) and Vaughan and Ridout (1971). The latter had prepared FeS from metallic Fe, while Bertaut et al. (1965) had bubbled H_2S through a Fe(II) solution. Bertaut et al. (1965) had even cooled their samples down to 1.7 K and still did not observe a magnetic ordering. Several properties can be deducted from the Mössbauer parameters of that single line phase reported here (Table 5.1) and by others (Bertaut et al., 1965; Mullet et al., 2002; Vaughan and Ridout, 1971). The isomer shift δ is indicative of the Fe spin state

(compare Fig. 12.8 in (Gütlich and Schröder, 2012)), and its value points to Fe in either a LS state (S=0) or an intermediate spin (IS) state (S=1). Magnetic ordering in the mineral phase would lead to the splitting of the single line into a six-line pattern resulting from magnetic dipole interaction, for which the nucleus must possess a magnetic dipole moment and there must be a magnetic field present at the nucleus. The Mössbauer-active ^{57}Fe nucleus possesses a non-zero magnetic dipole moment. The absence of magnetic ordering in this FeS phase therefore must stem from the absence of a magnetic field at the nucleus. Unpaired valence electrons in the electron shell produce a magnetic field below the magnetic ordering temperature (Curie temperature T_C or Néel temperature T_N). No magnetic ordering was observed down to 1.7 K, which suggests that Fe in this type of FeS phase must be in the LS state (S=0, i.e. no unpaired electrons).

A single line spectrum is unusual in Mössbauer spectra as most phases show quadrupole splitting resulting in a two-line pattern in the absence of magnetic interactions. Quadrupole splitting results from electric quadrupole interactions between the quadrupole moment of the nucleus and the electric field gradient (EFG) at the nucleus. Again, ^{57}Fe possesses a non-zero quadrupole moment. The EFG at the nucleus must then be zero, which is the case in the instance of cubic valence electron distribution and/or cubic lattice site symmetry. Taking these observations together suggests that the FeS phase investigated by us and reported on by others may in fact not be mackinawite but cubic FeS. Cubic FeS would then be diamagnetic because Fe is in the LS state. If the observed phase is not mackinawite but cubic FeS, the conflict between DFT and Mössbauer spectroscopy vanishes.

Cubic FeS generally forms from the reaction of metallic Fe with hydrogen sulfide and is metastable towards mackinawite at room temperature (De Medicis, 1970; Murowchick and Barnes, 1986; Shoesmith et al., 1980; Takeno et al., 1970). Synthesis from metallic Fe is the pathway chosen by Vaughan and Ridout (1971). We did not start with metallic Fe but all our reagants had been stored and our experiments took place in an anoxic glove box potentially providing the reducing conditions necessary. Furthermore, we reacted Fe not with H_2S but with Na_2S, and we protected our reaction bottle from light.

A single line subspectrum still dominates the spectrum of freeze-dried FeS but a magnetically ordered phase is now also present. During freeze-drying short exposures to oxygen are difficult to avoid. It may also be that cubic FeS was partially transformed into mackinawite during the freeze-drying process. Mullet et al. (2002) reported similar Mössbauer spectra. They had synthesized FeS from metallic Fe with sodium sulfide and produced larger, micrometer-sized mackinawite crystals. Rickard and Luther (2007) suggested that the presence of cubic FeS templates permits these larger mackinawite crystals to form in contrast to the nanoparticulate material produced through the direct solution reaction.

Mullet et al. (2002) confirm the formation of mackinawite on the basis or X-Ray Diffraction (XRD) patterns. They report a very similar magnetically ordered six-line subspectrum next to a dominant single line subspectrum (Mullet et al., 2002). However, they also report an additional magnetically ordered phase not apparent in our spectra (Mullet et al., 2002). This may be another Fe sulfide such as troilite or greigite or a result of partial oxidation as their X-ray photoelectron spectroscopy (XPS) data suggest additional Fe(II)-O and Fe(III)-S bonds. We have performed additional experiments where mackinawite should have formed through the sulfidation of iron (oxyhydr)oxides. Hellige et al. (2012) confirmed the formation of mackinawite through the sulfidation of lepidocrocite with TEM. We repeated these experiments to obtain Mössbauer spectra, and the peak positions due to FeS match the magnetically ordered phase in our freeze-dried samples (Fig. 5.1). When repeating these sulfidation experiments with a lower Fe/S ratio (c.f Materials and Methods) we should obtain pure FeS. The peak positions in the Mössbauer spectrum match those in the freeze-dried samples as well as those in the high Fe/S sulfidation experiments (Fig. 5.1).

This six-line subspectrum, however, is not symmetric, suggesting either strong influence of the quadrupole splitting ΔE_Q parameter or more than one Fe position in crystal lattice, i.e. a superposition of several sextets each resulting from a distinct Fe position in the lattice. The latter would not be expected for pure tetragonal FeS without vancancies or impurities where all Fe positions would be equal. We might deal with vacancies due to FeS stoichiometry being not exactly equal to 1 and/or oxygen playing a role (e.g. oxygen from reduced iron (oxyhydr)oxides). Alternatively, this FeS phase may exhibit a large quadrupole shift as a result of an intermediate spin

state (S=1), which would lead to Jahn-Teller distortion, or because the magnetical ordering leads to a distorted ‘octet’ pattern as observed for other magnetically order Fe(II)-compounds such as siderite (Ok, 1969).

5.5 Conclusions and outlook

Though we cannot exclude that single line and six-line subspectra represent the same FeS mineral form but at different degrees of particle size and/or purity, it is also possible that they represent two distinct mineral forms. The single line subspectrum would then represent cubic FeS, and the data presented here would be the first Mössbauer parameters from this mineral allowing conclusions on its Fe spin state and magnetic properties. The six-line subspectrum would in turn represent mackinawite (although a mixture of mackinawite with additional Fe-O-S compounds cannot be excluded). In that case, we would be able to confirm that mackinawite exhibits magnetic ordering at low temperatures, thus resolving a long-standing dispute on the magnetic properties of mackinawite arising from DFT calculations and conflicting Mössbauer results in the literature. However, to prove these hypotheses we need to obtain Mössbauer spectra from cubic FeS and mackinawite sample whose identity has been clearly confirmed by other methods.

Acknowledgements

This work was carried out in the framework of the research unit FOR 580, electron transfer processes in anoxic aquifers (e-TraP), funded by Deutsche Forschungsgemeinschaft. We thank Ayokunle Akindutire for help with mineral synthesis and George Luther III and Ian Butler for fruitful discussions.

5.6 References

Bertaut, E., Burlet, P., and Chappert, J., 1965. Sur l'absence d'ordre magnetique dans la forme quadratique de FeS. *Solid State Communications* **3**, 335-338.

De Medicis, R., 1970. Cubic FeS, a metastable iron sulfide. *Science* **170**, 1191-1192.

Devey, A., Grau-Crespo, R., and De Leeuw, N., 2008. Combined density functional theory and interatomic potential study of the bulk and surface structures and properties of the iron sulfide mackinawite (FeS). *The Journal of Physical Chemistry C* **112**, 10960-10967.

Gütlich, P. and Schröder, C., 2012. Mössbauer Spectroscopy, *Methods in Physical Chemistry*. Wiley-VCH Verlag GmbH & Co. KGaA.

Hafneb, S. and Kalvius, M., 1966. The Mössbauer resonance of Fe57 in troilite (FeS) and pyrrhotite (Fe0 88S). *Zeitschrift für Kristallographie-Crystalline Materials* **123**, 443-458.

Hazen, R. M., 2013. Paleomineralogy of the Hadean Eon: a preliminary species list. *American Journal of Science* **313**, 807-843.

Hellige, K., Pollok, K., Larese-Casanova, P., Behrends, T., and Peiffer, S., 2012. Pathways of ferrous iron mineral formation upon sulfidation of lepidocrocite surfaces. *Geochimica et Cosmochimica Acta* **81**, 69-81.

Jacob, C. R. and Reiher, M., 2012. Spin in density-functional theory. *International Journal of Quantum Chemistry* **112**, 3661-3684.

Kwon, K. D., Refson, K., Bone, S., Qiao, R., Yang, W.-l., Liu, Z., and Sposito, G., 2011. Magnetic ordering in tetragonal FeS: evidence for strong itinerant spin fluctuations. *Physical Review B* **83**, 064402.

Morice, J., Rees, L., and Rickard, D., 1969. Mössbauer studies of iron sulphides. *Journal of Inorganic and Nuclear Chemistry* **31**, 3797-3802.

Mullet, M., Boursiquot, S., Abdelmoula, M., Génin, J.-M., and Ehrhardt, J.-J., 2002. Surface chemistry and structural properties of mackinawite prepared by reaction of sulfide ions with metallic iron. *Geochimica et Cosmochimica Acta* **66**, 829-836.

Murowchick, J. B. and Barnes, H., 1986. Formation of cubic FeS. *American Mineralogist* **71**, 1243-1246.

Murphy, W. L., Andersen, J. M., and Ebelin, R. M., 2002. Assessment of geology as it pertains to modeling uplift in jointed rock :

a basis for inclusion of uncertainty in flow models. US Army Corps of Engineers, Engineer Research and Development Center, Geotechnical and Structures Laboratory, Information Technology Laboratory, Vicksburg, Miss.

Nakamura, R., Okamoto, A., Tajima, N., Newton, G. J., Kai, F., Takashima, T., and Hashimoto, K., 2010. Biological Iron-Monosulfide Production for Efficient Electricity Harvesting from a Deep-Sea Metal-Reducing Bacterium. *ChemBioChem* **11**, 643-645.

Ok, H. N., 1969. Relaxation effects in antiferromagnetic ferrous carbonate. *Physical Review* **185**, 472.

Rickard, D., Griffith, A., Oldroyd, A., Butler, I., Lopez-Capel, E., Manning, D., and Apperley, D., 2006. The composition of nanoparticulate mackinawite, tetragonal iron (II) monosulfide. *Chemical Geology* **235**, 286-298.

Rickard, D. and Luther, G. W., 2007. Chemistry of iron sulfides. *Chemical Reviews* **107**, 514-562.

Russell, M. J. and Hall, A., 1997. The emergence of life from iron monosulphide bubbles at a submarine hydrothermal redox and pH front. *Journal of the Geological Society* **154**, 377-402.

Shoesmith, D. W., Taylor, P., Bailey, M. G., and Owen, D. G., 1980. The formation of ferrous monosulfide polymorphs during the corrosion of iron by aqueous hydrogen sulfide at 21 C. *Journal of the Electrochemical Society* **127**, 1007-1015.

Subedi, A., Zhang, L., Singh, D. J., and Du, M.-H., 2008. Density functional study of FeS, FeSe, and FeTe: Electronic structure, magnetism, phonons, and superconductivity. *Physical Review B* **78**, 134514.

Takeno, S., Zoka, H., and Niihara, T., 1970. Metastable cubic iron sulfide-with special reference to mackinawite. *American Mineralogist* **55**, 1639-&.

Vaughan, D. and Ridout, M., 1971. Mössbauer studies of some sulphide minerals. *Journal of Inorganic and Nuclear Chemistry* **33**, 741-746.

Wan, M., Shchukarev, A., Lohmayer, R., Planer-Friedrich, B., and Peiffer, S., 2014. Occurrence of Surface Polysulfides during the Interaction between Ferric (Hydr)Oxides and Aqueous Sulfide. *Environmental Science & Technology* **48**, 5076-5084.

Contribution to the studies

Study 1

Occurrence of Surface Polysulfides during the Interaction between Ferric (Hydr)Oxides and Aqueous Sulfide

Published in 2014, *Environmental science & technology*, 48(9), 5076-5084.

Moli Wan	55%	concepts, laboratory work, manuscript preparation
Andrey Shchukarev	10%	XPS analysis, discussion of result, comments on manuscript
Regina Lohmayer	10%	HPLC analysis, discussion of results
Britta Planer-Friedrich	10%	concepts, comments on manuscripts
Stefan Peiffer	15%	concepts, discussion of result, comments on manuscript

Study 2

Pyrite formation and mineral transformation pathways upon sulfidation of ferric hydroxides depend on mineral type and sulfide concentration

Published in 2015, *Chemical Geology*, *400*, 44-55.

Stefan Peiffer	55%	concepts, discussion of results, manuscript preparation
Thilo Behrends	10%	concepts, discussion of results, manuscript preparation
Katrin Hellige	20%	Laboratory work, manuscript preparation
Philip Larese-Casanova	5%	Mössbauer spectroscopy analysis, discussion of results
Moli Wan	5%	laboratory test, comments on manuscript
Kilian Pollok	5%	TEM analysis, discussion of results

Study 3

Fe/S ratio controls pathway and kinetics of pyrite formation during Fe(III)-S(-II) interaction

Planned submission to *Geochimica et Cosmochimica Acta.* Manuscript in preparation.

Moli Wan	55%	concepts, laboratory work, manuscript preparation
Christian Schröder	10%	Mössbauer spectroscopy analysis, discussion of results, comments on manuscript
Stefan Peiffer	35%	concepts, discussion of results, comments on manuscript

Study 4

Electromagnetic Properties of FeS Phases: Insights from Mössbauer Spectroscopy

Planned submission to *Geochimica et Cosmochimica Acta.* Manuscript in preparation.

Christian Schröder	50%	concepts, Mössbauer spectroscopy analysis, discussion of results, manuscript preparation
Moli Wan	35%	concepts, laboratory work, discussion of results, comments on manuscript
Stefan Peiffer	15%	comments on manuscript

Acknowledgements

I would like to thank Stefan Peiffer for the opportunity to work at the department of Hydrology, the supervision and all helpful advices during the whole 'Ph.D' project.

The 'Ph.D' project should not be finished without the support from cooperation partners. I would like to thank

- Britta Planer-Friedrich, Regina Lohmayer and Sophie Fortenfant at the Environmental Geochemistry Group, university of Bayreuth for the help of polysulfide measurements;
- Andrey Shchukarev at the Umeå University, Sweden for the XPS analysis;
- Per Persson at the Lund University, Sweden for granting access to the XPS analysis;
- Stefan Haderlein at the University of Tübingen for the opportunity to work in the lab;
- Christian Schröder at the University of Tübingen (now at the University of Sirling, United Kingdom) for the help of measurements with Mössbauer spectroscopy and the data analysis.

I would like to thank Luisa Hopp for the valuable comments on the thesis and Maria Klug for the control on German translation.

Thank all people from reaserch group Etrap (FOR 580), FIMIN (ESF Research Networking Programme) and DAAD.

I would like to thank all people providing their help to the work: Bettina Kuppinger, Jutta Eckert, Martina Rohr, Heidi Zier, Silke Hammer, Karin Söllner, Katrin Hellige and Klaus-Holger Knorr, Ben Gilfedder, Sven Frei and Martina Heider.

I would like to thank Cornelia Nicodemus for her kindly help to make my life easier in Germany.

I would like to thank all friends for the good old days: skiing, hiking, table games, cooking, beer and alcohols. I would like to thank Sabine Thüns, Clara Laugsch, Kasia Zajac, Julia Beer, Markus Bauer, Christiane Neumann and her family, Michael Radke, Kerstin Grant, Uwe Kunkel, Julienne Schiebold, Jean-Lionel Payeur-Poirier, Kiyong Kim, Mario Chan, Xiaojun Chen, and hydro master students: Alana Steinbauer, Marco Pittroff, Maria Klug and Barbara Glaser and those who I've forgotten to mention here.

Special thank to my parents, my dear sister and my brothers for the support and understanding. Special thank to Beibei：感谢一路相伴。

Versicherungen und Erklärungen

(§8 S. 2 Nr. 6 PromO)

Hiermit erkläre ich mich damit einverstanden, dass die Elektronische Fassung meiner Dissertation unter Wahrung meiner Urheberrechte und des Datenschutzes einer gesonderten Überprüfung hinsichtlich der eigenständigen Anfertigung der Dissertation unterzogen werden kann

(§8 S. 2 Nr. 8 PromO)

Hiermit erkläre ich eidesstattlich, dass ich die Dissertation selbständig verfasst und keine anderen als die von mir angegebenen Quellen und Hilfsmittel benutzt habe

(§8 S. 2 Nr. 9 PromO)

Ich habe die Dissertation nicht bereits zur Erlangung eines akademischen Grades anderweitig eingereicht und habe auch nicht bereits diese oder eine gleichartige Doktorprüfung endgültig nicht bestanden.

(§8 S. 2 Nr. 10 PromO)

Hiermit erkläre ich, dass ich keine Hilfe von gewerbliche Promotionsberatern bzw. -vermittlern in Anspruch genommen habe und auch künftig nicht nehmen werde.

……..

Ort, Datum, Unterschrift